

**Titre:** Tool Condition Monitoring and Surface Topography Analysis During the Machining of CFRP Composites

**Auteur:** Xavier Rimpault

**Date:** 2016

**Type:** Mémoire ou thèse / Dissertation or Thesis

**Référence:** Rimpault, X. (2016). Tool Condition Monitoring and Surface Topography Analysis During the Machining of CFRP Composites [Thèse de doctorat, École Polytechnique de Montréal]. PolyPublie. <https://publications.polymtl.ca/2381/>

 **Document en libre accès dans PolyPublie**

Open Access document in PolyPublie

**URL de PolyPublie:** <https://publications.polymtl.ca/2381/>

**Directeurs de recherche:** Marek Balazinski, Jean-François Chatelain, & Jolanta-Ewa Sapieha

**Programme:** Génie mécanique

UNIVERSITÉ DE MONTRÉAL

TOOL CONDITION MONITORING AND SURFACE TOPOGRAPHY ANALYSIS DURING  
THE MACHINING OF CFRP COMPOSITES

XAVIER RIMPAULT

DÉPARTEMENT DE GÉNIE MÉCANIQUE  
ÉCOLE POLYTECHNIQUE DE MONTRÉAL

THÈSE PRÉSENTÉE EN VUE DE L'OBTENTION  
DU DIPLÔME DE PHILOSOPHIAE DOCTOR  
(GÉNIE MÉCANIQUE)

DÉCEMBRE 2016

UNIVERSITÉ DE MONTRÉAL

ÉCOLE POLYTECHNIQUE DE MONTRÉAL

Cette thèse intitulée :

TOOL CONDITION MONITORING AND SURFACE TOPOGRAPHY ANALYSIS  
DURING THE MACHINING OF CFRP COMPOSITES

présentée par : RIMPAULT Xavier

en vue de l'obtention du diplôme de : Philosophiae Doctor

a été dûment acceptée par le jury d'examen constitué de :

M. LAKIS Aouni A., Ph. D., président

M. BALAZINSKI Marek, Docteur ès Sciences, membre et directeur de recherche

Mme SAPIEHA Jolanta Ewa, Ph. D., membre et codirectrice de recherche

M. CHATELAIN Jean-François, Ph. D., membre et codirecteur de recherche

M. BOUKHILI Rachid, Doctorat, membre

M. FURET Benoit, Doctorat, membre externe

## ACKNOWLEDGEMENTS

I would never have been able to complete this thesis without the assistance of my committee members and colleagues, and the help and support of my friends and family.

Foremost, I would like to express my deepest gratitude to my advisor, Prof. Marek Balazinski, for the continuous support of my Ph. D. study and research, for his motivation and enthusiasm. I would like to thank my co-advisors, Prof. Jean-François Chatelain and Prof. Jolanta Klemberg-Sapieha, for their guidance, help and patience.

My sincere thanks also goes to the rest of my thesis committee: Prof. Diane Riopel, Prof. Rachid Boukhili, Prof. Aouni A. Lakis and Prof. Benoit Furet, for their encouragement, insightful comments and hard questions.

I would like to thank technicians at the virtual manufacturing research laboratory (LRFV) in Polytechnique Montreal, Guy Gironne, Vincent Mayer and François Ménard, and at the products, processes, and systems engineering laboratory (LIPPS) in ÉTS, Éric Marcoux, for their advice, time and assistance. I would like to thank our industrial partners in the CRIAQ MANU-413 project.

I would also like to thank Karina Mateo-Rodriguez, Marie-Michèle Vézina and Caroline Jodoin at Service des Étudiants de Polytechnique for giving me the job opportunity and help for students with disabilities.

Obviously, I am very grateful to my numerous colleagues and friends who supported me during all those years, with special thanks to my friend, colleague and love, Anna Łoś.

## RÉSUMÉ

Les composites polymères notamment FRP (fibre reinforced plastics) sont de plus en plus employés dans l'industrie manufacturière (aéronautique et automobile notamment) pour la confection de leurs produits. L'emploi de carbone dans les FRP est en particulier prisé pour ses caractéristiques mécaniques. Depuis quelques décennies, le mélange de matériaux composites et métalliques au sein de structures de produits apporte des défis supplémentaires lors de leur assemblage. Face à ces nouveaux matériaux, les scientifiques et industriels réemploient les techniques qui ont été bâties et fait leurs preuves pour des matériaux métalliques relativement homogènes. Cependant, de par les propriétés intrinsèques des composites FRP, l'état de surface est fondamentalement hétérogène et la caractérisation de l'état de surface en devient complexe. Un autre point, de par ces spécificités, usiner un tel matériau provoque des petites vibrations additionnelles que l'on pourrait qualifier de bruit sur des signaux vibratoires, en comparaison avec l'usinage de métaux.

Cette thèse vise à répondre aux problèmes de caractérisation de surface mais aussi au développement d'une technique novatrice de suivi de la qualité de coupe. La technique développée se base sur la théorie fractale et l'analyse fractale pour répondre aux besoins de la quantification du bruit sur les signaux de forces de coupe ou de vibration. L'analyse fractale permet de mettre en évidence le niveau de complexité et de rugosité d'objets. Pour bâtir et valider cette méthode, plusieurs tests ont été réalisés : détournage, perçage axial et orbital. Malgré le niveau élémentaire du développement de cette technique, les premiers résultats sont prometteurs. Mise en place sur une cellule de fabrication, cette méthode permet d'évaluer, en un temps très court, le niveau d'usure d'outil (en vue de son possible remplacement) ainsi que la qualité de coupe générée.

Pour la caractérisation de surface de composites laminés, l'étude s'est premièrement basée sur des relevés de profils de surface et de rugosité. Dans chacune des deux directions principales (dans le sens du pli et dans le sens de l'empilement), des problèmes spécifiques ont été mis en évidence. Et pour chacune des directions, un plan correctif des méthodes de caractérisation actuelles a été proposé. Le résultat de ces optimisations proposées permet de mieux évaluer l'état de surface au vue de la qualité de coupe ainsi que de la robustesse du procédé.

## ABSTRACT

Polymer composites such as FRPs (fiber reinforced plastics) have been increasingly used by the manufacturing industry (aerospace and automotive in particular) in the making of their products. The carbon selection in FRPs is especially preferred for its mechanical properties. For few decades, the combination of composite and metallic materials within products' structure has been raising up additional challenges during the assembly. To solve those issues, scientists and industrials often reused techniques that had been built and proved for relatively homogeneous metallic materials. However, due to the intrinsic properties of FRP composites, the surface condition is particularly heterogeneous and such surface condition characterization tend to be more complex. Furthermore, machining a FRP material generates additional short vibrations that could be evaluated as noise in the vibration signals in comparison with the machining of metals.

This thesis is a contribution to solutions to surface characterization issues and proposes an innovative technique of machining quality monitoring. The developed technique is based on the fractal theory and fractal analysis to meet the needs of the noise assessment in the cutting forces or vibration signals. Fractal analysis allows to evaluate the complexity and roughness of objects. To build and validate this method, several tests were performed: trimming, drilling axial and orbital. Despite the relatively low level of development of this technique, first results are promising. Set up in a manufacturing cell, this method allows to evaluate, in a very short time, the tool wear (for possible tool replacement) and the machining quality.

For laminated composites' surface characterization, the study is primarily based on surface profiles and roughness observations. For both two main directions (in the ply plane direction and in the direction of the stack sequence), specific problems have been highlighted. And for each direction, a corrective plan of current characterization methods proposed. The result of those proposed enhancements to better evaluate the surface condition in view of the machining quality and process robustness.

## TABLE OF CONTENTS

ACKNOWLEDGEMENTS .....	III
RÉSUMÉ.....	IV
ABSTRACT .....	V
TABLE OF CONTENTS .....	VI
LIST OF TABLES .....	X
LIST OF FIGURES.....	XII
LIST OF SYMBOLS AND ABBREVIATIONS.....	XVIII
LIST OF APPENDICES .....	XIX
PREAMBLE.....	XX
CHAPTER 1    INTRODUCTION.....	1
1.1    Problem description.....	1
1.2    Objectives.....	2
CHAPTER 2    LITERATURE REVIEW .....	4
2.1    Fibre reinforced plastics (FRP) .....	4
2.1.1    Generalities.....	4
2.1.2    Carbon fibre reinforced plastics (CFRP).....	4
2.1.3    Mechanical properties .....	6
2.2    Machining of FRPs.....	7
2.2.1    Orthogonal cutting.....	7
2.2.2    Chip formation .....	9
2.2.3    Tooling .....	10
2.3    Machining quality .....	11
2.3.1    Surface integrity .....	11

2.3.2	Surface topography .....	13
2.4	Surface roughness .....	15
2.5	Fractal objects .....	18
2.5.1	Concept and generalities .....	18
2.5.2	Fractal analysis techniques.....	19
CHAPTER 3	GENERAL PRESENTATION .....	21
CHAPTER 4	ARTICLE 1: TOOL WEAR AND SURFACE QUALITY ASSESSMENT OF CFRP TRIMMING USING FRACTAL ANALYSES OF THE CUTTING FORCE SIGNALS	24
4.1	Abstract .....	24
4.2	Introduction .....	24
4.2.1	CFRP .....	24
4.2.2	Fractal analysis .....	25
4.3	Workpiece, machine, setup and tooling specifications .....	26
4.4	Methodology .....	27
4.4.1	Design of experiments.....	27
4.4.2	Measurements.....	28
4.4.3	Analyses performed.....	29
4.5	Fractal dimension calculation methods .....	30
4.5.1	Box-counting fractal analysis.....	32
4.5.2	Correlation fractal analysis.....	33
4.5.3	Regularization fractal analysis .....	35
4.6	Results and discussion.....	37
4.6.1	Statistical parameters.....	37
4.6.2	Fractal parameters .....	39
4.6.3	Machined surface quality .....	44



4.7	Conclusion.....	45
4.8	Acknowledgements .....	46
4.9	References .....	46
CHAPTER 5 ARTICLE 2: A NEW APPROACH FOR THE SURFACE ROUGHNESS PROFILE CHARACTERIZATION OF LAMINATED COMPOSITES IN THE PLY PLANE DIRECTION .....		49
5.1	Abstract .....	49
5.2	Introduction .....	49
5.3	Methodology .....	51
5.3.1	Design of experiments.....	51
5.3.2	Experimental setup.....	52
5.3.3	Measurements.....	52
5.3.4	Calculated roughness parameters .....	54
5.4	Results and discussion.....	58
5.4.1	Roughness profiles .....	58
5.4.2	Autocorrelation.....	59
5.4.3	Fractal analysis .....	62
5.5	Conclusion.....	64
5.6	Acknowledgements .....	64
5.7	References .....	64
CHAPTER 6 ARTICLE 3: SURFACE PROFILE TEXTURE CHARACTERIZATION OF TRIMMED LAMINATED COMPOSITE IN THE STACKING SEQUENCE DIRECTION ....		66
6.1	Abstract .....	66
6.2	Introduction .....	66
6.2.1	Laminated composites .....	66

6.2.2	Surface profile characterization .....	68
6.3	Methodology .....	70
6.3.1	Primary profiles filtering .....	70
6.3.2	Machining experiments .....	75
6.3.3	Profile measurements .....	75
6.3.4	Parametrization and filtering method assessment .....	76
6.3.5	Complementary analysis .....	77
6.4	Results and discussion .....	78
6.4.1	Primary profiles .....	78
6.4.2	Roughness profiles obtained using linear Gaussian filter .....	81
6.4.3	Roughness profiles obtained using standards filtering for different stratified properties surface .....	81
6.4.4	Roughness profiles with valleys removing .....	83
6.5	Conclusion .....	89
6.6	Acknowledgements .....	90
6.7	References .....	90
CHAPTER 7	GENERAL DISCUSSION .....	92
7.1	Fractal analysis of CFRP machining signals .....	92
7.2	Topography analysis of laminated composite .....	93
CHAPTER 8	GENERAL CONCLUSION AND RECOMMENDATIONS .....	94
8.1	Original contributions .....	94
8.2	Future works .....	97
BIBLIOGRAPHY	.....	98
APPENDICES	.....	106

## LIST OF TABLES

Table 2.1: Carbon fibre general characteristics (Berthelot, 2012) .....	5
Table 2.2: Mechanical characteristics of epoxy resin (Berthelot, 2012).....	6
Table 4.1: Tool geometrical characteristics .....	26
Table 4.2: Chosen cutting parameters for the machining experiments using three tools with the same characteristics .....	27
Table 4.3: Picture samples of the clearance tool wear for the tool 1 along its tool life .....	28
Table 5.1: Chosen cutting parameters for the machining tests .....	52
Table 5.2: Profile length datasheet .....	53
Table 6.1: Profile characteristics datasheet .....	69
Table 6.2: Chosen profile parameters .....	77
Table 6.3: Averages and maximums of the relative standard deviations calculated on each face for up and down milling faces, for primary parameters (a); for roughness parameters from roughness profiles filtered using the linear Gaussian function with the 0.25 mm cut off length (b); for roughness parameters from profiles filtered using the filtering technique from ISO 13565-1, using the same 2.5 mm cut off length (c) and two different cut off lengths (2.5 mm and then 0.25 mm) (d) – (all values are in percentage).....	82
Table 6.4: Averages and maximums of the relative standard deviations calculated on each face for up- and down-milling faces and for plateau primary parameters and plateau roughness profiles (the values are presented in percentage) .....	86
Table 8.1: Journal publication list (ranked by chronological order using the submission date)....	95
Table 8.2: Communication list in conferences (ranked by chronological order using the conference/symposium date as reference).....	96
Table A.1: Conducted plans of experiments for the twist drills.....	113
Table A.2: Means of the titanium burr height ratios for each couple of feed and speed corresponding to the titanium layer.....	118

Table A.3: Means of the aluminium burr height ratios for each couple of feed and speed corresponding to the aluminium layer.....	120
Table A.4: Means of the calculated force signal fractal dimensions $D_R$ for each couple of feed and speed levels corresponding to the CFRP layer.....	124
Table B.1: Cutting parameters .....	132

## LIST OF FIGURES

Figure 2-1: Lay-up laminate (Campbell, 2010) .....	5
Figure 2-2: Longitudinal strength/ultimate strength ratio as function of ply angle (left); Tensile properties of fibers, matrix and composite material (right) (Campbell, 2010) .....	6
Figure 2-3: Orthogonal and oblique cutting process geometries (Altintas, 2012) .....	7
Figure 2-4: Crack propagation modes (Hudson & Harrison, 1997).....	8
Figure 2-5: McKenzie angles definition (Bonnet, 2010) .....	8
Figure 2-6: Cutting mechanisms for CFRP composites machining in parallel and perpendicular directions (Koplev et al., 1983).....	9
Figure 2-7: UD cutting mechanisms (Arola, Ramulu, & Wang, 1996) .....	9
Figure 2-8: Up- and down- milling (Sheikh-Ahmad, J. Y., 2009).....	10
Figure 2-9: Delamination types (Colligan, 1991) .....	12
Figure 2-10: Delamination factor (Davim, J. P. & Reis, 2005) .....	12
Figure 2-11: Fibre orientation effect on the profile surface roughness with different depth of cut (a) 0.001mm; (b) 0.050mm (Wang, X. M. & Zhang, 2003).....	15
Figure 2-12: Comparison of roughness profiles for four orientations using three set of cutting parameters (Chatelain et al., 2012).....	16
Figure 2-13: Different types of roughness profiles (Chatelain et al., 2012) .....	17
Figure 2-14: Koch curve iterations (Davim, J. et al., 2011).....	19
Figure 2-15: Fractal analysis evaluating the British coastline length using different stick lengths (Andrus, 2005) .....	20
Figure 3-1: Thesis organization plan.....	23
Figure 4-1: Experimental setup used for short cuts machining (100 mm).....	27
Figure 4-2: Cutting forces measured from the first cut of the 1 <sup>st</sup> pass of the tool 1 (for graph clarity, the signals were shifted one from another) .....	30

Figure 4-3: Weierstrass-Mandelbrot functions generated with different values of the parameter or fractal dimension $D$ .....	31
Figure 4-4: Total cutting force signal samples $F_T$ over three rotational periods for different tool wear of tool 1 (from 1 <sup>st</sup> pass with a new tool to the 22 <sup>nd</sup> pass with a worn tool).....	32
Figure 4-5: Box counting graph (box number containing the curve vs the size box) for different tool wear of the tool 1 .....	33
Figure 4-6: Correlation analysis graph ( $\log(\varepsilon)$ vs $\log \varepsilon$ ) for different tool wear of the tool 1 .....	34
Figure 4-7: Regularization analysis graph ( $\log la$ vs $\log a$ ) using the 1 <sup>st</sup> derivative Gaussian function kernel.....	36
Figure 4-8: Regularization analysis graph ( $\log la$ vs $\log a$ ) using the rectangular kernel.....	36
Figure 4-9: Evolution of the tool wear $VB_{avg}$ vs the length of CFRP cut.....	37
Figure 4-10: Averages and standard deviations of the total cutting force signals vs the averaged tool wear $VB_{avg}$ .....	38
Figure 4-11: Skewness (asymmetry) and kurtosis (flatness) of the total cutting force signals vs the averaged tool wear $VB_{avg}$ .....	38
Figure 4-12: Topothesis results vs the tool wear average $VB_{avg}$ .....	39
Figure 4-13: Fractal dimensions graph (fractal dimensions $D_{BC}$ , $D_C$ , $D_{RG}$ , $D_{RR}$ ) in comparison to the averaged tool wear $VB_{avg}$ .....	40
Figure 4-14: Coefficient of fractal dimension slope determination vs the averaged tool wear $VB_{avg}$ .....	41
Figure 4-15: Fractal index $If$ vs the tool wear $VB_{avg}$ .....	42
Figure 4-16: Cutting force signal samples over two tool rotational periods for different tool wear of tool 1: feed force signal $F_f$ (left), normal force signal $F_n$ (centre) and vertical force signal $F_z$ (right) .....	43
Figure 4-17: Fractal dimensions graph in comparison to the averaged tool wear $VB_{avg}$ .....	44
Figure 4-18: Coefficient of fractal dimension slope determination vs the averaged tool wear $VB_{avg}$ from the fractal analysis of the $F_n$ cutting force signals .....	44

Figure 5-1: Roughness profiles examples of $-45^\circ$ ply orientation giving similar $Ra$ , $Rsk$ and $Rku$ with low (left) and high (right) tool wear.....	51
Figure 5-2: Measurement area on the machined coupon face.....	53
Figure 5-3: Roughness profile samples for the four ply orientations and both face milling types and machined with different tool wear (first, ninth and twentieth passes respectively a, b and c, respectively with the tool wear of 0 mm, 0.07 mm and 0.19 mm) of tool 1 .....	55
Figure 5-4: Roughness parameters associated with the normalized autocorrelation function $acf$ .....	56
Figure 5-5: Regularization analysis graph using the rectangular kernel .....	57
Figure 5-6: Roughness parameter $Ra$ values average vs. the averaged tool wear $VB$ for the four ply orientations and both milling types .....	60
Figure 5-7: Autocorrelation results $RACa0$ average ( $acf$ average deviation towards zero) vs the averaged tool wear $VB$ for the four ply orientations and both milling types .....	61
Figure 5-8: Fractal parameter $RR2_{high}$ results average vs the averaged tool wear $VB$ for the four ply orientations and both milling types .....	63
Figure 6-1: Surface profile measurements in longitudinal and transverse direction on a trimmed laminated composite surface .....	67
Figure 6-2: Simplified chart of surface profile characterization .....	68
Figure 6-3: Examples of waviness profiles using the Gaussian probability density function filter and different cut-off lengths.....	69
Figure 6-4: Roughness profile examples using the Gaussian probability density function filter and different cut-off lengths (roughness profiles are in black based on the primary profile in grey) .....	70
Figure 6-5: Filtering technique using the modified ISO 13565-1 method.....	72
Figure 6-6: Simplified chart of the plateau roughness characterization.....	73
Figure 6-7: Plateau roughness profile example: removal of the profile deep valleys (left), primary and roughness plateau profiles (right).....	74
Figure 6-8: Surface profile measurement area on the coupon .....	76

Figure 6-9: Primary profiles examples for different tool wear and both up- and down-milling with the stacking sequence from left to right for each profile: $0^\circ/+45^\circ/-45^\circ/+45^\circ/-45^\circ/0^\circ/-45^\circ/+45^\circ/90^\circ/90^\circ/+45^\circ/-45^\circ/0^\circ/-45^\circ/+45^\circ/-45^\circ/45^\circ/0^\circ/+45^\circ/-45^\circ$ (uncut fibres are circled)	79
Figure 6-10: Amplitude Distribution Curves (ADC) and Bearing Area Curves (BAC) examples of primary profiles for different tool wear and both up- and down-milling	80
Figure 6-11: Amplitude Distribution Curves (ADC) and Bearing Area Curves (BAC) examples of roughness profiles for different tool wear obtained from filtered profiles using two different cut-off lengths during the ISO 13565-1 standard filtration	84
Figure 6-12: Mean and median of $R_t$ and $R_k$ roughness parameters for both milling type and different tool wear with the deviation of $\pm 2$ standard deviation on the mean	85
Figure 6-13: Plateau roughness profiles after removing the deep valleys and applying a second filtering	87
Figure 6-14: Mean and median of $PRa$ and $PRk$ roughness parameters for both milling type and different tool wear with the deviation of $\pm 2$ standard deviation on the mean	88
Figure A-1: Box counting example for a five circle inversion fractal	108
Figure A-2: Stack material specifications	111
Figure A-3: Experimental set-up of the fixture of the workpiece, mounted over the Kistler force measurement table and a junction part	112
Figure A-4: Top view of the holding table and frame of the stack	112
Figure A-5: Depths for the measurements of hole diameter and circularity (the references are at the top of each layer in the stack)	115
Figure A-6: Titanium burr height ratio versus the tool wear $VB_{Bmax}$	116
Figure A-7: Titanium burr height ratio versus the thrust force under same cutting parameters corresponding to the central point of the variation parameters for titanium	117
Figure A-8: Titanium burr height ratio versus the torque under same cutting parameters corresponding to the central point of the variation parameters for titanium	117



Figure A-9: Aluminium burr height ratio versus the tool wear $VB_{Bmax}$ .....	119
Figure A-10: Aluminium burr height ratio versus the thrust force under same cutting parameters corresponding to the central point of the variation parameters for titanium .....	119
Figure A-11: Measured thrust force signals for sharp and worn tools during CFRP machining .....	120
Figure A-12: Measured thrust force signals for sharp and worn tools over a period during CFRP drilling (magnification of the frames from Figure A-11).....	121
Figure A-13: Graphs $\ln l_a$ (length of the convolution product estimated for the size $a$ ) versus $\ln a$ computed from the thrust force signals obtained during the CFRP machining using one tool after drilling the holes 1, 17, 34, 55, 82 and 115.....	122
Figure A-14: Graphs $\ln l_a$ (length of the convolution product estimated for the size $a$ ) versus $\ln a$ from the thrust force signals obtained from the CFRP machining using one tool after drilling the holes 1, 17, 34, 55, 82 and 115 (magnification of the area between the vertical lines from Figure A-13).....	123
Figure A-15: Measured thrust force signals for sharp and worn tools over a period during titanium machining.....	123
Figure A-16: Relative standard deviations of fractal dimensions $D_R$ , calculated for different sampling lengths.....	124
Figure A-17: Fractal dimension $D_R$ versus the number of hole drilled for 100% CFRP cutting speed and feed levels (LS 1-3: Fractal dimension $D_R$ estimated with least square method for tools 1-3, Min: minimum limit of Fractal dimension $D_R$ , Max: maximum limit of Fractal dimension $D_R$ ) .....	125
Figure A-18: Fractal dimensions $D_R$ using least square (LS) method versus the tool wear $VB_{Bmax}$ .....	125
Figure A-19: Fractal dimensions $D_R$ using least square (LS) method versus titanium burr height ratio.....	126
Figure A-20: Fractal dimensions $D_R$ using least square (LS) method versus aluminium burr height ratio.....	126
Figure B-1: Experimental setup representation.....	132

Figure B-2: Filtered cutting forces (top), total cutting force (center) and filtered and root mean square (RMS) acoustic emission (AE – bottom) signals.....	133
Figure B-3: Zoom samples, from the analyzed section presented in Fig. 2, of the total cutting force ( $F_T$ ) signals – up – and of the acoustic emission (AE) signals – down – over two tool rotation periods for different holes .....	134
Figure B-4: Graph of curve samples for the fractal dimension determination using the rectangular kernel of total cutting force and acoustic emission signals .....	136
Figure B-5: Results of the fractal dimension $D$ , the topothesis $G$ and the $R^2$ from the analysis of $F_T$ and AE signals vs the number of holes drilled.....	137
Figure B-6: Fractal index, $I_F$ , results and the tool wear in function of the number of holes drilled .....	138
Figure C-1: Measurement positions on trimmed surfaces in the transverse direction .....	142
Figure C-2: Measurement positions diagram on hole surfaces .....	143
Figure C-3: Primary profiles of up- and down-milling trimmed surfaces for three different tool wear .....	144
Figure C-4: $Ra$ average results with $\pm 2$ standard deviations obtained on up- and down-milling faces .....	145
Figure C-5: Roughness parameters $Ra$ along the hole orientation for a sharp tool .....	146
Figure C-6: Roughness parameters $Ra$ for medium (left) and high (right) tool wear .....	147
Figure C-7: Profile samples for different tool wear at several hole angular positions (colored section in Figure C 5) .....	148

## **LIST OF SYMBOLS AND ABBREVIATIONS**

CFRP	Carbon fiber reinforced plastics
CVD	Chemical vapor deposition
FRP	Fiber reinforced plastics
PCBN	Polycrystalline cubic boron nitride
PCD	Polycrystalline diamond
PVD	Physical vapor deposition
RMS	Root mean square
UD	Unidirectional

## **LIST OF APPENDICES**

APPENDIX A – ARTICLE 4: BURR HEIGHT MONITORING WHILE DRILLING CFRP/TITANIUM/ALUMINIUM STACKS .....	106
APPENDIX B – ARTICLE 5: FRACTAL ANALYSIS OF CUTTING FORCE AND ACOUSTIC EMISSION SIGNALS DURING CFRP MACHINING .....	130
APPENDIX C – ARTICLE 6: SURFACE PROFILE TOPOGRAPHY OF TRIMMED AND DRILLED CARBON/EPOXY COMPOSITE .....	140

## **PREAMBLE**

The research presented herein started following my internship at Bombardier Aerospace in Montreal, within the framework of the CRIAQ project MANU-413. At this time, my research was focused on the optimization of the drilling process of multimaterials' stack composed of carbon epoxy composite and, titanium and aluminum alloys. To evaluate this process, different criteria were used, such as cutting forces average and amplitude, accelerometer signal root mean square, surface quality, burrs and hole sizing.

Firstly, while analyzing the cutting force signals to extract data such as mean and amplitude, I noticed that the averaging the signal caused a considerable amount of information lost, especially for the cutting forces acquired while drilling CFRP (carbon fiber reinforced plastic). For example, the shape patterns from the cutting force signal were evolving along the increase of the tool wear. This observation was particularly clear when the signal was observed for only few tool rotation periods. At high magnification range, it was noticed that the 'ruggedness' of the signals acquired from machining with different tool wear was changing as well. Literature review allowed to find an innovative technique to quantify the shape evolution and signal roughness: the fractal analysis. Thus, it was successfully used to estimate the burr heights from the cutting force signals acquired during the drilling of CFRP within the stack (Appendix A).

Secondly, while analyzing the hole quality of the CFRP layer, the surface texture profile was measured and roughness parameters calculated. The roughness parameters deviation found at this time was too high to be relevant at this point. I decided then to investigate further and propose new methods to evaluate the surface condition of laminated composites through their roughness profile.

## **CHAPTER 1 INTRODUCTION**

Aircrafts' structure design is mainly driven by weight reduction and safety. The latter is a particularly obvious airworthiness requirement. The former, weight reduction, is motivated by regulation compliance (in terms of e.g. noise reduction and gas emission) and by the competitive aerospace market (for instance aircraft range, gas consumption and noise level).

To reduce the weight of an aircraft, while maintaining or even improving mechanical properties of the parts, the aerospace industry uses new materials for their airplanes structure. In addition to metallic materials, such as aluminum or titanium alloys, traditionally being used in the last four decades, aircraft designers are increasingly selecting new types of materials, such as lithium aluminum alloy and composite materials. In composite materials, the most used are ply-laminated composites of carbon fiber and epoxy resin matrix. After manufacturing those composite parts, machining operations are required, either, drilling and riveting for assembly purposes, or trimming to finish the workpiece edges. Those machining operations need to be closely evaluated to maintain sufficient quality and to remain within the requirements.

The evaluation of machining processes can be assessed, among others, through the cutting force signals and/or vibrations generated during the operation. It can also be performed by investigating the integrity of the machined surface. Because of the heterogeneous nature of the carbon fiber reinforced plastics (CFRP), the quality of surface condition is poorly characterized using traditional roughness parameters.

Carbon Fiber Reinforced Plastics (CFRP) have a heterogeneous structure made of carbon fibres and epoxy matrix resin. Due to CFRP physical characteristics, the cutting mechanisms are more complex compared to metallic materials and their consequences are not sufficiently known. Machining quality, which is required to assess the process reliability in the industry, is therefore more difficult to evaluate. That is why current methods of monitoring and surface condition estimation need to be re-evaluated to this heterogeneous material.

### **1.1 Problem description**

The unidirectional fiber composite cutting process has been investigated in numerous studies over the last thirty years focusing on different aspects, such as the chip formation, the machining quality,

the surface condition and the cutting force prediction. When the surface roughness was evaluated, the traditional roughness parameter  $Ra$  was very often the only parameter used. Variations of the  $Ra$  parameter were studied multiple times, either in accordance with the feed or the cutting speed or even to different tooling types. However, reducing a surface characterization to a single value may be a subject to criticism. Such reduction is adequate in certain cases allowing to properly evaluate a surface roughness thanks to a single value. Indeed, surface profile parameters have been heavily used for homogeneous materials, such as metals. However, researchers note that the use of the  $Ra$  parameter is inadequate to composite materials due to their heterogeneity (Landon, Y. & Cherif, M., 2013). Depending on the orientation of the ply or direction of the roughness profile, this profile has various shapes (Chatelain, Zaghbani, & Monier, 2012).

In addition to surface characterization problems, determining appropriate cutting parameters can be challenging depending on the machining process and the requirements. Monitoring composite machining operations can turn machinists puzzled. The tool wear evolution follows the same trends as the one for metals. However, a worn tool, which could be acceptable for metals' machining, can generate e.g. delamination and resin damage. Different wear indicators could be proposed based, for instance, on vibrations and cutting force signals.

The tool wear indicators would greatly help in the FRP machining monitoring to avoid scrapped parts. Nowadays, ensuring a sufficient machining quality is difficult on a production line. For instance, a matrix thermal damage is practically impossible to detect without using a scanning electron microscope. Nevertheless, an appropriate model could predict the tool wear and the surface quality based on the analysis of the cutting forces signals and vibrations generated during the composite machining.

## 1.2 Objectives

The main objective of this thesis is to characterize and estimate the surface condition of trimmed CFRP samples.

The secondary objectives are defined as follows:

1. Understand characterization problems using traditional techniques of profile measurements for laminate composite surfaces.

2. Propose a new filtering process to obtain roughness profiles from surface measurements on laminate composite.
3. Propose new parameter(s) allowing a proper characterization of machined composite materials' surfaces.
4. Develop tool wear and surface condition estimating method based on the analysis of cutting force signals during the CFRP machining.



## **CHAPTER 2      LITERATURE REVIEW**

In this chapter, a state of the art is shortly presented, focusing on the trimming of carbon fibre reinforced plastics (CFRPs). However, the following literature review is only a familiarization and vulgarization of terms and concepts that are to be heavily discussed in the next chapters in order to avoid repetitive content. In each chapter or appendix containing an article, a separate state of the art oriented to the topic is presented.

Complementary subjects are highlighted in this literature review such as cutting force while CFRP machining, tool wear mechanisms, tool wear, surface integrity and roughness. Fractal analysis is mentioned in the machining framework as well. This technique, which has strong capabilities, is now unfortunately underused in manufacturing.

### **2.1 Fibre reinforced plastics (FRP)**

#### **2.1.1 Generalities**

Composite properties are characterized by both of the materials used: matrix and reinforcement. In addition to the constitutive materials, the interface plays a major role in the composite constitution. The reinforcement-matrix interface allows to maintain the composite structure and it permits the mechanical load transfer between both constituents.

In this study, unidirectional fibre composites with a plastic matrix are considered. Their fibrous structure is important. It allows the designer to increase composite mechanical properties in selected directions. The lay-up composite type is called laminate. Such laminate is manufactured by stacking unidirectional pre-impregnated fibre plies in different orientations (Figure 2-1).

#### **2.1.2 Carbon fibre reinforced plastics (CFRP)**

The FRP chosen in this study is the Carbon FRP (CFRP). The laminated CFRP used was prepared using pre-impregnated plies. The CFRP was manufactured using manual lay-up and then cured in autoclave.

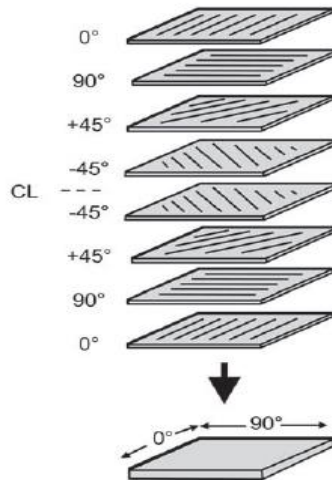


Figure 2-1: Lay-up laminate (Campbell, 2010)

### 2.1.2.1 Fibre

Fibres are used as reinforcement in the composite – they support the mechanical loads. The carbon fibre is known to have a high tensile and compressive strength and low density (Table 2.1). Carbon fibres are placed by threads of several thousand fibres, in a ply. Herein, fibres are all oriented in one direction per ply and impregnated with resin.

Table 2.1: Carbon fibre general characteristics (Berthelot, 2012)

	Carbone HR	Carbone HM	Carbone THM
<b>Volume mass <math>\rho</math> (g/cm<sup>3</sup>)</b>	1.75	1.81	1.95
<b>Diameter (<math>\mu\text{m}</math>)</b>		5 – 7	
<b>Young modulus <math>E_f</math> (MPa)</b>	230	400	600
<b>Specific modulus <math>E_f/\rho</math> (MNm/kg)</b>	130	210	310
<b>Fracture stress (MPa)</b>	3000 – 4000	2800	2000
<b>Specific fracture stress <math>\sigma_{fu}/\rho</math> (kNm/kg)</b>	1710 – 2290	1550	1000 – 1200

### 2.1.2.2 Resin

Two types of matrix can be used: thermoset and thermoplastic. For CFRP, the matrix is a thermoset resin which is the epoxy resin in this study. Contrary to thermoplastics, this resin can be irreversible when thermally damaged beyond relatively low temperature (Bonnet, 2010; Lasri, 2009). Epoxy resin is known to have good fatigue resistance (Table 2.2). It allows keeping the fibres attached to one part and transferring the mechanical loads to the fibres.

Table 2.2: Mechanical characteristics of epoxy resin (Berthelot, 2012)

<b>Density (g/cm<sup>3</sup>)</b>	1.1 – 1.5
<b>Tensile elastic modulus (GPa)</b>	3 – 5
<b>Tensile yield stress (MPa)</b>	60 – 80
<b>Bending yield stress (MPa)</b>	100 – 150
<b>Elongation upon break (%)</b>	2 – 5
<b>Shear strength (MPa)</b>	30 – 50
<b>Heat deflection temperature (°C)</b>	290

### 2.1.3 Mechanical properties

Main CFRP characteristics are high specific stiffness and strength, high fatigue and corrosion resistance, and light weight. Due to their laminated structure, CFRPs are anisotropic and their mechanical properties vary depending on the direction. For one unidirectional fibre ply, the elastic modulus is different depending on the angle between the fibre and the applied force (Figure 2-2).

The 0° fibre ply orientation admits the highest longitudinal tension load. In this case, the axial mechanical loads are supported by the fibres and the matrix prevents fibre buckling in compression and allows load distribution among fibres in tension.

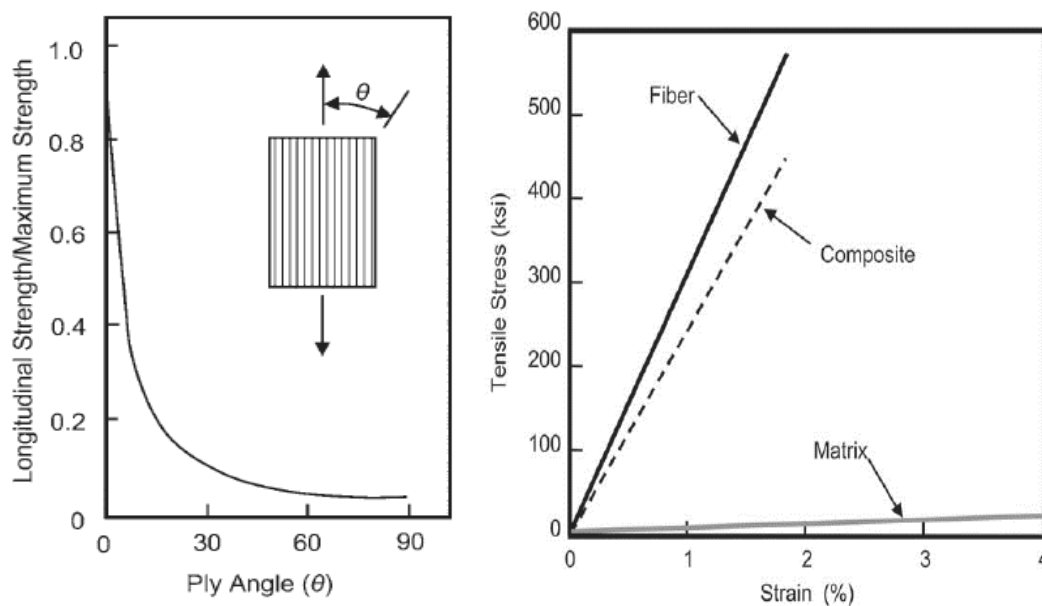


Figure 2-2: Longitudinal strength/ultimate strength ratio as function of ply angle (left); Tensile properties of fibers, matrix and composite material (right) (Campbell, 2010)

By stacking up plies in different fibre orientations, a laminate lay-up is obtained (Figure 2-1). The lay-up sequence is defined by the desired part thickness and mechanical properties.

## 2.2 Machining of FRPs

This study scope focuses on conventional machining by material removal. Non-conventional methods (laser, electric discharge, ultrasonic and waterjet machining) are left off in this study due to their shortcomings, such as production rate, affected zone and high price (Wang, D. H., 1993). Before presenting machining process of laminated composite materials, orthogonal cutting is shortly introduced.

### 2.2.1 Orthogonal cutting

#### 2.2.1.1 Metal / homogeneous material

To understand issues of CFRP machining, machining of homogeneous material is presented. The base of material removal machining process can be reduced to orthogonal and oblique cutting (Figure 2-3). In orthogonal cutting, the cutting edge is perpendicular to the feed/tool direction. In the oblique cutting situation, the cutting edge is angled to the plan normal to feed direction in the machined surface plan.

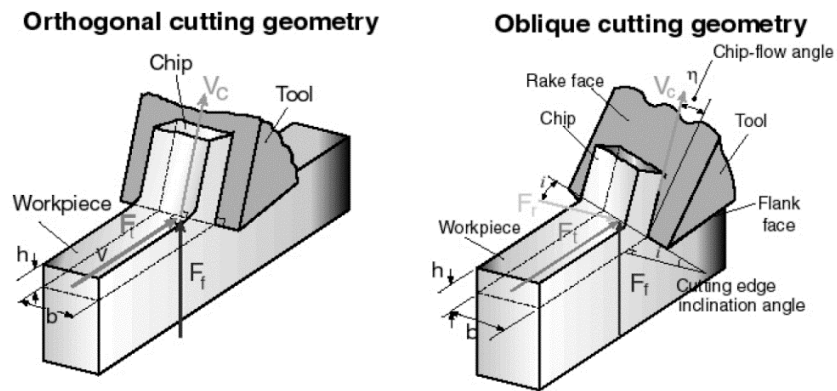


Figure 2-3: Orthogonal and oblique cutting process geometries (Altintas, 2012)

The material removal is caused by the shearing of the material. Regarding machining unidirectional fibre laminated composite, the material removal can be caused by various elementary mechanisms. Figure 2-4 depicts fracture mechanics with different crack propagation modes.

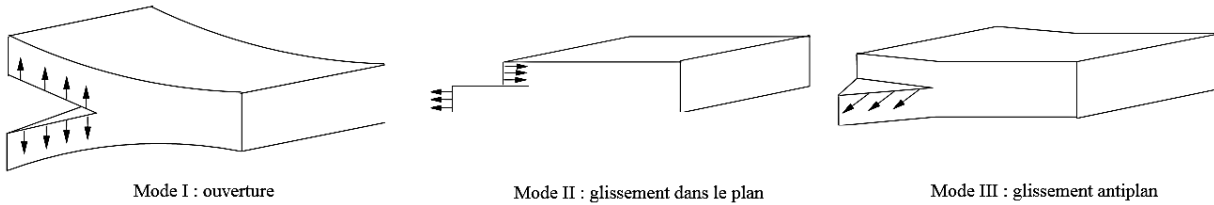


Figure 2-4: Crack propagation modes (Hudson & Harrison, 1997)

Different cases of chip formation are overviewed in the next section depending on the tool direction vs the fibre.

### 2.2.1.2 FRP material

FRP material machining is in some ways similar to wood cutting in particular with the position of the tool vs the wooden fibre. In the fifties, Kivimaa and McKenzie proposed notations to position the tool edge in the reference frame of the wooden fibres (McKenzie, 1960) (Kivimaa, 1950). Those notations can be used as well in the FRP machining (Figure 2-5).

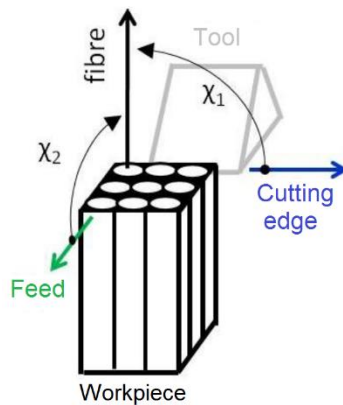


Figure 2-5: McKenzie angles definition (Bonnet, 2010)

First cutting mechanisms of unidirectional fibred composites were explored by Koplev *et al.* (Koplev, Lystrup, & Vorm, 1983), where material removal was studied for machining fibres at  $0^\circ$  and  $90^\circ$  (Figure 2-6).

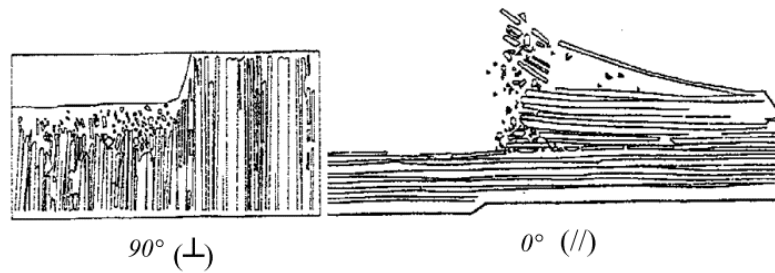


Figure 2-6: Cutting mechanisms for CFRP composites machining in parallel and perpendicular directions (Koplev et al., 1983)

### 2.2.2 Chip formation

The work started by Koplev et al. was followed by the one from Wang et al. which showed different chip formation ranked in five types, during CFRP machining, depending on the fiber orientation and the cutting edge rake angle (Figure 2-7) (Wang, D. H., Ramulu, & Arola, 1995a).

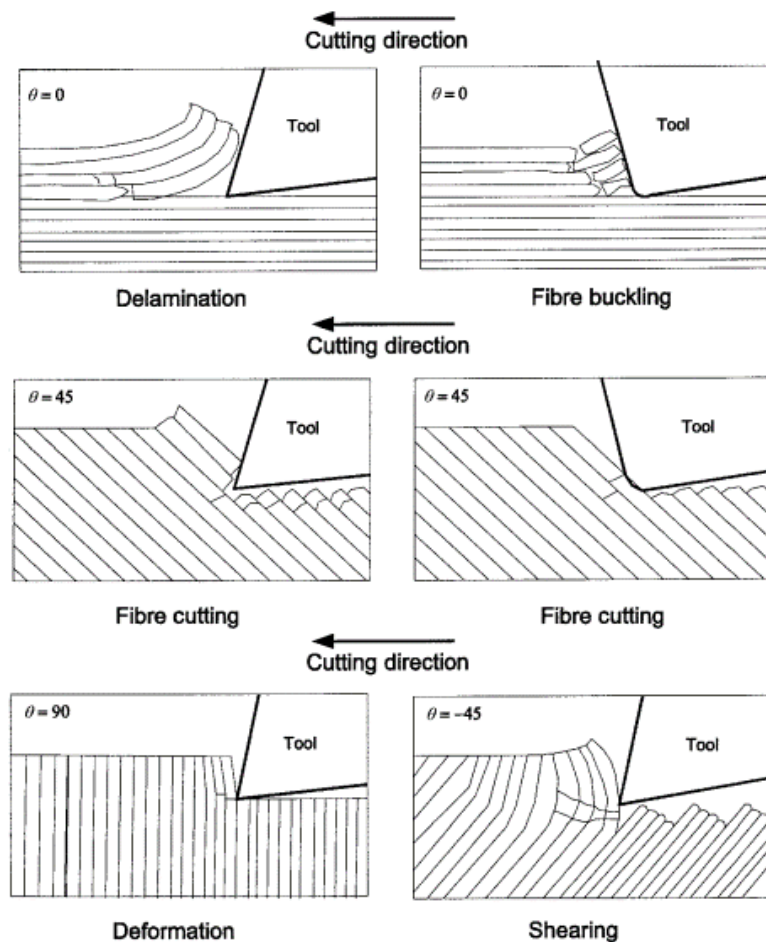


Figure 2-7: UD cutting mechanisms (Arola, Ramulu, & Wang, 1996)

Later, Arola et al. found the chip formation type was mainly due to relative position of the fibre orientation to the cutting edge feed direction (Arola et al., 1996).

In conventional cutting, two types of milling are possible: up- (opposite feed and tool rotational direction) and down- milling (same feed and tool rotational direction) (Figure 2-8). In the case of CFRPs, Bérubé et al. found up-milling generates a smoother surface and lower cutting forces during trimming (Bérubé, 2012).

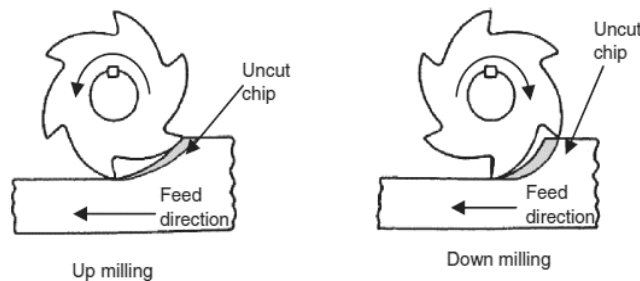


Figure 2-8: Up- and down- milling (Sheikh-Ahmad, J. Y., 2009)

### 2.2.3 Tooling

The chip formation is different between FRPs and metallic material machining. During the CFRP machining we can observe very severe level of abrasive wear of the cutting edge in particular due to the carbon fibres hardness. In consequence, the tool edge needs a relatively high hardness and toughness to resist to the fibre abrasiveness and to the mechanical loads during the cutting.

The chip formation during FRP machining tends to be more compression shearing or fibre fracturing whereas the chip formation during metal cutting leads to plastic deformation. In consequence, the tool edge should be relatively sharp and with a positive rake angle. Due to the carbon characteristics, the cutting tool needs to be hard and tough enough to bear the carbon abrasiveness and the machining loads as well (Sheikh-Ahmad, J. Y., 2009). Different tool material can be selected for this type of machining, e.g.:

- 1- Cemented tungsten carbides; composed of hard carbide particles cemented between each other using a metallic binder.
- 2- Coated carbides; tool material of cemented carbide coated with hard ceramics, the coating can be applied using the chemical vapor deposition (CVD) or physical vapor deposition (PVD).

- 3- Ceramics; composed of sintered alumina at high pressure and temperature. Ceramic tools have a relatively low toughness and tend to chip under heavy and scattering loads. Producing ceramic tools with sharp edges is also a source of concern.
- 4- Polycrystalline diamond (PCD); characterized by good thermal conductivity, low friction and high tool life. Composed of polycrystalline diamond compacted using cobalt binder at high temperature and pressure.
- 5- Polycrystalline cubic boron nitride (PCBN).
- 6- Diamond coated carbides; obtained by applying a low-pressured synthesized diamond on a carbide substrate using chemical vapor deposition. The diamond coating greatly improves the tool life length in CFRP machining although after the diamond deposition is altered the tool wear drastically increases.

## **2.3 Machining quality**

During machining, the cutting mechanisms of composite materials, in particular FRPs, are more complex compared to metallic materials. Phenomena, such as fibre pulling or matrix thermal damage, are part of machining problems and need to be assessed and controlled.

The tool wear is an important aspect in controlling a machining process. However, the tool wear is often used to assess the most important criteria in manufacturing: quality. The machining quality is identified by observing the surface integrity and the surface condition. In the CFRP case, the former can be affected with issues such as delamination and thermal damage. The latter may be evaluated through dimensional defects, surface roughness, waviness etc.

### **2.3.1 Surface integrity**

#### **2.3.1.1 Delamination**

#### **2.3.1.2 Delamination**

A delamination is a failure mode causing the fiber debonding from the matrix. Delamination within a FRP composite can be either intra- (delamination of the fiber within a ply) or inter-delamination (fiber delamination between plies) (Gouleau, Garnier, & Furet, 2007; Persson, Eriksson, & Zackrisson, 1997).



Delamination can be ranked based on its characteristics (Colligan, 1991) (Figure 2-9):

- Type I: The surface areas where ply fibers are missing;
- Type II: The uncut fibers overhung from the trimmed edge;
- Type I/II: A combination of both Type I, and Type II delamination;
- Type III: The loose fibers partially attached to the trimmed surface edge.

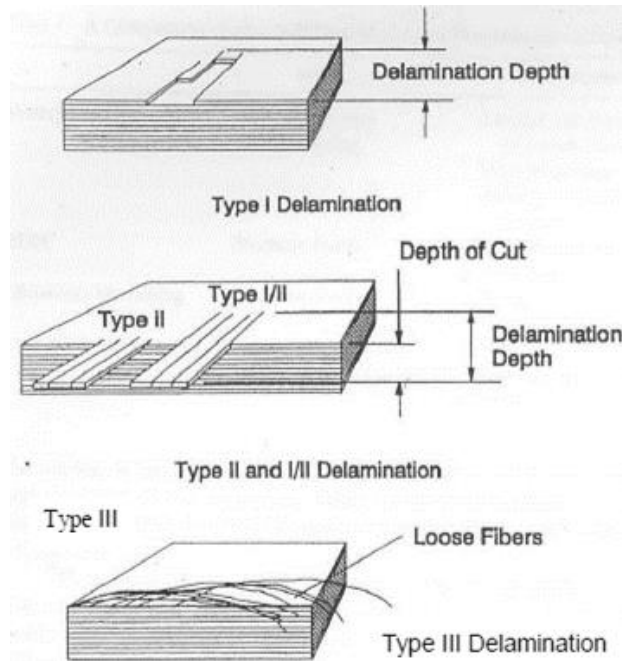


Figure 2-9: Delamination types (Colligan, 1991)

To evaluate the delamination level, Davim *et al.* proposed a delamination factor  $F_d$ , shown in Figure 2-10.

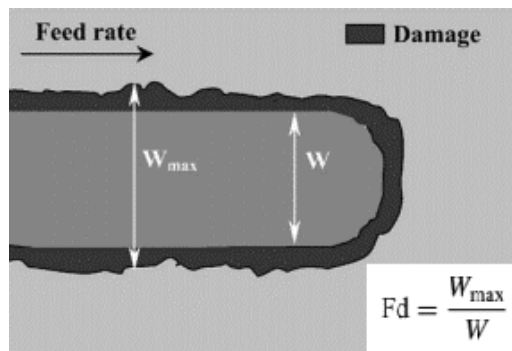


Figure 2-10: Delamination factor (Davim, J. P. & Reis, 2005)

In drilling, delamination phenomena are more eager to appear at the inlet (e.g. fiber pull-up) and at the hole outlet (Persson et al., 1997). Delamination can be also observed to a lower extent in the composite core next to the hole (Gouleau et al., 2007).

Different techniques of non-destructive control (such as ultrasounds, infrared thermography, tomography) are used to evaluate the manufacturing and machining quality in regards with the delamination (ECSS, 2011). In addition to those techniques, a visual check can be conducted as well. Surface resin microbreakages might be pinpointed. Depending on the size and orientation of those resin microbreakages, the ultrasound inspection may be preferred.

Regarding delamination symptoms, Sheikh-Ahmad et al. found that delamination often occurs closed to the surface with I and I/II delamination types (Sheikh-Ahmad, J., Urban, & Cheraghi, 2012). To limit those defects, it was proposed to decrease the cutting feed and increase the speed as well.

Hintze *et al.* observed CFRP delamination during milling using PCDs tools and noticed a high relationship between delamination and, the tool sharpness and the fibre orientation (Hintze, Hartmann, & Schütte, 2011).

### **2.3.1.3 Heat damage**

The other main damage is the thermal degradation of the matrix. The matrix thermal damage is characterized by the matrix vaporisation or melting next to the cutting zone. This degradation is caused by the friction between the tool cutting edges and the composite surfaces. The damage depth depends on the heat generated (Guegan, Lemaitre, & Hamann, 1992).

Two solutions can be applied to reduce the heat generated by the cutting (Bonnet, 2010):

- Selecting a better set of cutting parameters such as a cutting speed decrease and a feed increase.
- Redesigning the tool geometry by reducing the impact of the flute fillets (or increasing the clearance angle) on the composite surface.

### **2.3.2 Surface topography**

The surface topography includes all the surface shape at different scales but focuses only on the surface texture. This surface topography can have large defects vs the predicted surface. It also

represents the surface waviness and roughness. The roughness and waviness of a surface characterize the primary surface.

The surface condition depends on the cutting condition such as tool geometry, cutting dynamics, workpiece material characteristics, fibre orientation and cutting parameters. During their life cycle, the reliability of machined parts partly relies on the surface condition and therefore needs to be looked at. The surface finish is also important for assembly purposes e.g. riveting.

### **2.3.2.1 Dimensional defects**

Dimensional defects, such as the non-circularity of a hole, are mainly due to the composite anisotropy (Guegan et al., 1992; Piquet, Ferret, Lachaud, & Swider, 2000).

### **2.3.2.2 Waviness, roughness surfaces**

To evaluate a surface condition, a visual check can be performed. However, measurements are often preferred to improve reproducibility rates. Measurements can be performed by acquiring topography point mesh height over a surface or on a profile line. Even if the surface measurements have usually narrower result deviation, they are more time consuming to conduct than surface profile measurements. In the industry, the surface profile characterization is preferred. The characterization is a parametrization of the profiles reducing a scattered profile into a single value (e.g.  $Ra$  – average deviation of the profile).

Regarding the process leading to waviness and roughness profiles, the raw profile obtained from the measurement leads to the primary profile by slope correction. This primary profile is composed of the waviness profile and the roughness profile which can be extracted by filtration.

On the machined coupons, there are also two preferable directions of observation (Sheikh-Ahmad, J. et al., 2012):

- 1- Longitudinal direction (in the ply plane); very often the object of inspection since it is also the feed direction in trimming.
- 2- Transversal direction (in the stacking sequence direction); more concerned for hole inspection.

The following chapters deeply investigate problems encountered by the scientific community and propose characterization tools based on current standards.

## 2.4 Surface roughness

In the scientific community and to a higher extent in the industry, the surface condition is mainly characterized using roughness profile parameters (Jawahir et al., 2011). Those roughness parameters were built for homogeneous materials such as metals. However, a study shows the  $Ra$  roughness parameter is highly influenced by fibre orientations while other parameters such  $Rt$  and  $Rz$  allow to assess machining damages (Wern, Ramulu, & Colligan, 1993).

An experimental research involving orthogonal cutting of UD (unidirectional) composites shows roughness profiles with different fibre orientations (Wang, X. M. & Zhang, 2003). Figure 2-11 depicts variations of roughness profiles for different fibre orientations with different cutting angles and depth of cut. For a specific machining setup (tooling, machining angles and cutting parameters), the average value of roughness parameters can jump from one to seven times depending on the fibre orientation. The highest values were obtained for the  $120^\circ$ -fibre-orientation. This statement is confirmed in experimental trimming tests (Chatelain et al., 2012) (Figure 2-12, Figure 2-12 and Figure 2-13) and in experimental drilling tests as well (Landon, Y. & Cherif, M., 2013).

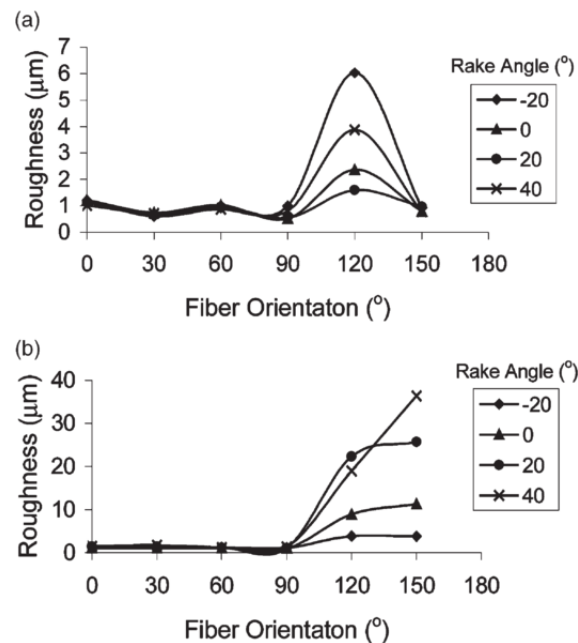


Figure 2-11: Fibre orientation effect on the profile surface roughness with different depth of cut

(a) 0.001mm; (b) 0.050mm (Wang, X. M. & Zhang, 2003).

Figure 2-12 depicts different roughness profiles for the main orientations of  $0^\circ$ ,  $+45^\circ$ ,  $90^\circ$  and  $-45^\circ$  and for three sets of cutting parameters. Those roughness profiles were measured in the ply plane, so the longitudinal direction, allowing to observe one fibre orientation only. For each fibre orientation, a specific pattern can be observed whatever the cutting parameters are.

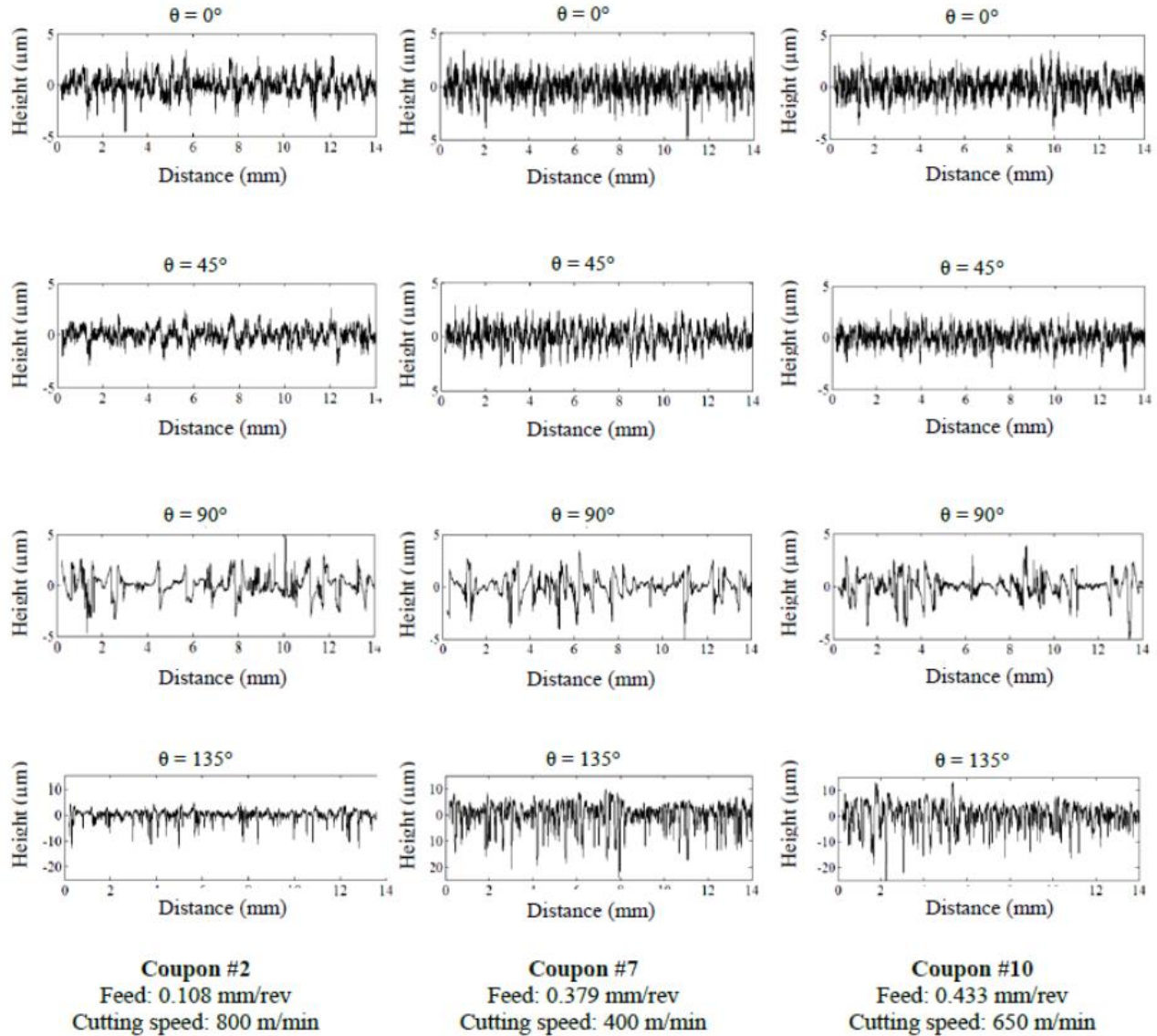


Figure 2-12: Comparison of roughness profiles for four orientations using three set of cutting parameters (Chatelain et al., 2012)

In Figure 2-13, different types of roughness profiles are displayed for each of the four main fibre orientations ( $0^\circ$ ,  $+45^\circ$ ,  $90^\circ$  and  $-45^\circ$ ). Each profile tends to have specific features depending on the fibre orientation.

Based on those observations, the current characterization of laminated composites in the ply plane direction should be reconsidered. Due to the high surface variations and patterns depending on the fibre orientation, the characterization in the transverse direction (in the stacking sequence direction) should be reassessed as well.

Nevertheless, the scientific community mainly uses current surface characterization tools (which were built for homogeneous materials) instead of challenging them in the perspective of heterogeneous and/or laminated materials. In such case, the *modus operandi* is also at stake. Performing a measurement on different plies successively could alter results in comparison with a single fibre orientation inspection.

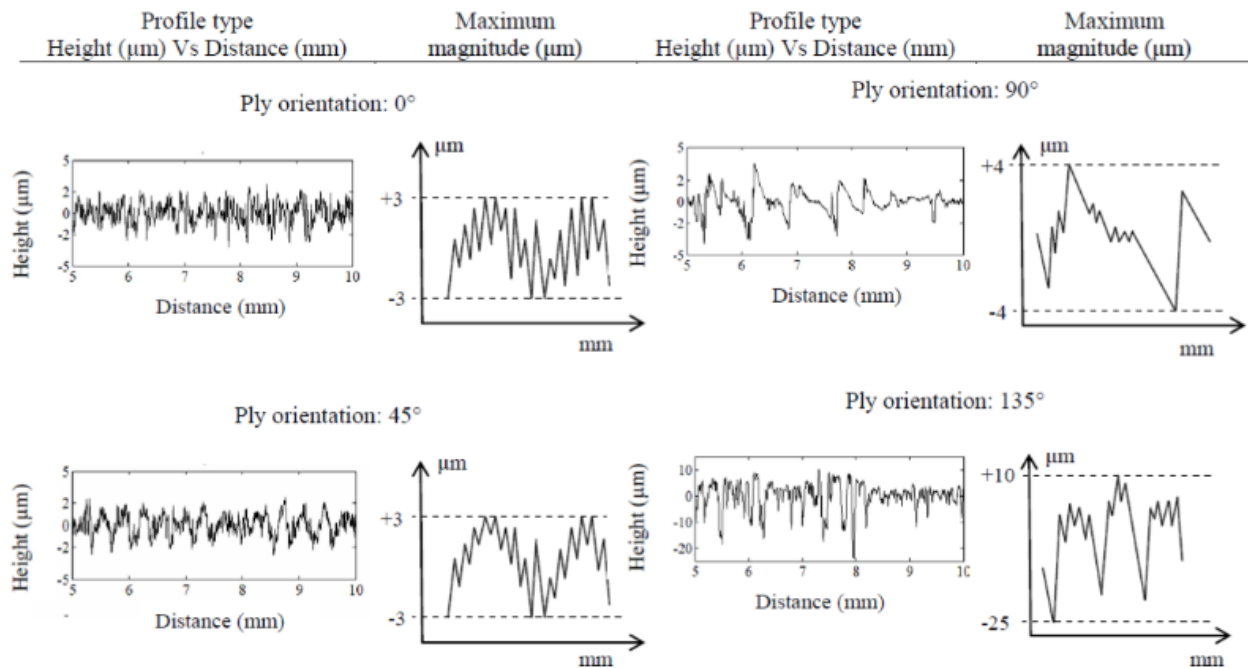


Figure 2-13: Different types of roughness profiles (Chatelain et al., 2012)

Besides research studies which evaluates impacts of tool wear, tool coating or cutting parameters, a article relates the machining quality monitoring using acoustic emissions and cutting force signals during the CFRP drilling (Arul, Vijayaraghavan, & Malhotra, 2007). However, the inspection of the hole surfaces is limited to hole diameter and uncut fibres at the hole outlet.

A thesis, focused on the CFRP/Aluminium stack drilling, evaluated the machining quality using neural network (Roudgé, 2011). In this study, several factors were taken into account, such as cutting forces, tool wear, hole dimensioning (diameter, circularity and cylindricity).

## 2.5 Fractal objects

Fractal generation and analysis are already used in multiple domains such as economy, weather forecast, medicine, engineering and graphics simulation. Fractal concepts and analysis are discussed at large in this chapter. The motivation of the fractal analysis used in therein and further details are to be heavily reviewed in the following chapters.

### 2.5.1 Concept and generalities

Fractal analysis was brought to light by Mandelbrot (Mandelbrot, B., 1975). The fractal principle stands in the fact that the area of a table is not necessarily a defined figure but can change depending on the scale of observation. The area of a table can be relatively easily calculated at a human scale (e.g.  $1\text{m} \times 1.5\text{m} = 1.5\text{m}^2$ ). However, if you zoom in a section of a table, the surface area increases as well. It even tends to an unlimited area with the continuous magnification increase. Fractal theory brings an answer to this problem by observing the scale dependency on the area (Mandelbrot, B. B., 1982).

A fractal can be described as a geometrical set with an auto-similarity characteristic, which can be observed as a ‘small’ part of the set representing the set itself (Robert, 2001; Russ, 1994). For instance, the Koch flake is one the most famous fractal object (Figure 2-14) (Davim, J., Barman, & Sahoo, 2011).

The different iterative steps to build the Koch curve are as follow:

- Step 0: a  $L$ -length line is chosen;
- Step 1: the central part of the third of the line is removed and replaced by the two other lines of the equilateral triangle (using this removed segment as base for the triangle);
- Step 2: the same operation is repeated on each of the four  $L/3$ -length segments at a lower scale;
- Step3 and so on: same iterative operation at each step.

The length of such object is indeed infinite and yet can be easily described by a single parameter: the fractal dimension. In this case, the Koch curve has a fractal dimension  $D$  that can be expressed by:

$$D = \lim_{n \rightarrow \infty} \frac{\ln(n)}{\ln(h)} \quad (2.1)$$

Where  $h$  is the homothetic scale factor ( $1/3$  in this case) and  $n$  is the number of sticks at the first step (4 in this case) (Sapoval, 1997). Herein, this fractal dimension  $D$  (also called homothetic fractal dimension) has a value close to 1.26.

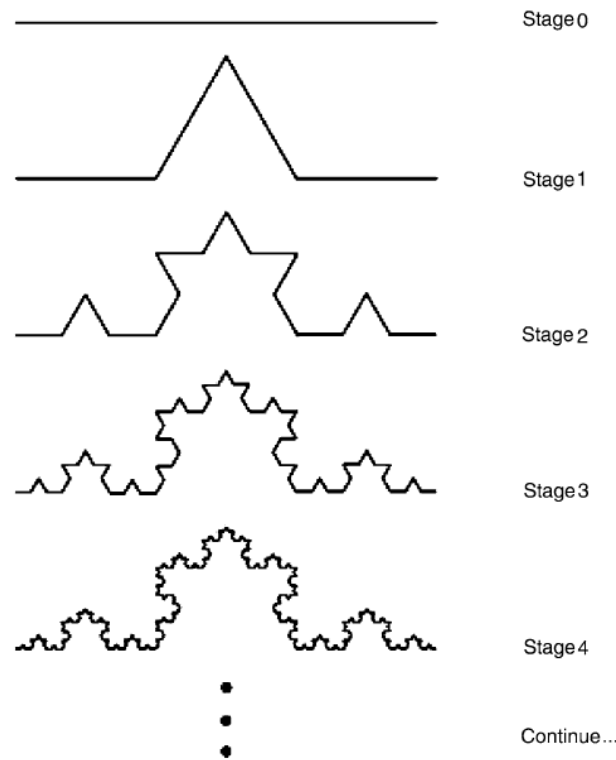


Figure 2-14: Koch curve iterations (Davim, J. et al., 2011)

The fractal dimension can admit non-integer values. For instance, an object contained in a two-dimension coordinate space can have a fractal dimension from 1 up to 2. The fractal dimension is considered as an index characterizing the level of complexity of a set.

Fractal objects can be drawn using this fractal dimension calculated e.g. from the equations of Weierstrass-Mandelbrot. Numerous fractal analysis techniques exist (three of them are presented and evaluated in Chapter 4) and the most known method is presented in the next section.

## 2.5.2 Fractal analysis techniques

Last section showed how to build fractal objects using a fractal dimension (Sapoval, 1997). However, fractal analysis evaluates the fractal dimension of a given object. The first and one of the



most known example of fractal analysis (stick-counting) is the measurement of the British coastline length (Figure 2-15).

The British coastline is approximated using sticks with different lengths. For each stick size, sticks can be easily counted. The fractal dimension is then assessed as the slope of the log-log graph with the stick size for the X-axis and the stick count in the Y-axis.



Figure 2-15: Fractal analysis evaluating the British coastline length using different stick lengths  
(Andrus, 2005)

In Chapter 4, three fractal analyses are presented and evaluated from experimental cutting force signals. In Appendix A and Appendix B, the regularization analysis (another type of fractal analysis) is used to monitor the tool wear.

### CHAPTER 3      GENERAL PRESENTATION

Previously, the introduction and the literature review were presenting the subject framework and previous research up to date. This chapter shows the general structure of the thesis with the introduction of the articles and objectives. The next three chapters, which compose the dissertation core, are three journal articles. Another three journal papers in appendix round off the study. The organization of the papers incorporated in this thesis is shown in Figure 3-1.

The fourth chapter is the paper “Tool wear and surface quality assessment of CFRP trimming using fractal analyses of the cutting force signals” which was accepted by peer reviewers for publication in *CIRP Journal of Manufacturing Science and Technology*. The research work presented therein is focused on the analysis and discussion of the cutting forces during the CFRP trimming. Aside traditional techniques, three types of fractal analysis were described and applied on the cutting forces signals. The use of fractal analysis was motivated by the different ‘noise’ levels identified along the tool life in the cutting force signals, which noise is difficult to evaluate using traditional methods. The results shown promising future developments in tool condition and machining quality online monitoring during CFRP trimming.

The fifth chapter is constituted of the article “A new approach for the surface roughness profile characterization of laminated composites in the ply plane direction” which was submitted to peer reviewers for publication in *Canadian Aeronautics and Space Journal*. In this research article, new roughness parameters are proposed based on the fractal analysis method. The surface of CFRP composite, which is composed of laminated unidirectional plies, admits relatively high variations and patterns depending on the direction of profile observation. Surface profile observations show possible correlation between the machining quality and the roughness profile ‘noise’ in the ply plane direction, regardless to the ply orientation. Experimental results of the newly introduced fractal analysis based roughness parameters are found better estimate than current roughness parameters.

The sixth chapter exhibits the journal article “Surface profile texture characterization of trimmed laminated composite in the stacking sequence direction” which was accepted by peer reviewers for publication in the journal *Measurement*. In the perpendicular direction to the CFRP ply plane, so in the transverse direction, different problems occur. For instance, during hole inspections, depending on the angular position of the measurement, roughness parameter results can widely

vary and are improper to evaluate the machining quality. In this research article, a new filtering method is proposed to reduce the problem. To evaluate this new technique, numerous measurements were performed on CFRP trimmed coupons in the transverse direction and roughness parameters from the current and the new proposed filtering methods are presented. The introduced filtering method allows reducing by up to half the roughness parameter dispersion.

The Appendix A presents the journal paper “Burr height monitoring while drilling CFRP/Titanium/Aluminium stacks” which was accepted by peer reviewers for publication in *Mechanics and Industry*. The research work presented therein was the first application of fractal analysis on CFRP drilling cutting force signals in order to evaluate the tool wear and the burr generated at the outlet of titanium and aluminium layers in a multimaterial stack. At this point the results were promising.

Another article “Fractal analysis of cutting force and acoustic emission signals during CFRP machining” is shown in the Appendix B. This article was presented during the conference *High Performance Machining* (Chemnitz, Germany) in 2016 and published in the peer reviewed *Procedia CIRP* journal. The fractal analysis was applied on both cutting force signals and acoustic emission signals during the orbital drilling of the multimaterial stack of CFRP/titanium. The results show great potential and is currently under investigation for further development.

The Appendix C presents the paper “Surface profile topography of trimmed and drilled carbon/epoxy composite” which was presented during the Conference on Surface Integrity (Charlotte, North Carolina, U.S.A.) in 2016 and published in the peer reviewed *Procedia CIRP* journal. The research presented therein states the different problems of surface profile characterization. The surfaces at stake were from drilled holes and straight trimmed coupons.

The thesis ends with a general discussion of the articles, followed by the general conclusion and recommendations. This allows to sum up the original contributions of the research herein and propose orientations for future work.

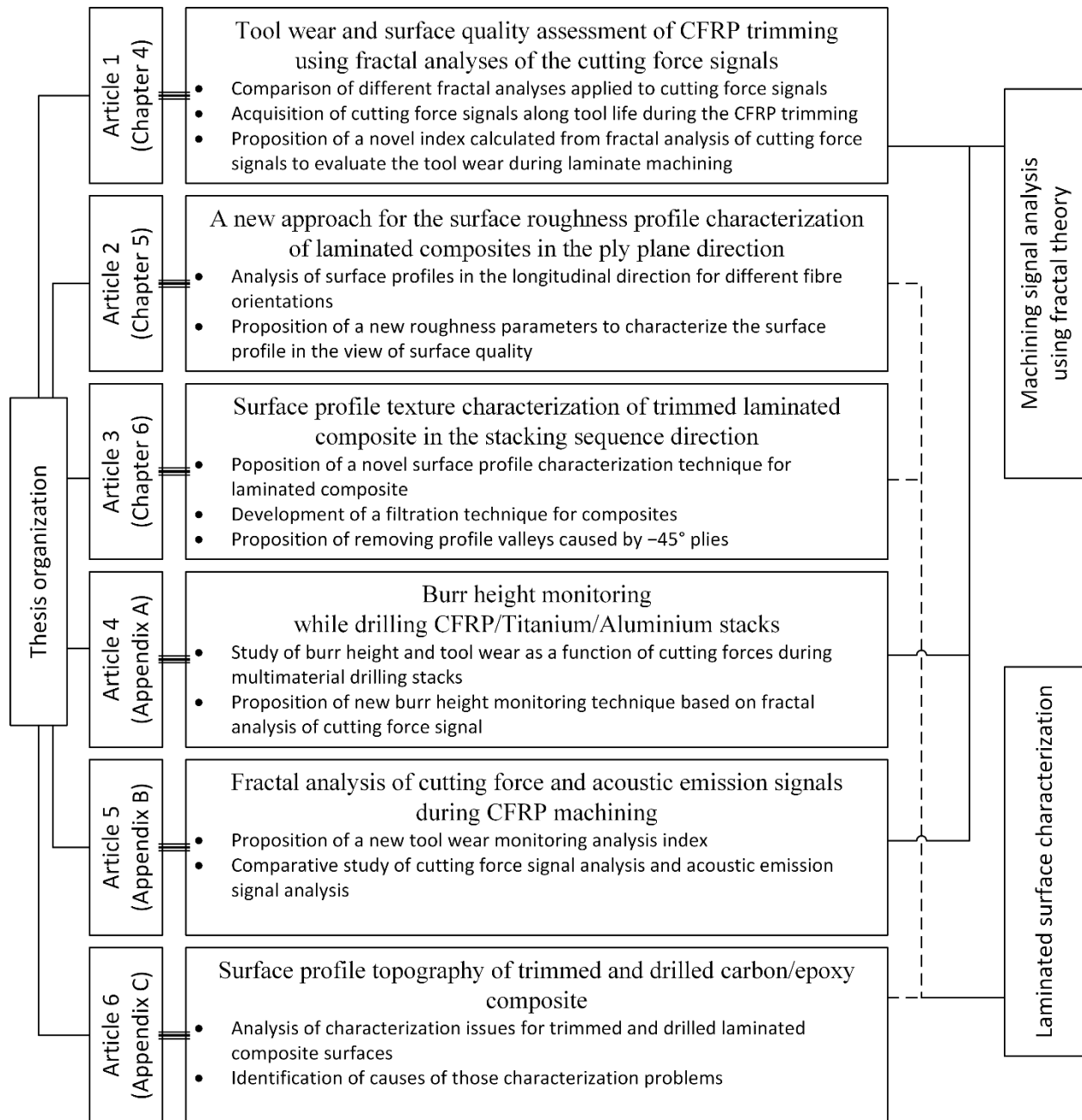


Figure 3-1: Thesis organization plan

# CHAPTER 4      ARTICLE 1: TOOL WEAR AND SURFACE QUALITY ASSESSMENT OF CFRP TRIMMING USING FRACTAL ANALYSES OF THE CUTTING FORCE SIGNALS

Xavier Rimpault<sup>a</sup>, Jean-François Chatelain<sup>b</sup>, Jolanta E. Klemberg-Sapieha<sup>c</sup>, Marek Balazinski<sup>a</sup>

<sup>a</sup>Department of Mechanical Engineering, Polytechnique Montréal, Canada

<sup>b</sup>Department of Mechanical Engineering, École de Technologie Supérieure, Canada

<sup>c</sup>Department of Engineering Physics, Polytechnique Montréal, Canada

\* Published in *CIRP Journal of Manufacturing Science and Technology*, vol.16, pp.72-80, 2017.

## 4.1 Abstract

The surface quality of machined carbon fibre reinforced plastics (CFRP) differs depending on cutting conditions e.g. cutting parameters and tool wear. Fractal analyses were performed on the cutting force signals, acquired during the trimming of CFRP, to describe the signal complexities variations. Fractal parameters, such as dimension and topothesy, were used to describe the signal irregularity and complexity. Statistical parameters, e.g. average and amplitude, and fractal parameters were compared related to the tool wear and to the surface quality. The fractal results from cutting force signals can estimate the tool wear and the surface quality.

*Keywords:* Fibre reinforced plastic, trimming, cutting force signal, fractal analysis, tool wear.

## 4.2 Introduction

### 4.2.1 CFRP

Thanks to their high strength-to-weight ratios, carbon fibre reinforced plastics (CFRP) have been more and more used in the aerospace industry. However, the heterogeneity and anisotropy of those materials implies rethinking or developing new machining and metrology techniques commonly used for metal alloy parts.

As a result of the use of moulds to manufacture composite, CFRP components obtained are close to their final shape and does not need several finishing operations. However, some processes remain inevitable e.g. drilling and trimming. Several problems may occur during fibre reinforced

plastic (FRP) machining, such as inter-ply and intra-ply delamination, uncut fibres, pulled fibres and burnt resin [1-3]. Jahanmir *et al.* found that the thermal damage of the resin is caused by the high heat generated during the machining bound with the low heat conductivity of the resin matrix [4].

Due to the abrasiveness and hardness of the carbon fibres, abrasion is considered as the foremost wear mechanism [5, 6]. The coating and tool geometry can be optimized to increase the tool life. In the industry, diamond coating is the most commonly used coating to machine CFRP. To obtain a higher surface quality, the radius angle of the tool cutting edge can be reduced. However, this geometry change weakens the cutting edge and may induce a faster wear. Following the tool condition, the heat generated in the cutting zone becomes higher with the dullness of the tool. Hamedanianpour *et al.* found that, even if the tool wear is still considered as functional, the resin may be burnt during the CFRP machining leading to imply a lower surface quality [7].

#### **4.2.2 Fractal analysis**

Fractals were introduced by the mathematician Benoit Mandelbrot to describe the length of Britain coastline [8]. Nowadays, fractals are seen as an object which owns a self-affine pattern or singularity [9]. In metrology, fractal analyses have already been investigated and used to define the roughness of surfaces. However, only few research articles show interest to apply this analysis technique to machining such as for signal analysis of machining acoustic emissions. Bukkapatnam *et al.* proposed analysis methods based on chaos theory and fractal analysis to extract information from signals such as acoustics emissions, cutting force signals and accelerometers during the machining of steel in lathe [10, 11].

The cutting force acquired during trimming can be estimated for homogeneous materials such as aluminium and titanium alloys [12]. For laminate composites, the cutting force prediction is more complicated due to its composition. For example, the CFRP used in this study is made of two different components – carbon, which is very hard to cut, and epoxy resin, which has a high machinability index. Karpas *et al.* and Kalla *et al.* proposed mechanistic force models for milling laminated composites [13-15]. However, those models do not integrate the tool wear impact and the noise of the cutting force signals.

Kabaldin *et al.* and Fu *et al.* used fractal analysis techniques to characterize the noise in the signals of, respectively, accelerometer and acoustic emission sensors while machining steel [16, 17]. The results showed trends towards the tool wear in both studies with an increase of the vibration noise.

Throughout the machining of the CFRP, the carbon fibres are fractured due to a charge of the tool on the fibre. The fracture of the carbon fibres during the CFRP machining generates an additional noise in the vibratory and cutting force signals in comparison with the machining of homogenous metallic material. This noise is usually not taken into account in the analysis of the cutting forces. However, this signal noise may give additional information about the machining such as the tool wear and the quality of the generated surface. For example, the cutting force signal noise diminishes with the increase of the tool wear.

### 4.3 Workpiece, machine, setup and tooling specifications

The machined composite was an autoclave-cured 24-ply CFRP laminate. This quasi-isotropic composite was produced using pre-impregnated plies oriented in the stacking sequence  $[90^\circ/-45^\circ/+45^\circ/0^\circ/+45^\circ/-45^\circ/+45^\circ/-45^\circ/0^\circ/-45^\circ/+45^\circ/90^\circ]_s$ . This resulted in a flat laminated composite part with a 4.44 mm thickness and a 64% fibre volume fraction.

The machining experiments were carried out using the K2X10 Huron<sup>®</sup> high-speed machining centre. This 3-axis computerised numerical control (CNC) machine allows a maximum spindle speed of 28 000 RPM at 30 kW. For health and safety purposes, a dust extraction system was mounted onto the machine.

The cutting tool used was an end mill router with six straight flutes. The geometrical characteristics of this cutter are listed in Table 4.1. This end-mill was a carbide tool coated using a diamond chemical vapour deposition.

Table 4.1: Tool geometrical characteristics

Rake angle	Clearance angle	Helix angle	Diameter
8°	10°	10°	3/8"

Two setups were used for our experiments. One allowed to machine 100 mm test coupons in order to proceed to a full inspection of the trimmed surface e.g. roughness evaluation, machined surface quality, thermal damage. This first setup is depicted in Figure 4-1. The other setup allowed to trim longer cuts – 900 mm in length – in order to generate tool wear. No coupon was kept after

machining with this second configuration. In this operation, all the laminate part machined was transformed into “chips and dust”. The fixture of both setups was screwed to a dynamometer table (Figure 4-1).

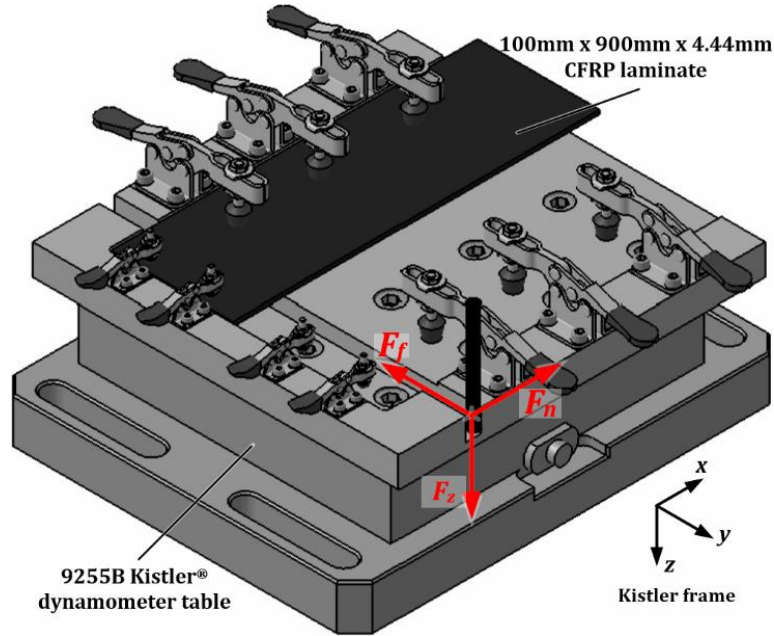


Figure 4-1: Experimental setup used for short cuts machining (100 mm)

## 4.4 Methodology

### 4.4.1 Design of experiments

The machining tests were performed with the parameters listed in Table 4.2. The cutting parameters were selected according to the best operational cutting conditions for a similar tool and CFRP material in the literature [18]. Three tools were used herein, sharing the same characteristics, and one set of cutting parameters was assigned to each one (Table 4.2).

Table 4.2: Chosen cutting parameters for the machining experiments using three tools with the same characteristics

Test/Tool	Feed (mm/min)	Speed (m/min)
1	1524	400
2	2794	300
3	4064	200










For each cutting parameter set, one tool had been used until the end test criterion was reached. This selected criterion was the end of the tool life defined by the wear limit. The average tool wear limit on the flank wear was set at a maximum average of 0.3 mm, as alleged in ISO 8688-2 standard [19].

Each tool was used to machine, at first, one short cut and, then, alternatively short cuts and long cuts until the tool life criterion was reached. Machining experiments were performed at the same tool height position and in full engagement for both setups.

#### 4.4.2 Measurements

The cutting tool was inspected before each short cut by recording pictures using the VHC-600+500F Keyence® optical microscope. The images were taken on the clearance face of each flute of the tool. Table 4.3 shows the clearance cutting edge of the tool 1 along the tool life. The maximum tool wear,  $VB_{max}$ , was estimated based on those pictures according to ISO 8688-2 standard recommendations [19]. The tool wear  $VB_{avg}$  is introduced as the average of the six tool wear  $VB_{max}$  values estimated for the six flutes of the tool.

Table 4.3: Picture samples of the clearance tool wear for the tool 1 along its tool life

Estimated tool wear $VB_{avg}$ (mm)						
0	0.057	0.072	0.078	0.100	0.116	0.254
Length of cut (m)						
0	4	8	12	19.6	18	20
						

0.75 mm

The cutting forces were measured using the 9255B Kistler® dynamometer table during each short cut. The forces  $F_x$ ,  $F_y$  and  $F_z$  were acquired respectively for the x-, y- and z-axis in the dynamometer table frame as depicted in Figure 4-1. The data acquisition system was set with a 24 kHz frequency rate allowing to acquire simultaneously all the signals without any post-synchronisation needed.

Systematic error and intercept of the force signals were corrected. The feed force  $F_f$  was determined as the force in the feed direction and orientation. The normal force  $F_n$  was the force obtained as follows:

$$F_n = -F_f \times F_z \quad (4.1)$$

The resultant force or total force was calculated as follows:

$$F_T = \sqrt{F_f^2 + F_n^2 + F_z^2} \quad (4.2)$$

The samples of the machined CFRP were examined using the Keyence® optical microscope and the Hitachi® S-3600N scanning electron microscope (SEM).

#### 4.4.3 Analyses performed

Analyses were carried out on the cutting force signals  $F_f$ ,  $F_n$ ,  $F_z$  and  $F_T$  during the stable section (signal section between the dot lines in Figure 4-2) identified during the machining (signal section between the dash lines in Figure 4-2).

Statistical parameters (average, peak-to-peak amplitude, standard deviation, kurtosis and skewness) of the resultant force signals  $F_T$  were calculated. These parameters were compared to the tool wear  $VB_{avg}$ .

This research focuses on the fractal analysis of the resultant force signals  $F_T$ . The results of fractal analyses were compared related to the evolution of the tool wear  $VB_{avg}$  and to the machined surface quality of the CFRP.

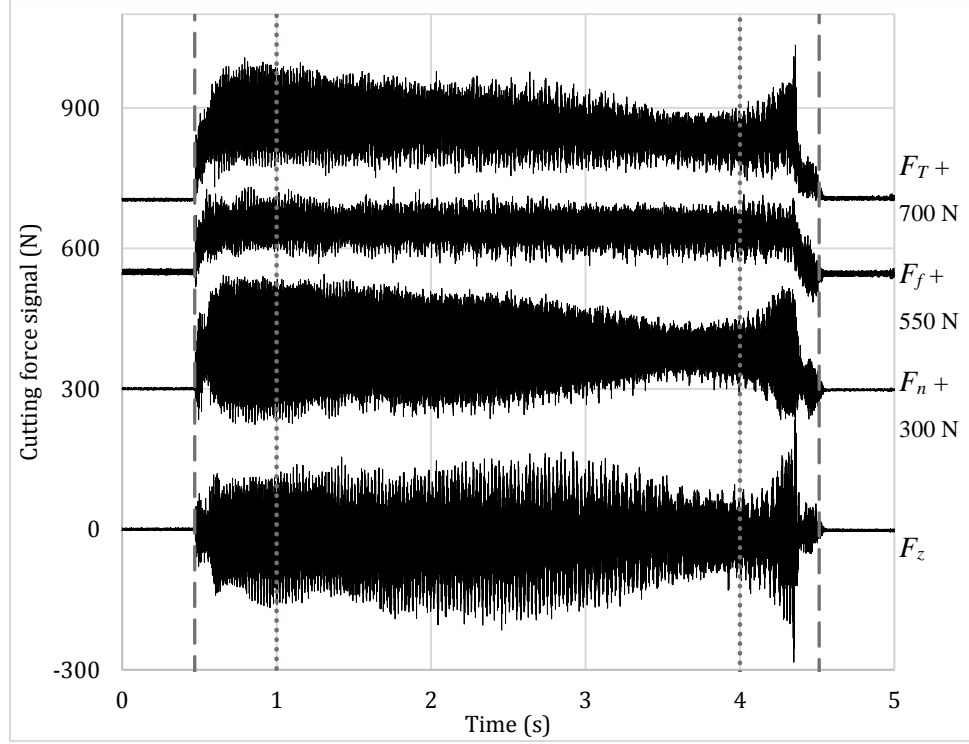


Figure 4-2: Cutting forces measured from the first cut of the 1<sup>st</sup> pass of the tool 1 (for graph clarity, the signals were shifted one from another)

## 4.5 Fractal dimension calculation methods

Fractal dimensions were initially used to depict some irregular geometries. Mathematicians found that “rough” surfaces have a self-affine behaviour, and use fractal dimension to estimate its roughness.

Evaluating the fractal dimension of an object or a curve is not an easy task to proceed. The function of Weierstrass-Mandelbrot (WM) allows drawing a self-affine curve [20]:

$$z(x) = G^{D-1} \sum_{n=n_1}^{\infty} \frac{\cos 2\pi\gamma^n x}{\gamma^{(2-D)n}} \quad (4.3)$$

The shape of the profile is determined only by two parameters –  $D$  and  $G$  – which are independent from the sampling length or the frequency.  $D$  is the fractal dimension, this is a regularity parameter of the function.  $G$  is called the topothesy of the analysed set. Traditionally, the topothesy determines

the ruggedness of a set.  $\gamma^n$  is the discrete frequency spectrum of the set roughness and  $n_1$  is the low cut-off frequency of the signal.

The WM function allows building a curve of given fractal dimension (Figure 4-3). Numerous techniques of fractal analysis can be used to obtain the fractal dimension from a profile. Three of them were employed in this study: box counting analysis, correlation analysis and regularization analysis. The fractal analysis provides an estimation of the complexity, regularity of a curve or set through its auto-scale nature.

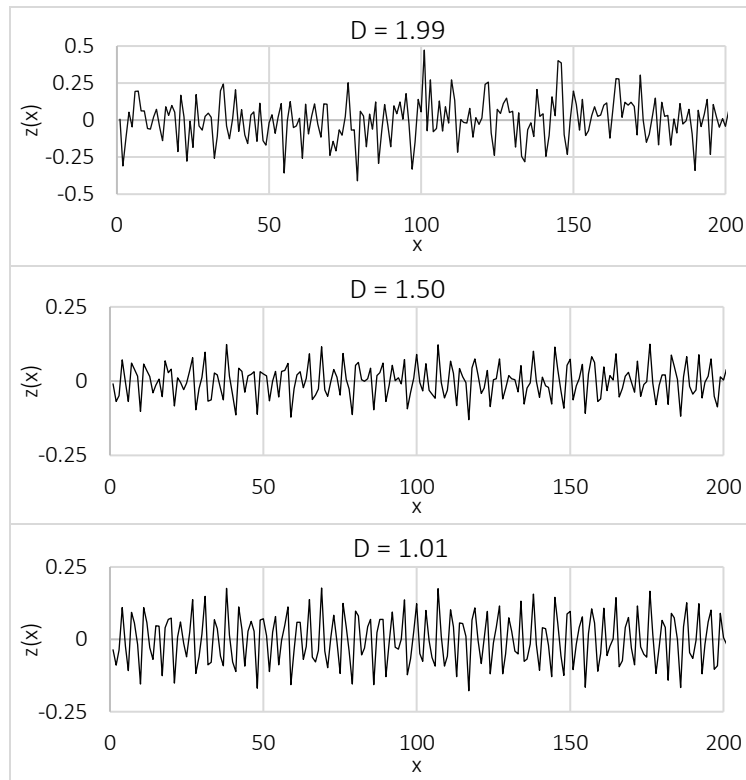


Figure 4-3: Weierstrass-Mandelbrot functions generated with different values of the parameter or fractal dimension  $D$

Figure 4-4 depicts samples of total cutting force signals for different tool wear. Those signals were acquired during the machining using the tool 1 at four spots from the first, seventh, fifteenth and twenty second passes. From the observation of the samples obtained during the first pass and, to a lesser extent, for the seventh pass, the signal behaviour seems erratic and affected by noise. In contrast, the twenty-second pass signal is relatively similar to the cutting force signals acquired during the machining of a homogeneous material. This cutting force signal obtained with an extremely worn tool has a more regular nature and seem less affected by noise. This observation

of the signal noise decreasing with the tool wear increase is reversed compared with the signals from homogeneous material machining such as steel. The four passes of the tool 1, shown in Figure 4-4, were chosen to present major phases of the impact of the tool wear evolution onto the cutting force signals. The same four passes were used to illustrate each fractal analysis method as well.

The fractal analysis is an adequate technique to describe the signal features and shapes and its changes with the tool wear variations, and so, with the surface quality. Each selected fractal analysis type is first presented with preliminary results of the evolution of the graphs so that the fractal parameters can be determined.

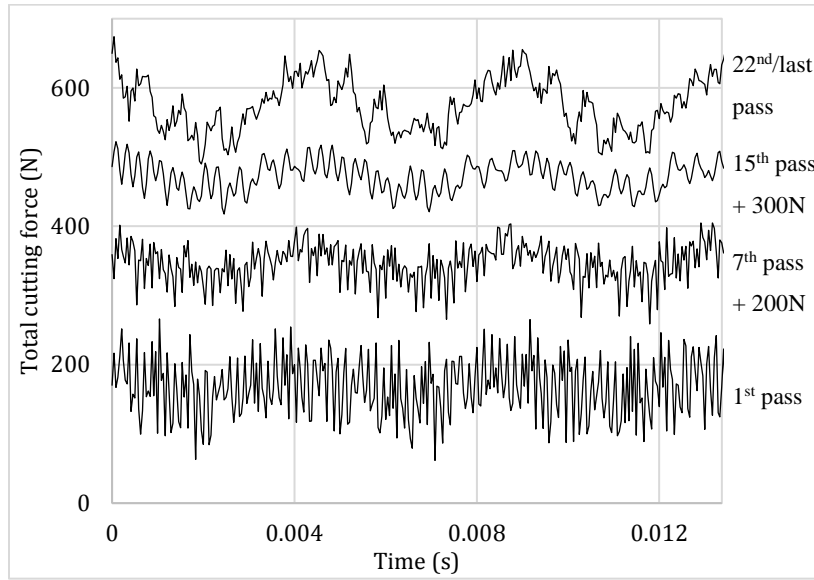


Figure 4-4: Total cutting force signal samples  $F_T$  over three rotational periods for different tool wear of tool 1 (from 1<sup>st</sup> pass with a new tool to the 22<sup>nd</sup> pass with a worn tool)

#### 4.5.1 Box-counting fractal analysis

The box-counting is probably the easiest and most used analysis to estimate the fractal dimension of a set. The box-counting dimension  $D_{BC}$  can be estimated using the following formula [21, 22]:

$$D_{BC} = \lim_{\varepsilon \rightarrow 0} \frac{\log N(\varepsilon)}{\log(1/\varepsilon)} \quad (4.4)$$

where  $\varepsilon$  is the size of the box and  $N(\varepsilon)$  is the number of boxes containing a fragment of the curve.

Usually, the dimension  $D_{BC}$  is calculated on the straightest portion of the curve  $\log N(\varepsilon)$  vs  $\log(1/\varepsilon)$  as shown in Figure 4-5.

The curves, shown in Figure 4-5, tend to be relatively similar at different heights. The box-counting analysis seems to generate a stable fractal dimension – slope of the curve – whatever the tool wear is. However, the topothesy – which is represented by the intercept – seems strongly influenced by the tool wear.

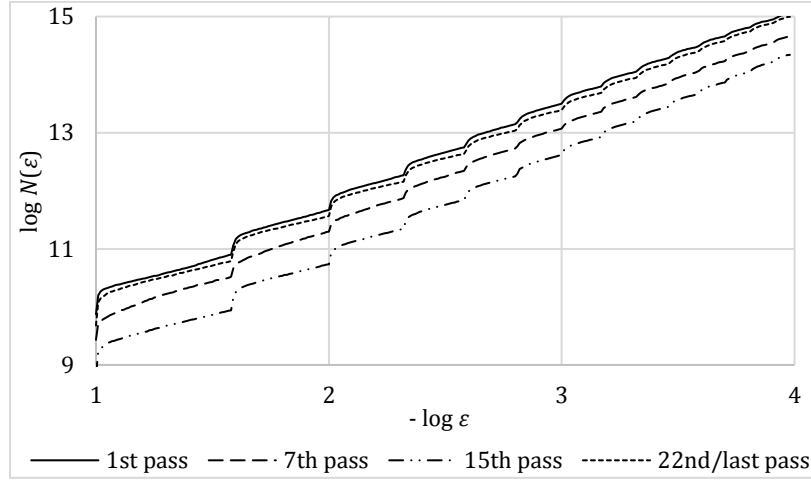


Figure 4-5: Box counting graph (box number containing the curve vs the size box) for different tool wear of the tool 1

#### 4.5.2 Correlation fractal analysis

The correlation analysis is one of the most used to estimate the fractal dimension of a curve. For this technique, a set of vectors are extracted from the discrete time series signal  $x(t)$  [23]:

$$\begin{aligned}
 \mathbf{X}_1 &= \{x(1), \quad x(1 + \tau), \quad \dots, x(1 + (M - 1)\tau)\} \\
 \mathbf{X}_2 &= \{x(1 + k), \quad x(1 + k + \tau), \quad \dots, x(1 + k + (M - 1)\tau)\} \\
 \vdots & \quad \quad \quad \vdots \quad \quad \quad \vdots \quad \quad \quad \vdots \quad \quad \quad \vdots \\
 \mathbf{X}_{N+1} &= \{x(1 + Nk), x(1 + Nk + \tau), \dots, x(1 + Nk + (M - 1)\tau)\}
 \end{aligned} \tag{4.5}$$

where  $N$  is the number of vectors,  $k$  is the space between the vectors,  $M$  is the phase space or embedding dimension or the number vector points and  $\tau$  is the space between two points within vectors.

Then, the correlation dimension  $D_C$  can be estimated as follows:

$$D_C = \lim_{\epsilon \rightarrow 0} \frac{\log C(\epsilon)}{\log \epsilon} \tag{4.6}$$

where the correlation function  $C(\varepsilon)$  can be calculated by:

$$C(\varepsilon) = \frac{1}{N(\varepsilon)(N(\varepsilon) + 1)} \sum_{i=1}^{N+1} \sum_{\substack{j=1 \\ j \neq i}}^{N+1} \theta(\varepsilon - |\mathbf{X}_i - \mathbf{X}_j|) \quad (4.7)$$

where  $\theta$  is the Heaviside step function and  $|\mathbf{X}_i - \mathbf{X}_j|$  is the distance between the vectors  $\mathbf{X}_i$  and  $\mathbf{X}_j$ . In this study, the input parameters were fixed as follows:  $N = 4000$  vectors,  $k = 1$  sampling points,  $M$  corresponds to the number of sampling points for one rotational period and  $\tau$  was selected in order to analyse the highest range of the machining stable part.

Figure 4-6 depicts the log/log graphs determining the fractal dimension for the four chosen passes of the tool 1.

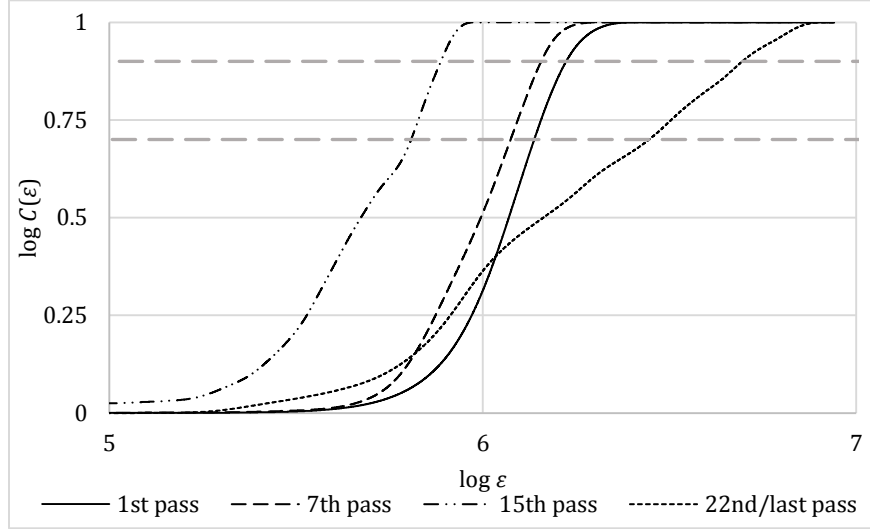


Figure 4-6: Correlation analysis graph ( $\log C(\varepsilon)$  vs  $\log \varepsilon$ ) for different tool wear of the tool 1

Once the log/log graph was plotted, three parameters were extracted from each curve: the dimension  $D_C$ , the topothesy  $G_C$  and the coefficient of determination  $R^2_C$ . The correlation dimension  $D_C$  was estimated as the curve slope between the 0.7 and 0.9 fixed values of  $\log C(\varepsilon)$  (as shown in Figure 4-6). This range was selected after the preliminary analysis. The topothesy  $G_C$  was calculated as the intercept of the slope for the same range and the correlation determination coefficient  $R^2_C$  was calculated for the same slope. Despite that four fractal dimension determination log/log graph are plotted in Figure 4-6, the range and the parameters selections are based on all the 224 results.

### 4.5.3 Regularization fractal analysis

The regularization fractal analysis was selected for its relative robustness and because it had been already used to assess gear damage with the use of accelerometer signals [24]. This regularization dimension is estimated from the convolutions of the signal 's' with different kernels  $g_a$  with a width of 'a' [25, 26]. Each convolution product  $s_a$  can be written:

$$s_a = s * g_a \quad (4.8)$$

Two kernels  $g_a$  were used in our calculation: a Gaussian kernel which is the first derivative of the 1-D Gaussian function, and a rectangle kernel which is an affine function.

Then, the hypothesis that  $s_a$  has a finite length called  $l_a$ , for the size of 'a', is set.

For both cases, the regularization dimension  $D_R$  can be calculated by:

$$D_R = 1 - \lim_{a \rightarrow 0} \frac{\log l_a}{\log a} \quad (4.9)$$

The limit, in the equation 9, is usually estimated as the slope value, where the 'a' values are close to 0 and the coefficient of determination,  $R^2$ , of the linear regression of a part of the curve is close to 1. From the preliminary analyses, the range of the slope determination was selected between nine sampling points and a value depending on the tool rotational speed. For the Gaussian kernel, this superior limit was selected for the number of sampling points acquired during one rotation per tooth. For the rectangular kernel, this high range limit was selected for the number of sampling points acquired during one entire rotation.

Figure 4-7 and Figure 4-8 depict the fractal dimensions determination graphs for both kernels and different tool wear of the tool 1. Fractal dimensions  $D_{RG}$  and  $D_{RR}$  were determined as the slope estimation for, respectively, Gaussian and rectangular kernels within the designated graph sections. The topographies  $G_{RG}$  and  $G_{RR}$  were the intercept calculated from the same slope estimation.

Concerning the log/log graph generated by the rectangular kernel analysis (Figure 4-8), the log/log curves are strongly impacted by the behaviour change of the cutting force signals and thus with the tool wear: the curve is bumpy with an unused cutter, and the curve is smoother with a worn tool. Two additional fractal parameter were added for this case:  $R_1^2$  and  $R_3^2$ , which are the coefficient



of determination of, respectively, the linear regression and the third-degree polynomial regression within the graph section.

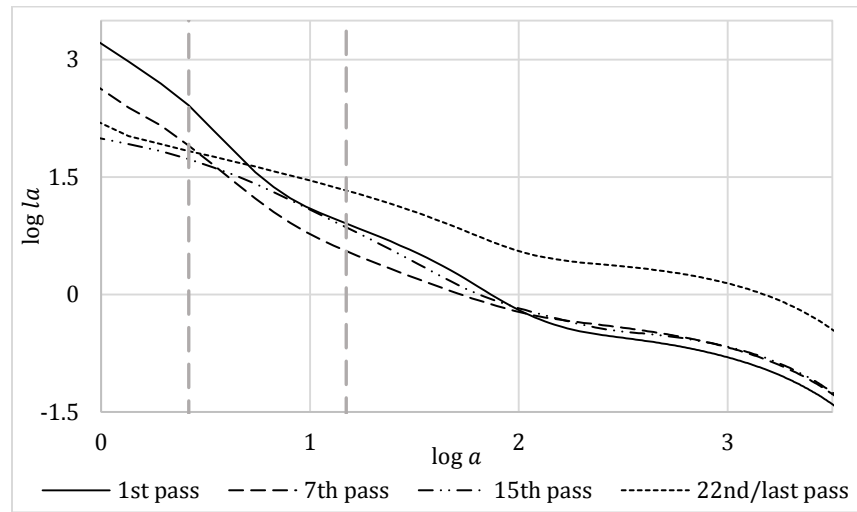


Figure 4-7: Regularization analysis graph ( $\log la$  vs  $\log a$ ) using the 1<sup>st</sup> derivative Gaussian function kernel

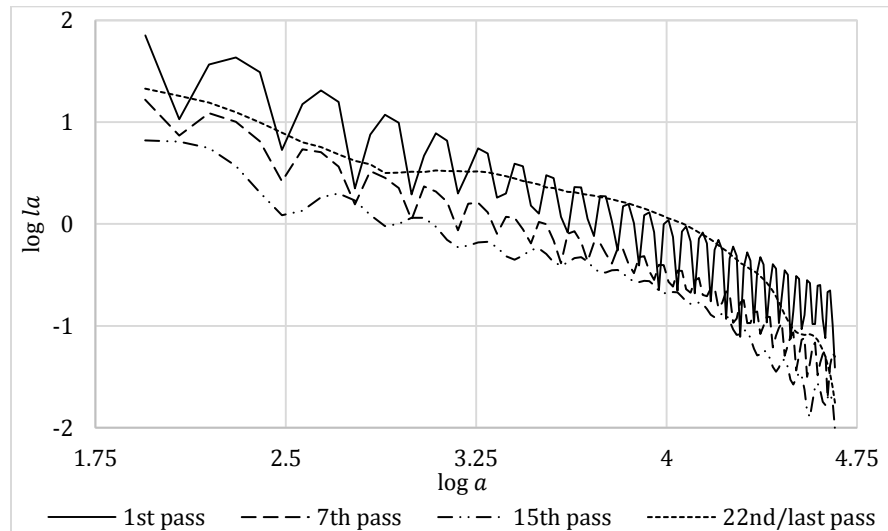


Figure 4-8: Regularization analysis graph ( $\log la$  vs  $\log a$ ) using the rectangular kernel

From the chaos theory and its branch, the fractal theory, the real fractal dimension  $D$  of a curve in the plan can reach the value range between 1 and 2. However, the main goal of this study is to present a new approach to predict the tool wear and so on the surface quality with the cutting force signal analysis. Thus, finding the best estimation of the signal fractal dimension is not crucial. In this paper, the so-called fractal dimensions can be outside this range. Such results are obviously

not accurate estimations of real fractal dimensions. Equivalent statement can be set for the topothesis results.

## 4.6 Results and discussion

The tool wear evolution is shown in Figure 4-9 towards the length of material cut. The tool wear is preferred to the length of cut in order to compare the results of the statistical and fractal parameters with it. In fact, the surface quality characteristics, such as delamination length or roughness parameters, might not be pertinent enough. For example, the roughness parameter  $Ra$  (average deviation of the roughness profile) was found inadequate to evaluate the surface finish of fibre reinforced plastic (FRP) composites. Thus, the tool wear was selected as comparative factor for the results.

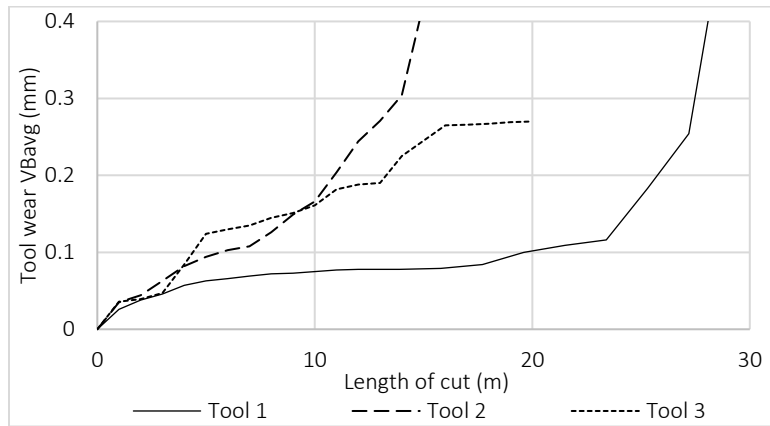


Figure 4-9: Evolution of the tool wear  $VB_{avg}$  vs the length of CFRP cut

### 4.6.1 Statistical parameters

Statistical parameters were calculated on the entire stable section of the total cutting force signal. In Figure 4-10, signal averages and signal standard deviations are presented vs the tool wear  $VB_{avg}$ . In Figure 4-11, signal skewness (asymmetry) and signal kurtosis (flatness) are shown towards the tool wear  $VB_{avg}$ . Variations are noticeable for the results of both figures, but they depend on the cutting parameters, in particular for the average and the standard deviation of the cutting force signal. For the signal average and a low tool wear, the value varies from 140 N to 340 N depending on the cutting parameters. Similar observations can be established for the standard deviation, the kurtosis or the skewness of the cutting force signals.

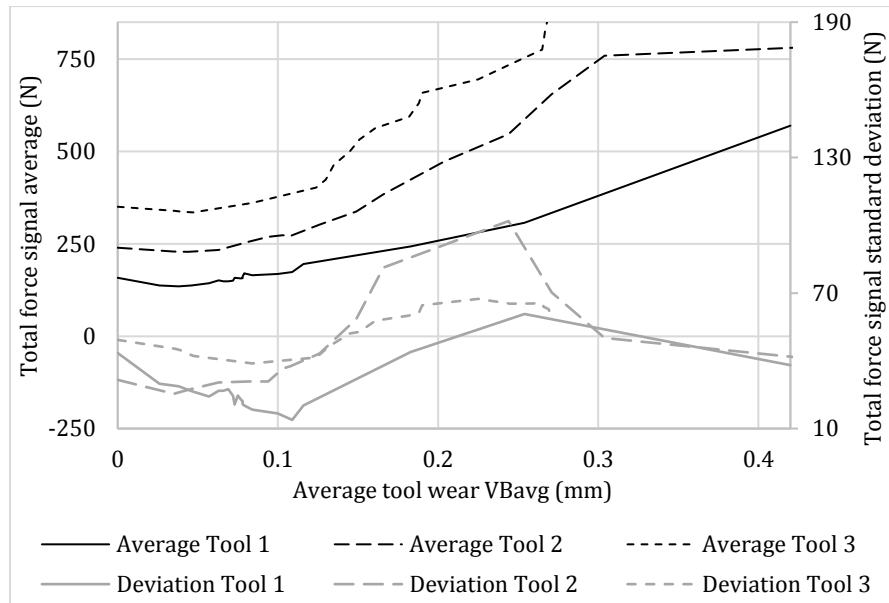


Figure 4-10: Averages and standard deviations of the total cutting force signals vs the averaged tool wear  $VB_{avg}$

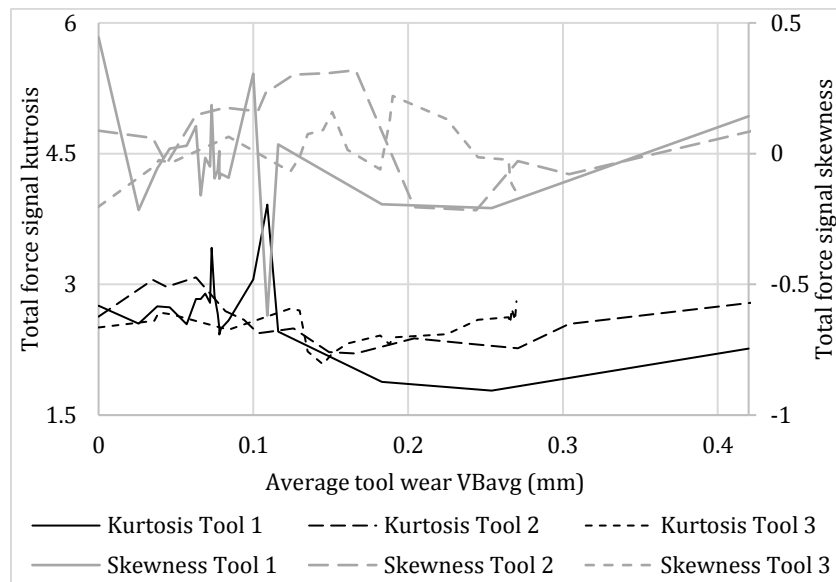


Figure 4-11: Skewness (asymmetry) and kurtosis (flatness) of the total cutting force signals vs the averaged tool wear  $VB_{avg}$

Moreover, the skewness (asymmetry) variations of the cutting force signals do not seem to evaluate the tool wear due to too little changes of this parameter. The kurtosis (flatness) of the cutting force signals allows to observe at least two of the three stages of wear, especially between the second and the third wear stages. The initial or primary wear which is a rapid wear increase at the beginning

of the tool life, the stationary or second stage wear which is the relatively steady state of the wear, and the third wear stage which is a rapid wear increase leading to the failure. The transition between the first and second stages was observed for a tool wear around 0.04 mm. The other change was observed for a tool wear of nearly 0.12 mm.

Although some of these statistical parameters permit to identify a change of wear stage type in certain cases, it requires a learning process for each of the cutting forces signals of different cutting parameters.

#### 4.6.2 Fractal parameters

All the fractal dimensions are calculated for each tool (or each cutting parameters set) and compared with the averaged tool wear  $VB_{avg}$  (Figure 4-13). The observations of the differently calculated fractal dimensions do not seem to help estimating the tool wear, either due to a high dispersion of the results, e.g. for the correlation dimension, or due to too low variations and with different directions, e.g. for the box counting dimension.

In Figure 4-12, the calculated topographies are presented towards the tool wear  $VB_{avg}$ . For one test, variations of the topographies vs the tool wear are similar. The variations are different, probably depending on the cutting parameters. A variation change of the topography vs the tool wear can be observed around the transition from the second to the third wear stage.

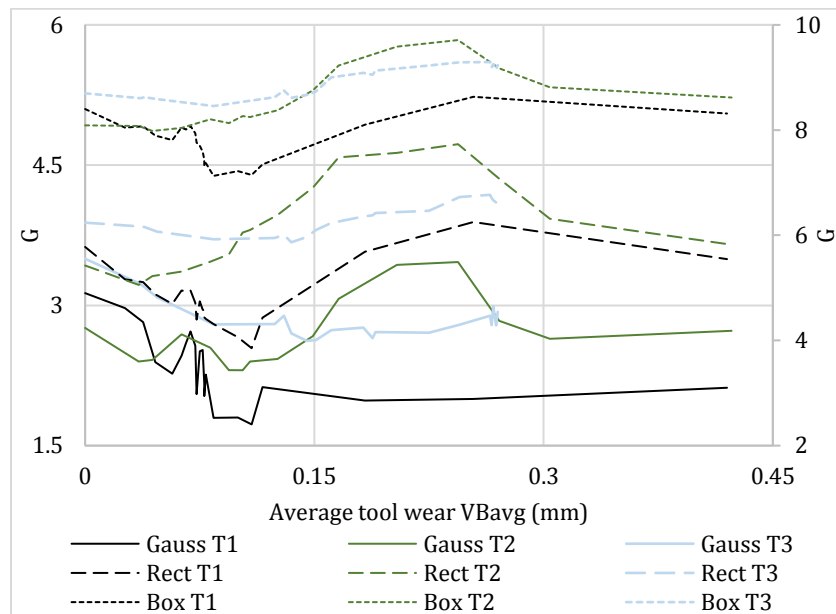


Figure 4-12: Topography results vs the tool wear average  $VB_{avg}$

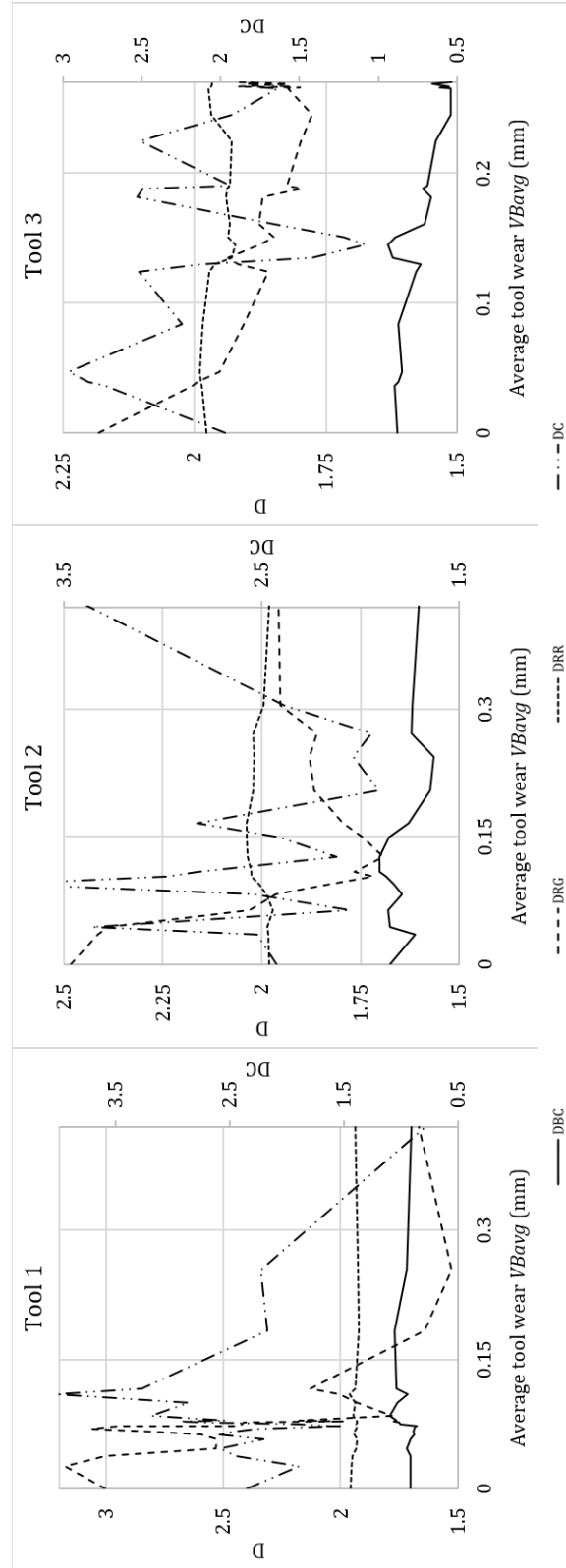


Figure 4-13: Fractal dimensions graph (fractal dimensions  $D_{BC}$ ,  $D_C$ ,  $D_{RG}$ ,  $D_{RR}$ ) in comparison to the averaged tool wear  $VB_{avg}$

In Figure 4-14, the variations of the determination coefficients with the tool wear  $VB_{avg}$  are depicted. Some of the  $R$ -squared results allow to distinguish different wear stages. For example, the first stage is illustrated by a high increase of the  $R_3^2$  coefficient. Then, the second wear stage is represented by a high value of this  $R$ -squared coefficient until its decreasing for the last stage and the rapid tool wear increase. With this calculation method, the cutting parameters have no relevant impact on the  $R$ -squared results.

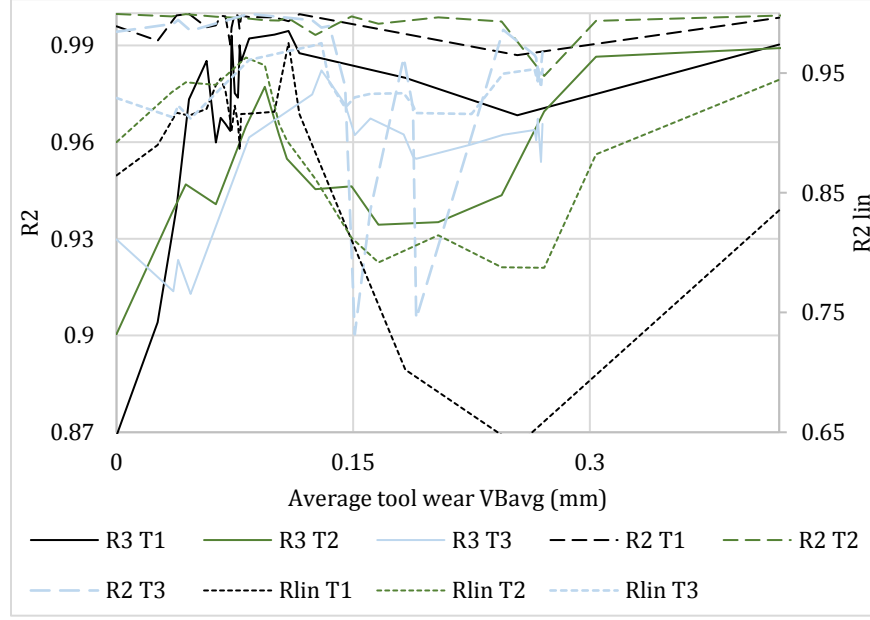


Figure 4-14: Coefficient of fractal dimension slope determination vs the averaged tool wear  $VB_{avg}$

However, even if the tool wear stage transitions can be seen on certain fractal parameters, the detection is not straight forward. Each parameter characterizes a specific feature of the cutting force signal. That is why a fractal index  $I_f$  is proposed based on combinations of few fractal parameters. Building this index based on the combination of the fractal parameters allows merging the key detections of each parameter to monitor more accurately the turning points of tool wear or surface quality during the entire tool life.

The empirical index proposed herein can be calculated as followed:

$$I_f = \frac{D_{RR}}{D_{RR}(o)} \frac{G_{RR}}{D_{RR}(o)} \frac{R_3^2 - R_1^2}{R_3^2(o) - R_1^2(o)} \quad (4.10)$$

where  $o$  corresponds to the initial value (obtained with a new tool) of each parameter.

Figure 4-15 depicts this fractal index towards the tool wear. This index allows to clearly observe a step variation at the transition point between the second and the third tool wear stages (occurring around 0.12 mm tool wear).

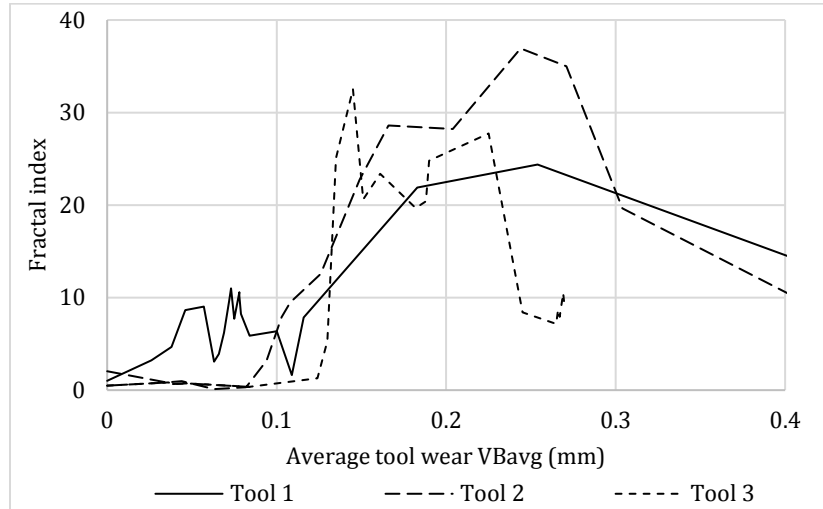


Figure 4-15: Fractal index  $I_f$  vs the tool wear  $VB_{avg}$

Some of the fractal parameters calculated from the total cutting force signals are suitable to evaluate the tool wear and the different wear stages. However, their technique estimation efficiency can be improved using additional fractal parameters calculated from different cutting force component signals such as the feed force signal  $F_f$ , the normal force signal  $F_n$  and the vertical force signal  $F_z$ .

In Figure 4-16, cutting force signals are shown for the feed, normal and vertical directions and different tool wear. The cutting force signal samples have a change of behaviour depending on the tool wear. The first pass corresponds to the primary wear stage, the eleventh to the steady wear state and the last one to an extremely worn tool. Each cutting force signal direction has a particular signal sample behaviour. Separate analysis of each force direction ( $F_f$ ,  $F_n$  and  $F_z$ ) can provide more information than the total cutting force signal.

For example, in Figure 4-17, for low tool wear (inferior to a 0.04 mm  $VB_{avg}$ ), the primary wear stage is observable on the regularization fractal dimensions with the Gaussian kernel.

Another example of complementary information obtained with the analysis of the normal cutting force signal  $F_n$  is depicted in Figure 4-18. The coefficients of determination of the regularization fractal analysis graph with the rectangular kernel can identify the transition between the steady state and the final rapid wear state.

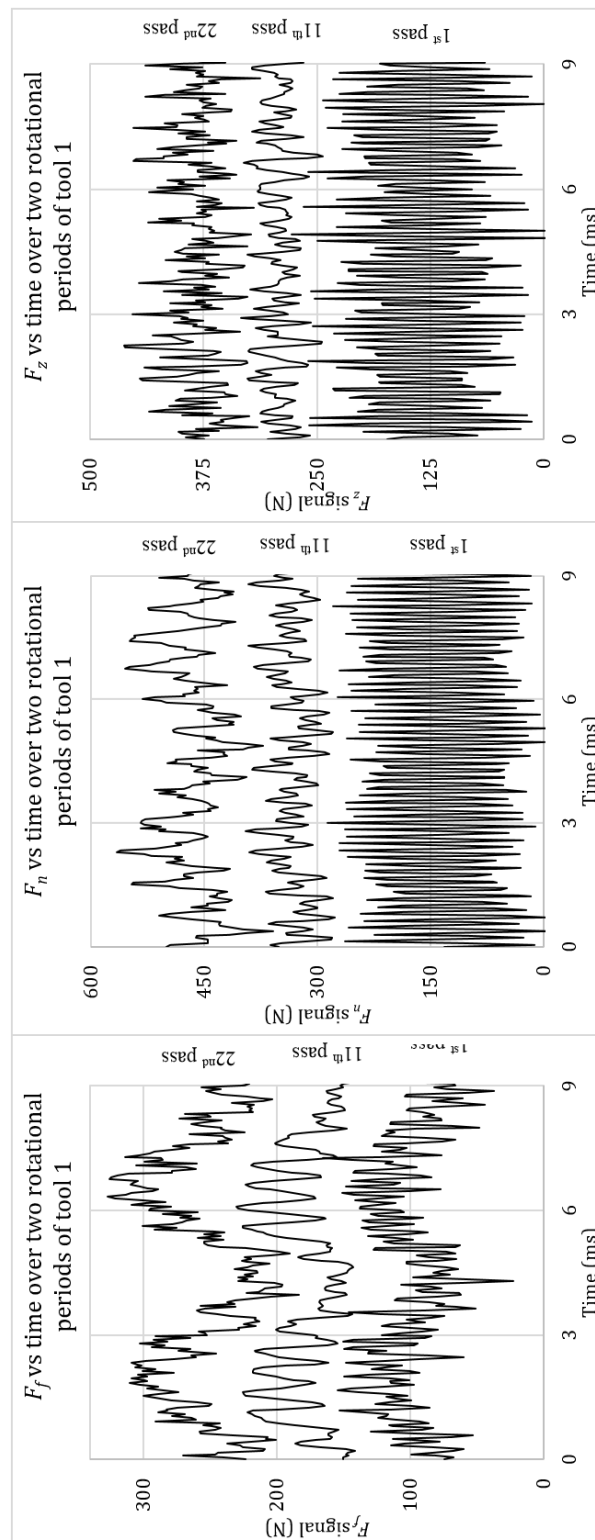


Figure 4-16: Cutting force signal samples over two tool rotational periods for different tool wear of tool 1: feed force signal  $F_f$  (left), normal force signal  $F_n$  (centre) and vertical force signal  $F_z$  (right)



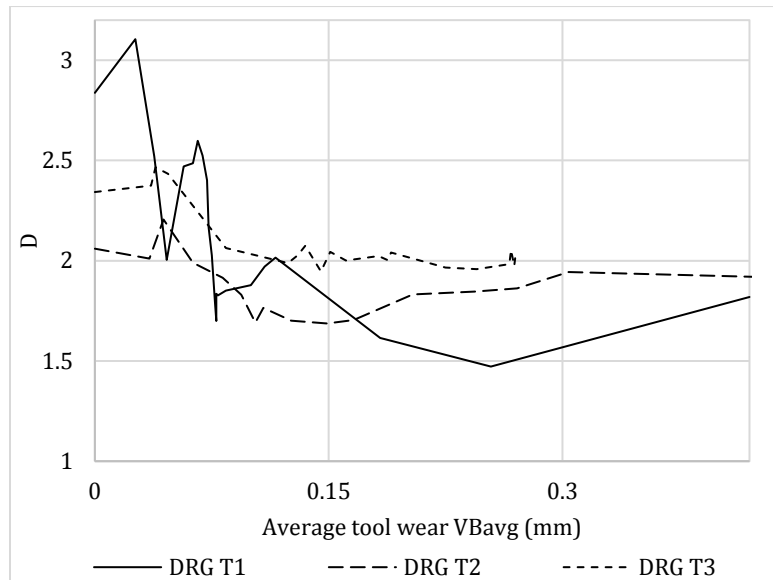


Figure 4-17: Fractal dimensions graph in comparison to the averaged tool wear  $VB_{avg}$

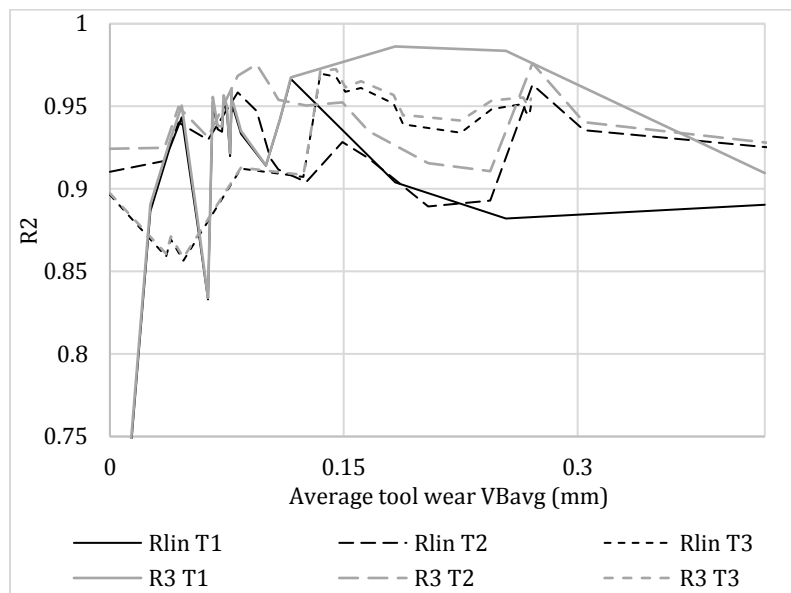


Figure 4-18: Coefficient of fractal dimension slope determination vs the averaged tool wear  $VB_{avg}$  from the fractal analysis of the  $F_n$  cutting force signals

### 4.6.3 Machined surface quality

The fractal results (fractal parameters and index) showed the tool wear can be well followed using the cutting force signals. Their efficiency is excellent to evaluate the quality of the machined surface and can be a complementary criterion during the online monitoring to maintain a sufficient

machining quality. Depending on the machined surface integrity requirements, a tool wear that is still considered acceptable and suitable for further machining operations may generate surface damage. From the conducted experiments for this study, it was noticed that for a tool wear higher than 0.12 mm, the surface integrity is affected, and the tool life end is reached. Moreover, close to a 0.30 mm tool wear, burning smoke from the matrix was generated from the CFRP trimming.

The results of the different cutting force signal, e.g. the feed force signal  $F_f$ , the normal force signal  $F_n$  and the vertical force signal  $F_z$  could be linked to different aspects of the surface quality such as delamination, the regularity of the machining surface, burnt resin, etc. Certain fractal parameters of the cutting force signals are excellent estimators to predict the surface quality than to predict the tool wear. However, the estimation of the tool wear, as performed in this study, has some limitations. Faraz *et al.* found that the cutting edge rounding (CER) could be a better estimator of the tool wear [27], and thus the prediction accuracy towards this CER would tend to be higher than the current tool wear estimation.

Regarding the machining and the acquired cutting force signals for a low tool wear, the tool radius is relatively small. By this, fibres are fractured according to the fracture mechanisms described by Arola *et al.* [28]. For this tool condition, the apparent noise on the cutting force signals is due to the fracture of the fibres under the tool loadings and so the noise added to the acquired cutting force signals reflects the loads to break small groups of fibres.

In the case where the tool wear is higher, the tool radius is greater as well. Cutting force signals remains affected by noise but at a lower level. From the observations of the obtained signals (Figure 4-4 and Figure 4-16), the total cutting force signal is relatively similar to the one acquired during the machining of a homogeneous material. This statement raises the question if the fibres are still fractured as described in the studies of Arola *et al.* or if the impact of certain modes of fractures has evolved.

## 4.7 Conclusion

An innovative approach to adaptive fractal analyses of cutting force signals was presented in this study. Fractal dimensions, other fractal parameters and the fractal index were the results of fractal analyses of the cutting force signals during the trimming of CFRP allowing to estimate the tool

wear and to assess the machined surface quality. The fractal parameters allow describing the regularity, complexity and auto-scale dependency of the cutting force signals partially.

Those fractal results were also compared with statistical parameters such as signal average, standard deviation, skewness and kurtosis. In this study, fractal results, in particular the proposed fractal index, are more efficient to estimate the tool wear and the surface quality than the statistical parameters can be. This technique is also less dependent on the cutting parameters than the statistical parameters. Thus, this online monitoring method allows ensuring that no scrapped part is machined during the CFRP trimming. Additionally, this method is not only limited to the CFRP trimming but can also be used for the trimming of laminated composite and could even be employed for other composite types such as metal matrix composites. Besides for this method to work efficiently, the machined part material needs to have a heterogeneous composition in order to distinguish and to identify changes in the cutting force signals behaviour.

This technique could also be adapted for monitoring the machining through the signals of acoustic emission sensors or accelerometers. The implementation of this type of device can easily be mounted onto the machine and could be performing quality checks of the surface machined or the tool condition.

## **4.8 Acknowledgements**

The authors wish to thank Mr. Hossein Hamedanianpour for conducting the experiments at the Centre Technologique en Aérospatial with the help of Mr. Réjean Roy.

The regularization dimensions were computed using a program fragment from the software FracLab engineered by INRIA in France.

This work was funded by the Consortium for Research and Innovation in Aerospace in Québec (CRIAQ) and its partners, the Natural Sciences and Engineering Research Council of Canada (NSERC), Bombardier Aerospace, Avior Integrated Products, Delastek and AV&R Aerospatiale.

## **4.9 References**

- [1] Persson E, Eriksson I, Zackrisson L. Effects of hole machining defects on strength and fatigue life of composite laminates. *Composites Part A: Applied Science and Manufacturing*. 1997;28:141-51.

- [2] König W, Wulf C, Graß P, Willerscheid H. Machining of Fibre Reinforced Plastics. CIRP Annals - Manufacturing Technology. 1985;34:537-48.
- [3] Guegan P, Lemaitre F, Hamann J. Contribution a l'usinage des materiaux composites. 1992.
- [4] Jahanmir S, Ramulu M, Koshy P. Machining of ceramics and composites New York: Marcel Dekker; 1999.
- [5] Stephenson DA, Agapiou JS. Metal cutting theory and practice: CRC press; 2005.
- [6] Tsao CC, Hocheng H. Effect of tool wear on delamination in drilling composite materials. International Journal of Mechanical Sciences. 2007;49:983-8.
- [7] Hamedanianpour H, Chatelain JF. Effect of Tool Wear on Quality of Carbon Fiber Reinforced Polymer Laminate during Edge Trimming. Applied Mechanics and Materials. 2013;325-326:34-9.
- [8] Mandelbrot B. Les objets fractals : Forme, hasard et dimension France: Flammarion; 1975.
- [9] Sapoval B. Universalités et fractales. Science Edition France: Flammarion; 1997.
- [10] Bukkapatnam STS, Kumara SRT, Lakhtakia A. Fractal Estimation of Flank Wear in Turning. Journal of Dynamic Systems, Measurement, and Control. 1999;122:89-94.
- [11] Bukkapatnam STS, Lakhtakia A, Kumara SRT. Analysis of sensor signals shows turning on a lathe exhibits low-dimensional chaos. Physical Review E. 1995;52:2375-87.
- [12] Altintas Y. Manufacturing automation : metal cutting mechanics, machine tool vibrations, and CNC design Cambridge; New York: Cambridge University Press; 2012.
- [13] Karpat Y, Bahtiyar O, Değer B. Mechanistic force modeling for milling of unidirectional carbon fiber reinforced polymer laminates. International Journal of Machine Tools and Manufacture. 2012;56:79-93.
- [14] Karpat Y, Bahtiyar O, Değer B. Milling Force Modelling of Multidirectional Carbon Fiber Reinforced Polymer Laminates. Procedia CIRP. 2012;1:460-5.
- [15] Kalla D, Sheikh-Ahmad J, Twomey J. Prediction of cutting forces in helical end milling fiber reinforced polymers. International Journal of Machine Tools and Manufacture. 2010;50:882-91.
- [16] Kabaldin YG, Seryi SV, Prosolovich AV, Burdasov EN. Improving the stability of cutting on the basis of fractal, dimensional, and wavelet analysis. Russian Engineering Research. 2010;30:587-95.
- [17] Fu P, Li WL, Zhu LQ. Cutting Tool Wear Monitoring Based on Wavelet Denoising and Fractal Theory. Applied Mechanics and Materials. 2011;48-49:349-52.
- [18] Bérubé S. Évaluation de la performance d'outils de coupe dédiés au détournage de structures composites carbone/époxy: École de Technologie Supérieure (Université du Québec à Montréal); 2012.

- [19] International Standard Organization I. Tool life testing in milling. Part 2: End milling 1989. p. 26.
- [20] Majumdar A, Tien CL. Fractal characterization and simulation of rough surfaces. *Wear*. 1990;136:313-27.
- [21] Gagnepain JJ, Roques-Carmes C. Fractal approach to two-dimensional and three-dimensional surface roughness. *Wear*. 1986;109:119-26.
- [22] Mandelbrot BB. *The fractal geometry of nature* San Francisco: W.H. Freeman; 1982.
- [23] Logan D, Mathew J. Using the correlation dimension for vibration fault diagnosis of rolling element bearings—I. Basic concepts. *Mechanical Systems and Signal Processing*. 1996;10:241-50.
- [24] Feng Z, Zuo MJ, Chu F. Application of regularization dimension to gear damage assessment. *Mechanical Systems and Signal Processing*. 2010;24:1081-98.
- [25] Lévy Véhel J, Legrand P. Signal and image processing with Fraclab. In: *Proceedings of Fractal04 CaFiN*, editor. Eighth International Multidisciplinary Conference Vancouver, Canada 2004.
- [26] Roueff F, Lévy Véhel J. A Regularization Approach to Fractional Dimension Estimation. In: Novak MM, editor. *Fractals 98*: World Scientific; 1998.
- [27] Faraz A, Biermann D, Weinert K. Cutting edge rounding: An innovative tool wear criterion in drilling CFRP composite laminates. *International Journal of Machine Tools and Manufacture*. 2009;49:1185-96.
- [28] Arola D, Ramulu M, Wang DH. Chip formation in orthogonal trimming of graphite/epoxy composite. *Composites Part A: Applied Science and Manufacturing*. 1996;27:121-33.

## **CHAPTER 5      ARTICLE 2: A NEW APPROACH FOR THE SURFACE ROUGHNESS PROFILE CHARACTERIZATION OF LAMINATED COMPOSITES IN THE PLY PLANE DIRECTION**

Xavier Rimpault<sup>a</sup>, Jean-François Chatelain<sup>b</sup>, Jolanta E. Klemberg-Sapieha<sup>c</sup>, Marek Balazinski<sup>a</sup>

<sup>a</sup>Department of Mechanical Engineering, Polytechnique Montréal, Canada

<sup>b</sup>Department of Mechanical Engineering, École de Technologie Supérieure, Canada

<sup>c</sup>Department of Engineering Physics, Polytechnique Montréal, Canada

\* Submitted to *Canadian Aeronautics and Space Journal* in July 2015.

### **5.1 Abstract**

Based on observations, current surface profile roughness parameters have some limitations of describing a surface texture. Characterizing the surface texture of a machined laminated composite is even more complex due to its anisotropic and heterogeneous nature at a micrometric scale. In this study, novel roughness parameters are proposed to characterize the surface texture of a composite. These parameters are based on the fractal analysis and the autocorrelation function allowing to describe the complexity, the regularity and the auto-scale dependency of the profile. To depict these parameters and demonstrate their estimation method, experiments of carbon fibre reinforced polymer (CFRP) trimming were conducted and roughness profiles were measured using a contact profilometer. Both up- and down-milling faces were inspected in the feed direction also within the ply plane, for each ply orientation ( $0^\circ$ ,  $90^\circ$  and  $\pm 45^\circ$ ), for different tool wear and three cutting parameters. The fractal analysis adjusted to the profile method seems better adapted to the surface texture definition. Even though autocorrelation and fractal roughness parameters proposed show some limitations, they are good estimators for the composite surfaces characterization, especially towards the tool wear evolution.

*Keywords:* Laminate composite, surface texture, roughness parameter.

### **5.2 Introduction**

Laminated composites, especially carbon fibre reinforced polymer (CFRP), have been gradually used in the aerospace industry thanks to their high strength-to-weight ratio. During the assembly

process and the product lifetime, the integrity of a machined composite surface is crucial. Besides damages occurring during machining such as inter- or intra-ply delamination or burnt resin, the surface texture needs to be optimized depending on the use. Thus, the surface texture requires to be characterized. The texture of polymer composite machined surface began to be investigated in the 1990s. Wern *et al.* discovered that the roughness average deviation parameter  $Ra$  is inaccurate to describe the CFRP surface roughness [1]. Years later, Palanikumar *et al.* investigated possible factors which could influence the surface roughness on machined glass fiber-reinforced polymer composites [2]. However, they based their study of the surface roughness on the same inadequate parameter  $Ra$ . Ghidossi *et al.* conclude that roughness criteria is not representative enough of the subsurface damage and so, of the machining quality during the machining of glass/epoxy laminated composite [3]. There again, the surface roughness was characterized only by one roughness parameter –  $Ra$ , which was found inadequate to describe the surface roughness of a laminated polymer composite. In the aerospace industry, areal roughness parameters are preferred to profile ones to describe the surface roughness. Contrary to profile roughness parameters which are indexes of a surface roughness using measured surface profiles, areal roughness parameters are roughness indexes calculated over a surface area. Consequently, the roughness check becomes more complex and more time consuming using areal roughness parameters.

Chatelain *et al.* investigated the effect of ply orientations on surface roughness using various roughness parameters ( $Ra$ ,  $Rq$ ,  $Rp$ ,  $Rv$ ,  $Rz$ ) [4]. Those parameters were measured and calculated in the ply plane from specific ply orientations ( $0^\circ$ ,  $90^\circ$  and  $\pm 45^\circ$ ). Relatively high value variations were noticed between the different ply orientations. That is why each ply orientation is treated separately in this study. Due to the CFRP anisotropy at a micrometric scale, the surface profile measurements is relatively different depending on the measurement orientation on the trimmed surface and, if applicable, depending on the fibre orientation.

This study is limited to the texture description of the trimmed surface in the ply plane – so is the feed direction in – for specific fibre orientations ( $0^\circ$ ,  $90^\circ$  and  $\pm 45^\circ$ ) and taking into account different tool wear. From different cutting conditions, surface profiles that have very different shapes can be represented with the same roughness parameters values. It results in a limit of characterization of composite surfaces using current roughness parameters.

In Figure 1, different roughness profiles with the same roughness parameters values are presented (profile average deviation  $Ra$ , profile skewness – asymmetry –  $Rsk$ , kurtosis – flatness –  $Rku$ ). Although the roughness parameters are similar, profiles behaviours are obviously different. That is why new roughness parameters are proposed in this study. Those parameters are extracted from the autocorrelation function and from the log-log graph determining the fractal dimension.

Introduced by the mathematician Benoit Mandelbrot, fractal theory and fractal analysis concepts have been used for the last twenty years in the metrology area [5, 6]. Even though this technique is known to have an excellent capability of describing the complexity of a surface or a curve, the use of the fractal analysis and its fractal parameters mainly remains at a trial level.

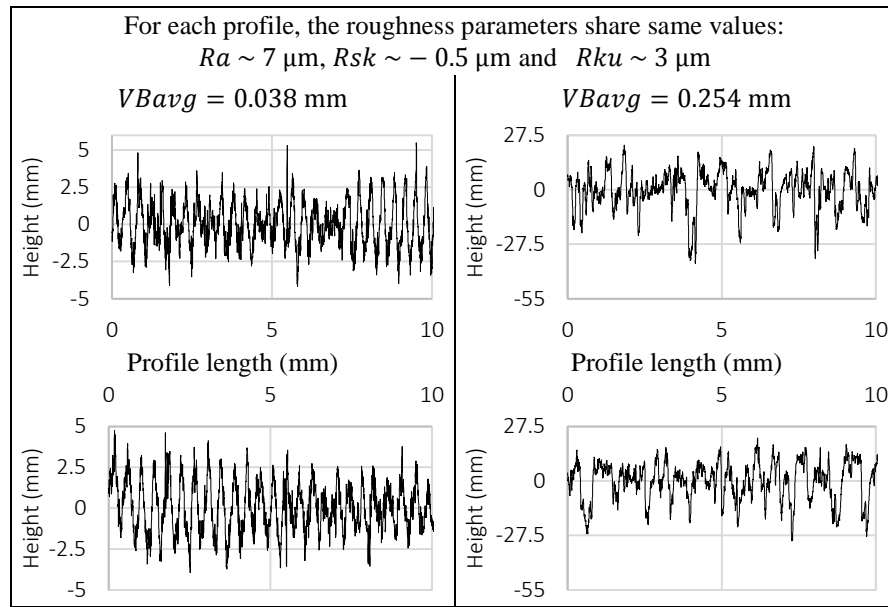


Figure 5-1: Roughness profiles examples of  $-45^\circ$  ply orientation giving similar  $Ra$ ,  $Rsk$  and  $Rku$  with low (left) and high (right) tool wear

## 5.3 Methodology

### 5.3.1 Design of experiments

The machining tests were performed with the parameters listed in Table I using three tools sharing the same characteristics. The cutting parameters were selected from the literature according to the best operational cutting conditions for a similar tool and CFRP material [7]. One tool was used for each test. The tools were used until the tool life criterion was reached. The limit was fixed at the



0.3 mm maximum average wear, named  $VB$  in this study, as described in ISO 8688-2:1989 standard [8].

Table 5.1: Chosen cutting parameters for the machining tests

Test Tool	Feed (mm/min)	Speed (m/min)	Feed (mm/rev)	Feed ( $\mu\text{m}/\text{rev}/\text{tooth}$ )
1	1524	400	0.114	19
2	2794	300	0.279	46
3	4064	200	0.608	101

### 5.3.2 Experimental setup

The machining experiments were performed with a 3-axis Huron<sup>®</sup> K2X10 computerized numerical control (CNC) machine-tool. This high-speed machining center, allowing a 28 000 RPM maximum spindle speed at 30 kW, was geared up with a dust extraction device for health and safety purposes. The setup mounted on the CNC machine allows to machine short and long cuts: the long cut setup was used to generate tool wear only, the short cut setup was used to machine coupons in order to inspect them fully. Short and long cuts were performed alternatively until the tool life criterion was reached.

An end mill router with six flutes was selected to conduct the machining tests. This tool has a 3/8" diameter, a 10° relief and helix angle and a 8° rake angle as geometrical properties and a diamond chemical vapour deposition as coating property.

The laminated composite is a quasi-isotropic CFRP composite, prepared using pre-impregnated plies with the  $[90^\circ/-45^\circ/+45^\circ/0^\circ/+45^\circ/-45^\circ/+45^\circ/-45^\circ/0^\circ/-45^\circ/+45^\circ/90^\circ]_s$  stacking sequence. This autoclave-cured composite has a 4.44 mm thickness with a 64 % fibre volume fraction.

### 5.3.3 Measurements

The CFRP coupons were inspected using the Keyence<sup>®</sup> VHC-600+500F optical microscope and Hitachi<sup>®</sup> S-3600N scanning electron microscope (SEM).

The cutting tool was observed using the Keyence<sup>®</sup> optical microscope allowing to give an estimation of the tool wear  $VB_{max}$ . The tool wear  $VB$  was then calculated as the average of the tool wear  $VB_{max}$  estimated for each of the clearance faces of the six tool flutes.

The surface texture of the coupon was examined using the Mitutoyo® SV-CS3200 profilometer. To compare all the measurements with each other, a common sampling length was selected, as shown in Table II. The measurements were performed for both up- and down-milling coupon faces, in the feed direction, which is also oriented in the ply plane. Figure 2 depicts the measurement area where the measurements were performed. For each face, only the eight central plies were inspected, and four measurements were realized by ply orientation. The stylus used was the 12AAC731 standard stylus with a 2  $\mu\text{m}$  tip radius and a 60° tip angle.

Table 5.2: Profile length datasheet

<b>Roughness sampling length or cut-off length</b>	2.5 mm
<b>Evaluation length</b>	12.5 mm
<b>Waviness sampling length</b>	25 mm
<b>Lowest roughness sampling length</b>	0.008 mm

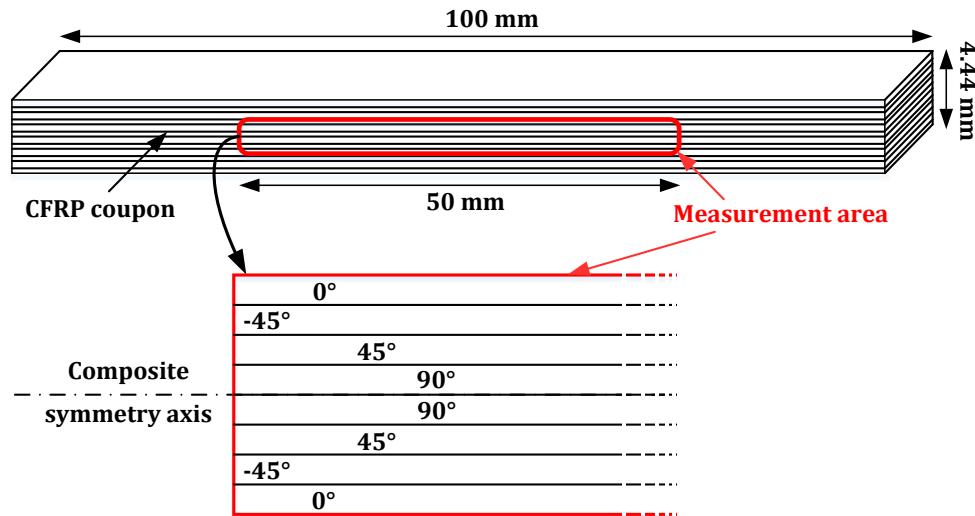


Figure 5-2: Measurement area on the machined coupon face

To ensure the stylus remains in contact with one ply only during the measurement of one whole profile, the CFRP coupon was gripped into a vice which was mounted on a compact compound cross table. This cross table allows to orientate and to position the coupon towards the stylus trajectory with micrometric screws.

The primary profiles measured were filtered using the phase correct function filter based on the Gaussian probability density function as described in the ISO 11562:1996 standard [9] and for a 2.5 mm cut-off length as presented in Table II. This filter was selected because it is currently the

most commonly used filter nowadays even though it may be affected by outliers and induce profile edge distortion. To evaluate the negative impacts of this filtering, other filters were used such as the robust Gaussian filter but no major impact was observed on the roughness parameters values.

### 5.3.4 Calculated roughness parameters

Before parametrizing the surface roughness using the autocorrelation function and the fractal analysis, preliminary analysis has been conducted by observing the roughness profiles. Some examples of the roughness profiles are presented in Figure 3. Surface profiles vary depending on the tool wear, the cutting parameters and the ply orientation. The main pattern in the roughness profiles shows a periodic oscillation (e.g. curves “a” for  $0^\circ$  and  $+45^\circ$  ply orientations in Figure 3). However, its period is not related to the feed per tooth and the period value is different depending on the face milling type. Concerning the tool condition impact, the main profile oscillating pattern variations induced by the tool wear increase are a decrease of the oscillating pattern amplitude and an increase of the same oscillating pattern period. With a highly worn tool, the roughness profile seems to be more erratic and affected by noise.

Due to the noise in the measured roughness profiles, the power spectral density function was not selected to determine this main periodic pattern. Instead, on the one hand, if there is a periodic pattern, its period length can be identified with the autocorrelation function. On the other hand, the fractal analysis is able to quantify the profile complexity and regularity.

From the roughness surface profiles, the current surface profile roughness parameters were calculated based on the standard recommendations of ISO 4287:1997 [10] and 13565-2:1996 [11].

Besides those roughness parameters calculations, the autocorrelation function was computed giving the normalized autocorrelation function  $acf$  (Figure 4). Six roughness parameters were based on the  $acf$  presented in Figure 4: the abscissae – called  $R_{AC_{min\ or\ max}}x$  – and ordinates – called  $R_{AC_{min\ or\ max}}z$  – of the first local minimum and maximum reached (black squares in Figure 4), the first abscissa – called  $R_{AC_0}x$  – when the  $acf$  curve reaches the y-axis (grey rhombus in Figure 4) and the average deviation towards zero of the  $acf$  curve – called  $R_{AC}a_0$  – (dash-dot line in Figure 4).

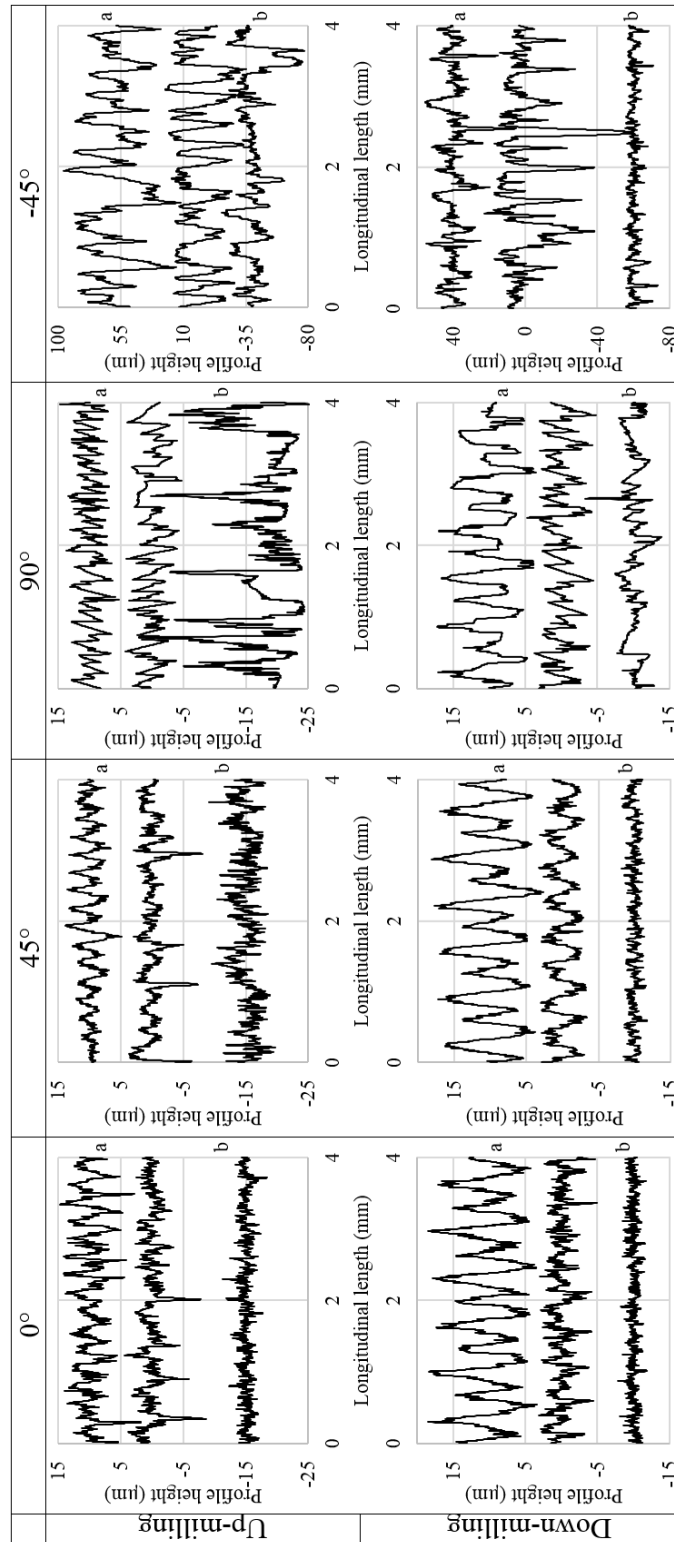


Figure 5-3: Roughness profile samples for the four ply orientations and both face milling types and machined with different tool wear (first, ninth and twentieth passes respectively a, b and c, respectively with the tool wear of 0 mm, 0.07 mm and 0.19 mm) of tool 1

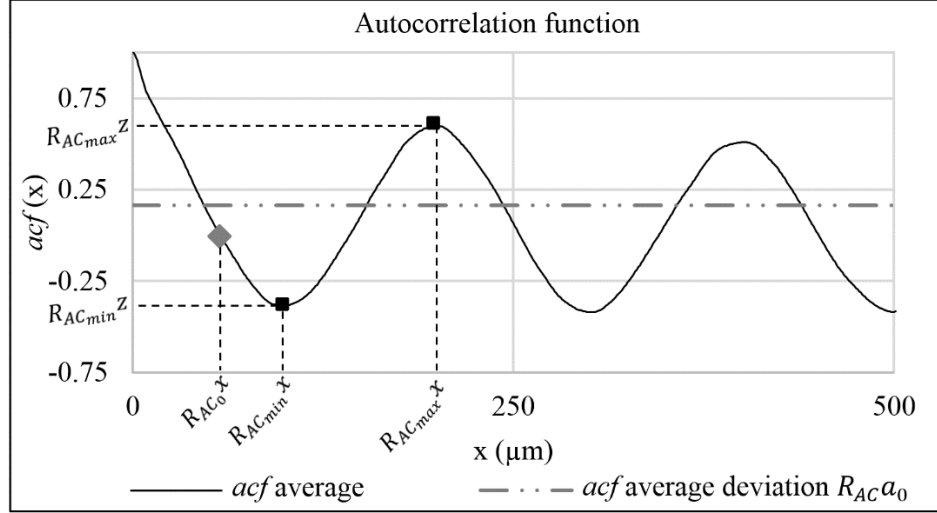


Figure 5-4: Roughness parameters associated with the normalized autocorrelation function  $acf$

The abscissae are correlated with the repetitive pattern period, and the ordinates reflect the importance of those patterns. The  $R_{AC}a_0$  average deviation towards zero of the  $acf$  curve provides information about the autocorrelative profile behaviour.

In this study, the regularization analysis was selected from numerous existing fractal analyses, due to its relative robustness. For example, this technique has already been used to assess any gear damage with the use of accelerometer signals [12]. The regularization analysis consists in the estimation of fractal parameters such as fractal dimension using convolutions of the signal called  $s$  with different kernels  $g_a$  with a width of  $a$  [13, 14]. Each convolution product  $s_a$  can be written:

$$s_a = s * g_a \quad (5.1)$$

The kernel  $g_a$  which was used in our calculation with a width of  $a$  was the rectangle kernel which is an affine function. Then, the hypothesis that  $s_a$  has a finite length called  $l_a$ , for the size of  $a$ , is set. The regularization dimension  $D_R$ , which is an estimation of the profile fractal dimension, can be calculated by:

$$D_R = 1 - \lim_{a \rightarrow 0} \frac{\log l_a}{\log a} \quad (5.2)$$

The limit, in the equation 2, is usually estimated as the slope value when  $a$  values are close to 0 and when the coefficient of determination  $R$ -squared of the linear regression of a part of the curve

is close to 1. Figure 5 depicts the fractal dimensions determination graphs for different tool wear of tool 1.

From preliminary analyses, two ranges of the slope determination were selected and identified in Figure 5. One which is in a high range scale, was chosen between one and two cut-off lengths (section between dot lines in Figure 5) and the second one which is in a low range scale, was selected across four and twelve lowest roughness sampling lengths (section between dash lines in Figure 5). Although other selections can be done, from preliminary analysis and observations, the choice of these two ranges is particularly fitting to the tool wear evolution whatever the selected cutting parameters are.

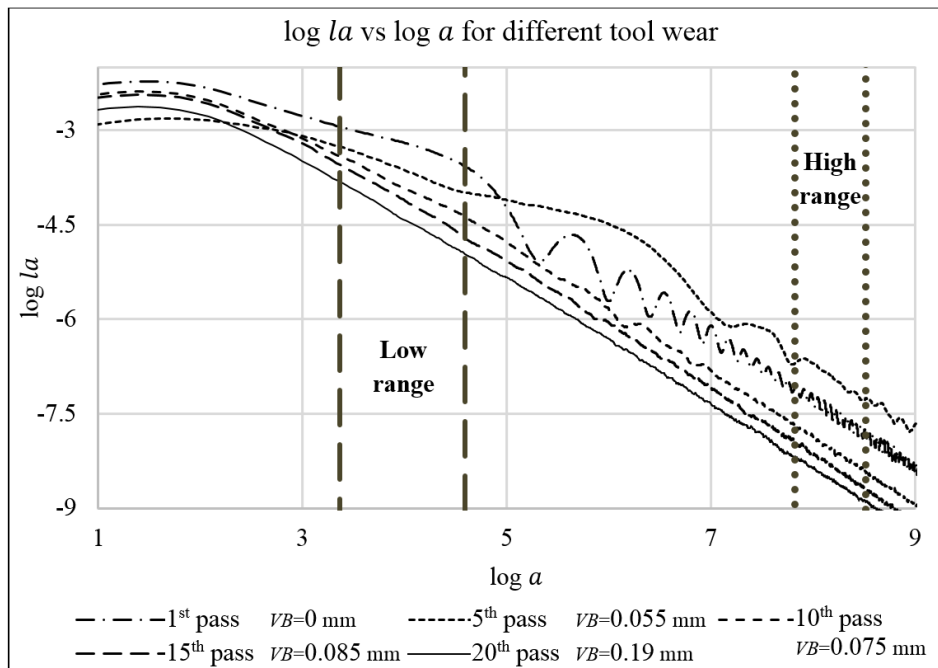


Figure 5-5: Regularization analysis graph using the rectangular kernel

Fractal dimensions were estimated as the slope estimations using the rectangular kernel within the designated graph section. Those fractal dimensions are called  $R_{D\ low}$  and  $R_{D\ high}$ , respectively for the low and high range scales. The topographies  $R_{G\ low}$  and  $R_{G\ high}$  were the intercept calculated from the same slope estimations for respectively for the low and high range scales.  $R_{D\ low}$  and  $R_{D\ high}$  are parameters which are the fractal dimensions, characterizing the regularity or auto-scale behaviour of the profile. ( $R_{G\ low}$  and  $R_{G\ high}$ ) are parameters characterizing the ruggedness of the roughness profile at the range scale selected.

An additional fractal parameter ( $R_{R^2\ low}$  and  $R_{R^2\ high}$  for respectively for the low and high range scales) was the coefficient of determination of the linear regression from the same slope estimation of the graph section. This additional fractal parameter was also introduced due to observations of the log-log curve in Figure 5. The curve seems strongly impacted by the behaviour change of the profile roughness with the tool wear: with a new tool, the curve is bumpy, and with a worn tool, the curve is smoother. This last parameter  $R^2$  can be perceived as an index of the roughness profile complexity variation at the range scale selected.

## 5.4 Results and discussion

### 5.4.1 Roughness profiles

From the observations of the different roughness profiles in Figure 3, for  $0^\circ$  and  $45^\circ$  ply orientation with a low tool wear, a periodic oscillation pattern can be identified (e.g. curve “a” for the  $0^\circ$  ply orientation in up-milling in Figure 3). The period value is different depending on the milling type, for example it reaches  $270\ \mu\text{m}$  for the up-milling side of the coupon and  $670\ \mu\text{m}$  for the down-milling side of the coupon for  $0^\circ$  or  $45^\circ$  ply orientation in Figure 3. Both observed periods are different compared to the feed per tooth. For a homogeneous material such as aluminium and titanium alloys, the periodic oscillation patterns are tool marks that can be correlated with the cutting feed. During the machining, the tool is not fracturing the fibres one by one when the pressure is applied by the tool cutting edge. Because, in this case, the tool mark length would be similar to the observed roughness profile period. Instead, the fibres are fractured by relatively small fibre groups apparently due to bending or shearing. This may be due to the structure of the composite. The inner part of the CFRP used is constituted of resin and threads of carbon fibres. The number of fibres within a thread may influence the size of the fractured fibre group and so on the noticeable period on the roughness profiles.

With the tool wear increase, the observed periods are increasing as well. At the same time, the profiles seem more affected by noise and these oscillation periods tend to be more difficult to detect (e.g. curve “c” for the  $+45^\circ$  ply orientation in up-milling in Figure 3).

Concerning the  $90^\circ$  ply orientation roughness profiles, no main oscillation period is easily observable, especially on the up-milling side of the coupon. The profile behaviour seems erratic.

With the tool wear increase, the measured profiles remain similar until reaching a high tool wear generating an apparently more erratic behaviour.

The profiles measured on the down-milling side of the  $-45^\circ$  ply orientation does not allow to distinguish a periodic pattern easily. With the tool increase, the surface texture is similar to deeper narrow cavities and then becomes extremely smooth for the highly worn tool. On the up-milling side of the  $-45^\circ$  ply orientation, relatively similar observations can be formulated.

Average values of the roughness parameter  $Ra$  are plotted vs the tool wear  $VB$  in Figure 6. The  $Ra$  parameter variations are different and are essentially depending on the tool. Furthermore, the ranges of the  $Ra$  parameter values does not allow to identify a change of surface quality for the three tools. Thus, as said in introduction, this parameter  $Ra$  is not adequate to describe the surface texture of machined CFRP.

Main results obtained with the autocorrelation analysis and the fractal analysis are presented in the following sections. Only one parameter from each is presented to illustrate the new proposed roughness parameters characterization capabilities. The average values of each illustrating parameter can be then compared with the results of the parameter  $Ra$ .

### 5.4.2 Autocorrelation

From the autocorrelation analysis, the  $R_{AC}a_0$  average deviation towards zero of the  $acf$  curve (dot-dash line in Figure 5) was selected to be presented. The lowest value – closest to zero – corresponds to a profile with a very low profile autocorrelation. No specific repetitive pattern can be easily identified in this case. Figure 7 displays autocorrelation functions samples calculated from roughness profiles for up- and down-milling sides, for the four ply orientations and for different tool wear. This parameter allows to identify relatively easily the tool wear and so the surface quality machined, whatever the ply orientation of  $0^\circ$ ,  $45^\circ$  or  $90^\circ$ .

Contrary to  $Ra$  results, for the average values of this roughness parameter, variations towards tool wear are relatively similar for ply orientations of  $0^\circ$ ,  $45^\circ$  and  $90^\circ$ , for each tool and each milling type. However, the roughness parameter variations trends vs the tool wear are different for the results obtained with the  $-45^\circ$  ply orientation.



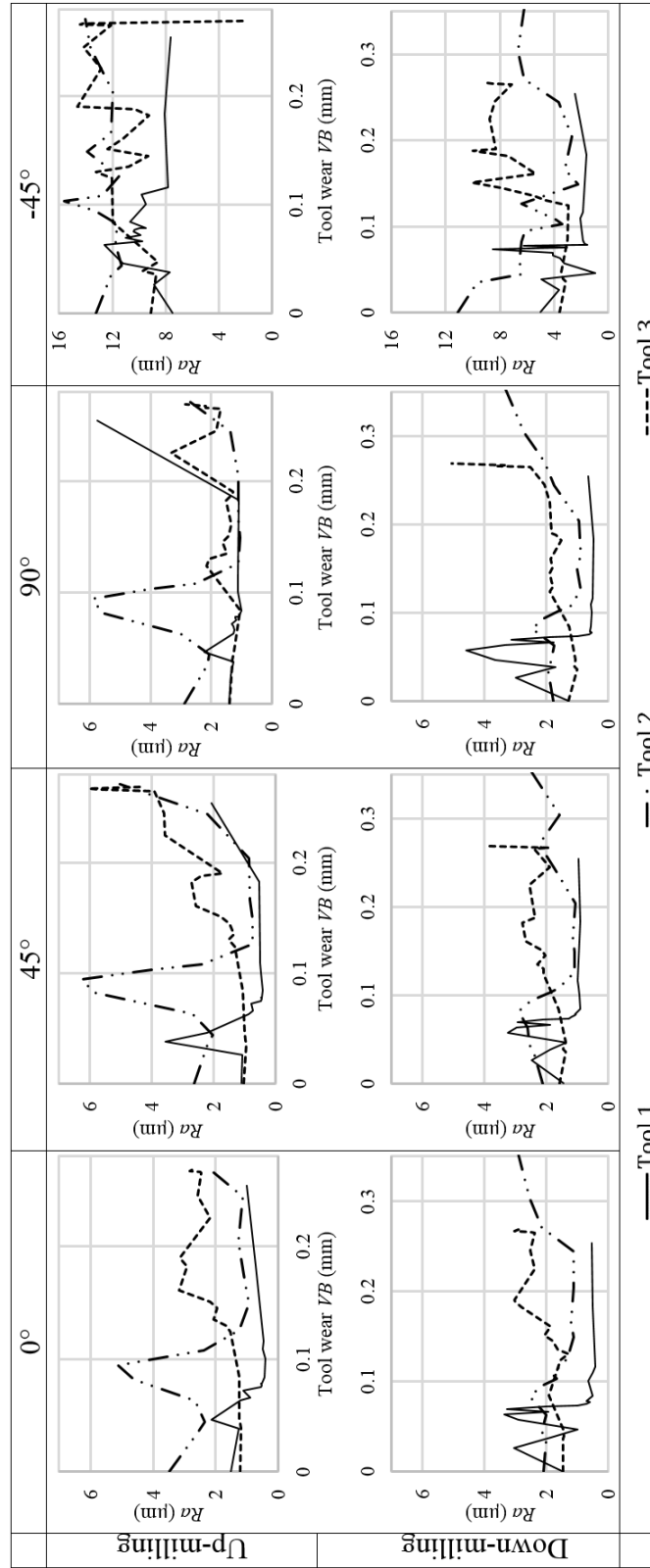


Figure 5-6: Roughness parameter  $Ra$  values average vs. the averaged tool wear  $VB$  for the four ply orientations and both milling types

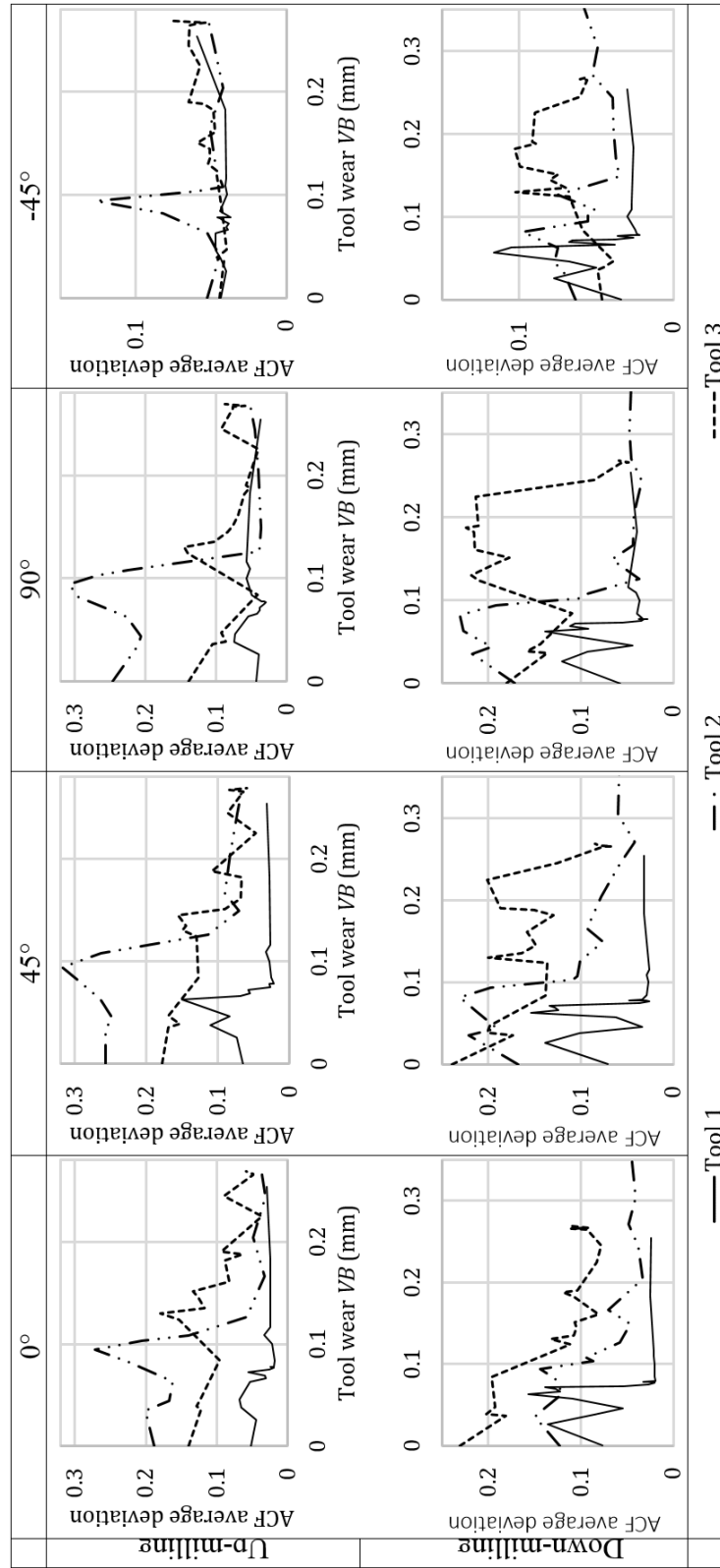


Figure 5-7: Autocorrelation results  $R_{AC}a_0$  average ( $acf$  average deviation towards zero) vs the averaged tool wear  $VB$  for the four ply orientations and both milling types

Similar variations are also noticeable between the tools e.g. for the results from the three tool for a  $0^\circ$  orientation ply in down-milling. The decrease of the  $R_{AC}a_0$  parameter can be associated with an increase of the tool wear, and so on with the surface quality decline. This parameter could be a trigger criterion for the surface quality. For e.g., if its value drops below around 0.05 for  $0^\circ$ ,  $+45^\circ$  and  $90^\circ$  ply orientations, the surface should be investigated further in order to check that the machined surface quality is according to the requirements.

### 5.4.3 Fractal analysis

From the fractal analysis, only the coefficient of determination  $R_{R^2 \text{ high}}$  of the highest range was selected to illustrate those new roughness parameters characterization capabilities. In Figure 8, the coefficient of determination of the highest range is displayed with both milling types, the four different ply orientations and different tool wear. In each figure from Figure 8, the results of the three different cutting parameters from identical tools are presented. Similarly, the results obtained with the average deviation towards zero of the  $acf$  curve, the fractal parameter curves have comparable variations between ply orientations of  $0^\circ$ ,  $45^\circ$  and  $90^\circ$  for each tool and each milling type as opposed to the results obtained with the  $-45^\circ$  orientation ply. Similar variations are also noticeable between the tools e.g. for  $0^\circ$  orientation ply in down-milling. In this last case, for a low tool wear, the parameter  $R_{R^2 \text{ high}}$  value admits a relatively wide range of variation to, then, with the increase of the tool wear, increase and stabilize around a value close to 1.

To improve the monitoring process through the surface texture check, the ratio of the  $R_{R^2 \text{ high}}$  over its value calculated for a 0 mm tool wear could be introduced. In this case, it could also be a trigger criterion for further investigations of the surface quality (e.g. for a ratio over than 20%).

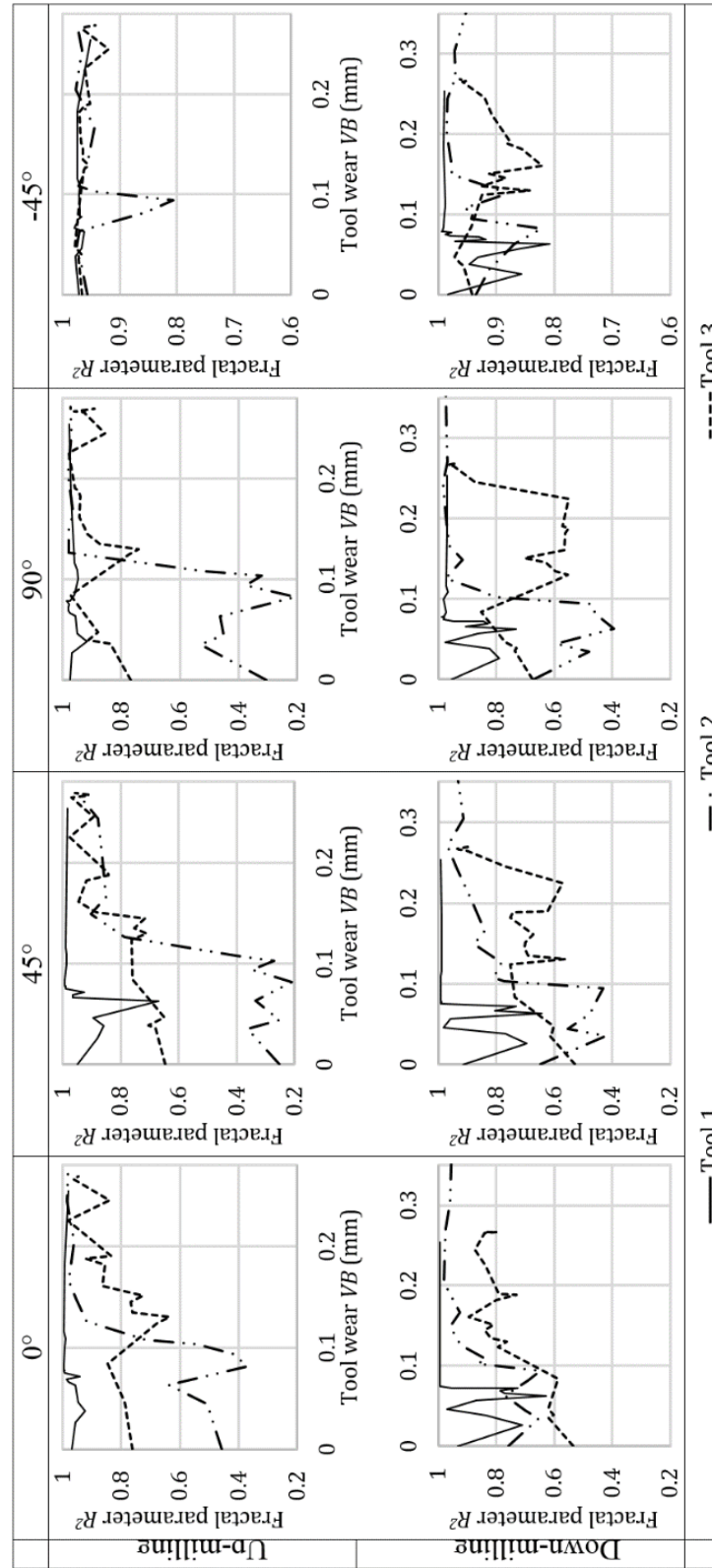


Figure 5-8: Fractal parameter  $R_{R^2 \text{ high}}$  results average vs the averaged tool wear  $VB$  for the four ply orientations and both milling types

## 5.5 Conclusion

Current roughness parameters (such as  $Ra$ ) have some limitations to describe the surface profiles of machined composites. In this study, new roughness parameters are proposed to characterize the surface texture of CFRP composites. Those new parameters are based on the autocorrelation function and on the fractal theory using the fractal parameters. Results show their efficiency to describe the regularity and complexity of the profiles. Observations of roughness profiles show surface marks due to the breakage by groups of the fibres. Those marks are relatively similar to tool marks on a homogenous material machined surface but cannot be correlated with the feed but seem strongly correlated with the tool wear. Those repetitive profile patterns can also be identified and their period can be estimated using the roughness parameters introduced in this study. However, the presented results of the proposed roughness parameters have some limitations but are accurate for most cases and may be complementary to current roughness parameters. A combination of those new parameters and the current ones could be the solution to accurately describe the surface texture of a laminated composite in the ply plane.

## 5.6 Acknowledgements

This work was funded by the Consortium for Research and Innovation in Aerospace in Québec (CRIAQ) and its partners, the Natural Sciences and Engineering Research Council of Canada (NSERC), Bombardier Aerospace, Avior Integrated Products, Delastek and AV&R Aerospatiale. The authors wish to thank Mr. Hossein Hamedanianpour for conducting the experiments with the help of Mr. Réjean Roy, and Mr. David Chapelier for measuring the surface profiles. To develop those novel roughness parameters, a program fragment was used from the software FracLab engineered by INRIA in France.

## 5.7 References

- [1] Wern CW, Ramulu M, Colligan K. A study of the surface texture of composite drilled holes. *Journal of Materials Processing Technology*. 1993;37:373-89.
- [2] Palanikumar K, Karunamoorthy L, Karthikeyan R. Assessment of factors influencing surface roughness on the machining of glass fiber-reinforced polymer composites. *Materials & Design*. 2006;27:862-71.

- [3] Ghidossi P, Mansori M, Pierron F. Influence of specimen preparation by machining on the failure of polymer matrix off-axis tensile coupons. *Composites Science and Technology*. 2006;66:1857-72.
- [4] Chatelain JF, Zagbani I, Monier J. Effect of Ply Orientation on Roughness for the Trimming Process of CFRP Laminates. *World Academy of Science, Engineering and Technology*. 2012;68:987 - 94.
- [5] Mandelbrot B. *Les objets fractals : Forme, hasard et dimension* France: Flammarion; 1975.
- [6] Davim J, Barman T, Sahoo P. *Fractal Analysis in Machining*: Springer Berlin Heidelberg; 2011.
- [7] Bérubé S. Évaluation de la performance d'outils de coupe dédiés au détournage de structures composites carbone/époxy: École de Technologie Supérieure (Université du Québec à Montréal); 2012.
- [8] International Standard Organization I. Tool life testing in milling. Part 2: End milling 1989. p.26.
- [9] International Standard Organization I. Geometrical Product Specifications (GPS) -- Surface texture: Profile method. Metrological characteristics of phase correct filters 1996. p. 7.
- [10] International Standard Organization I. Geometrical Product Specifications (GPS) -- Surface texture: Profile method. Terms, definitions and surface texture parameters 1997. p. 25.
- [11] International Standard Organization I. Geometrical Product Specifications (GPS) -- Surface texture: Profile method. Surfaces having stratified functional properties -- Part 2: Height characterization using the linear material ratio curve 1997. p. 6.
- [12] Feng Z, Zuo MJ, Chu F. Application of regularization dimension to gear damage assessment. *Mechanical Systems and Signal Processing*. 2010;24:1081-98.
- [13] Lévy Véhel J, Legrand P. Signal and image processing with Fraclab. In: *Proceedings of Fractal04 CaFiN*, editor. Eighth International Multidisciplinary Conference Vancouver, Canada 2004.
- [14] Roueff F, Lévy Véhel J. A Regularization Approach to Fractional Dimension Estimation. In: *Novak MM*, editor. *Fractals 98*: World Scientific; 1998.

## **CHAPTER 6      ARTICLE 3: SURFACE PROFILE TEXTURE CHARACTERIZATION OF TRIMMED LAMINATED COMPOSITE IN THE STACKING SEQUENCE DIRECTION**

Xavier Rimpault<sup>a</sup>, Jean-François Chatelain<sup>b</sup>, Jolanta E. Klemberg-Sapieha<sup>c</sup>, Marek Balazinski<sup>a</sup>

<sup>a</sup>Department of Mechanical Engineering, Polytechnique Montréal, Canada

<sup>b</sup>Department of Mechanical Engineering, École de Technologie Supérieure, Canada

<sup>c</sup>Department of Engineering Physics, Polytechnique Montréal, Canada

\* Published in *Measurement*, vol.91, pp.84-92, 2016.

### **6.1 Abstract**

The surface texture characterization of laminate composites is complex due to its heterogeneous structure and to the different stratified surface properties. Profile roughness parameters are highly impacted by those different layer properties, and their distributions are relatively spread out. A new filtering technique is proposed to improve the surface roughness parameter efficiency. To present issues from current filtering methods and to highlight this new approach, profile surface roughness taken from trimmed carbon fibre reinforced plastics samples are inspected in the composite stacking sequence using a contact profilometer. For each measurement, several roughness parameters are calculated. The efficiency of different filtering techniques is investigated through the roughness parameters distribution, calculated for up- and down-milling and for different tool wear. The new proposed technique, based on the separate characterization of plateaus and large deep valleys of the composite surface profiles, is found to be particularly efficient on the down milling face.

*Keywords:* Fiber reinforced plastics, topography, roughness, trimming.

### **6.2 Introduction**

#### **6.2.1 Laminated composites**

Laminated composites have been gradually used in the aerospace industry mainly thanks to high strength-to-weight ratios. Due to current manufacturing processes, composites are produced close

to their final shape. However, some machining operations are still required, such as trimming and drilling, to finish the parts. The surface texture needs to be investigated to evaluate the machining quality. The topography can be measured by profile evaluation. In this case, two main directions are considered for the trimmed composite surface. Figure 6-1 depicts both longitudinal and transverse surface profile measurements of a trimmed laminated composite surface.

Surfaces profiles in the ply plane direction and roughness parameters are strongly impacted by e.g. the tool wear and the fibre angle [1]. In other studies [2, 3], it was found a substantial difference of surface profile behaviour of trimmed  $0^\circ$  and  $45^\circ$  ply orientation towards  $-45^\circ$ .

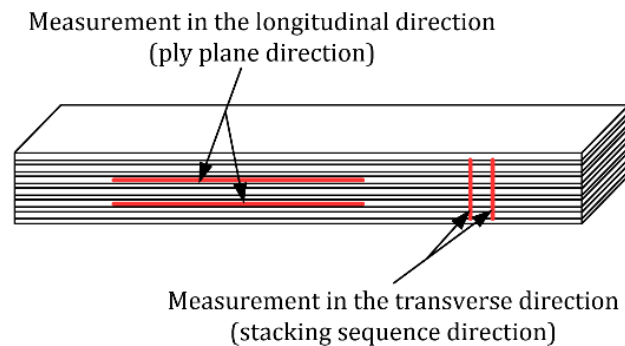


Figure 6-1: Surface profile measurements in longitudinal and transverse direction on a trimmed laminated composite surface

In the transverse direction, the surface texture characterization is more complex. Landon *et al.* found a very poor reproducibility rate for the roughness parameter  $Ra$  from measurement taken both at different heights and at different angular positions towards the hole axis [4]. The issue of high roughness parameter deviation in the ply stacking sequence is due to the inner structure of laminated composites. The composite surface of a trimmed edge or a hole has different stratified texture properties. Those different properties are caused by the different cutting mechanisms of the fibre orientation towards the cutting angle [5]. To perform an accurate roughness texture check, each part should be analysed separately. However, this procedure is time-consuming and cannot be used for industrial applications. Besides this difficulty, it was noticed that each ply admits a relatively high thickness variation. Thus, an automation procedure would be extremely complicated to implement.

Due to the different texture properties of the stratified composite surface, characterization parameters are strongly depending on the measurement position.



### 6.2.2 Surface profile characterization

To characterize a surface profile texture, two main operations are performed: profile filtering and parametrization (Figure 6-2). According to ISO standards, the roughness profile is extracted by filtering the primary profile [6]. The primary profile is obtained by removing the profile nominal form from the measured raw profile using best-fit least-square methods as mentioned in the ISO 4287:1997 standard [6].

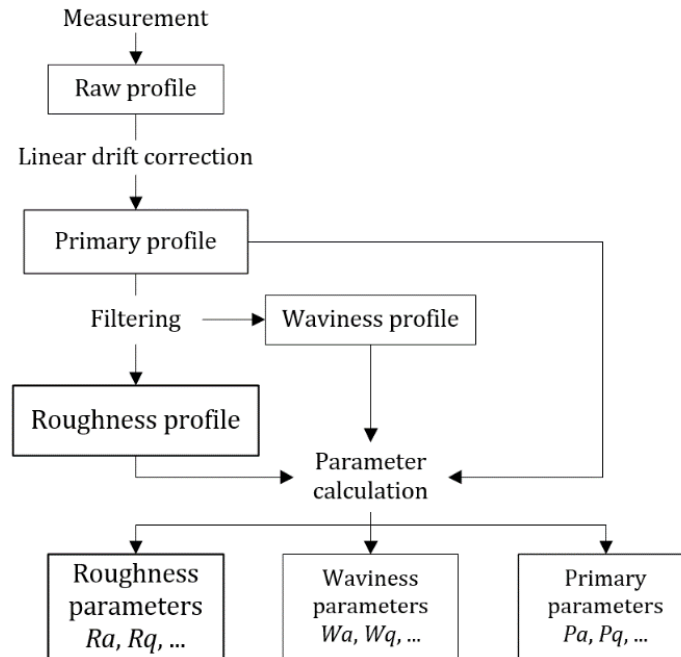


Figure 6-2: Simplified chart of surface profile characterization

The roughness profile is obtained by successively suppressing longwave and shortwave components using the filter characteristics  $\lambda_c$  and  $\lambda_s$ , respectively (Table 6.1). From the primary profile, the waviness profile is extracted as well, using the filter characteristics  $\lambda_c$  and  $\lambda_f$ , which are, respectively, the cut-off length and the intersection between the waviness and the even longer wave components.

Filter can be regrouped in three categories: linear, robust and morphologic filters [7]. The linear filters are traditionally used, such as the phase correct function filter based on the probability Gaussian density function. Robust filters are less sensitive to input data, and morphologic filters can also be called geometric filters.

Table 6.1: Profile characteristics datasheet

<b>Roughness sampling length or cut-off length <math>\lambda_c</math></b>	0.25 mm
<b>Evaluation length</b>	3.75 mm
<b>Waviness sampling length <math>\lambda_f</math></b>	2.5 mm
<b>Pitch</b>	0.0002 mm
<b>Lower roughness sampling length <math>\lambda_s</math></b>	0.0025 mm

Both filtering and parametrization operations may cause additional problems for the composite surface characterization. The former process problem may be inherent to the filter type and its characteristics. The linear Gaussian based filter, described in the ISO 11562:1996 standard [8], is the most commonly used in the industry and for research as well. However, this type of filter may engender edge distortion on the profile and may be altered by outliers. Figure 6-3 shows an example of primary profiles, filtered using different cut-off lengths. In Figure 6-4, roughness profiles are obtained from a primary profile filtered with the Gaussian probability density function and different cut-off lengths. Due to this filtering, various artefacts appears such as artificial peaks (in areas B, C, and E in Figure 6-4), edge distortion (area A), mis-filtered profile (areas C, D, E and G) and valleys (area F).

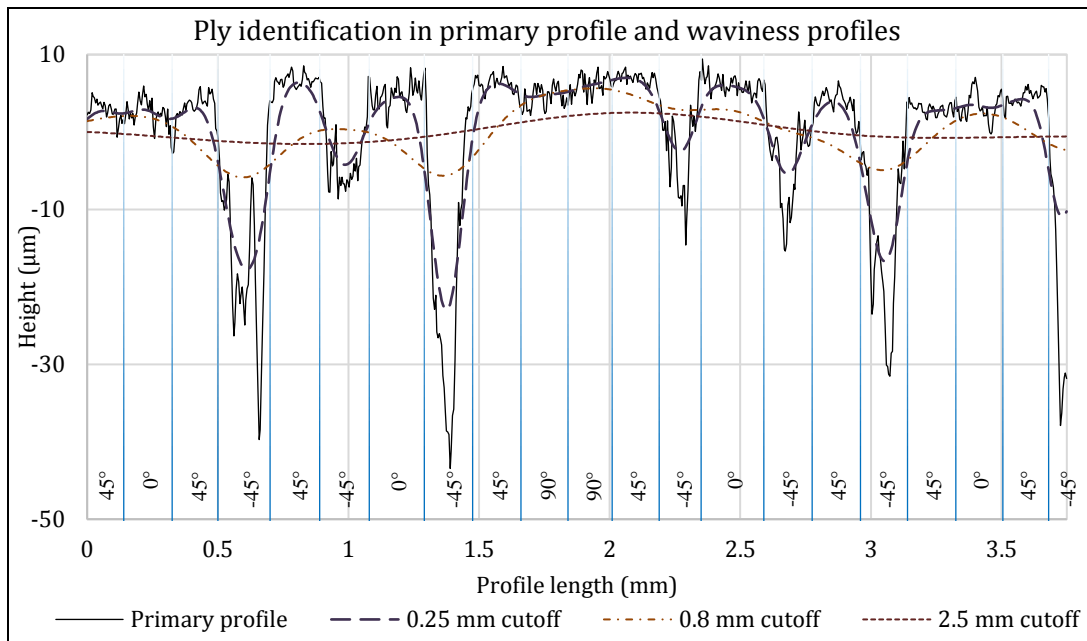


Figure 6-3: Examples of waviness profiles using the Gaussian probability density function filter and different cut-off lengths

Other linear, robust and morphologic filters were used in a preliminary investigation but none of them was really able to limit the problems. Besides its issues, the Gaussian based linear filter is

substantially used in surface roughness analysis. Instead of optimizing filters, this Gaussian based linear filter is used along this study and filtering techniques are to be investigated to limit the filter drawbacks.

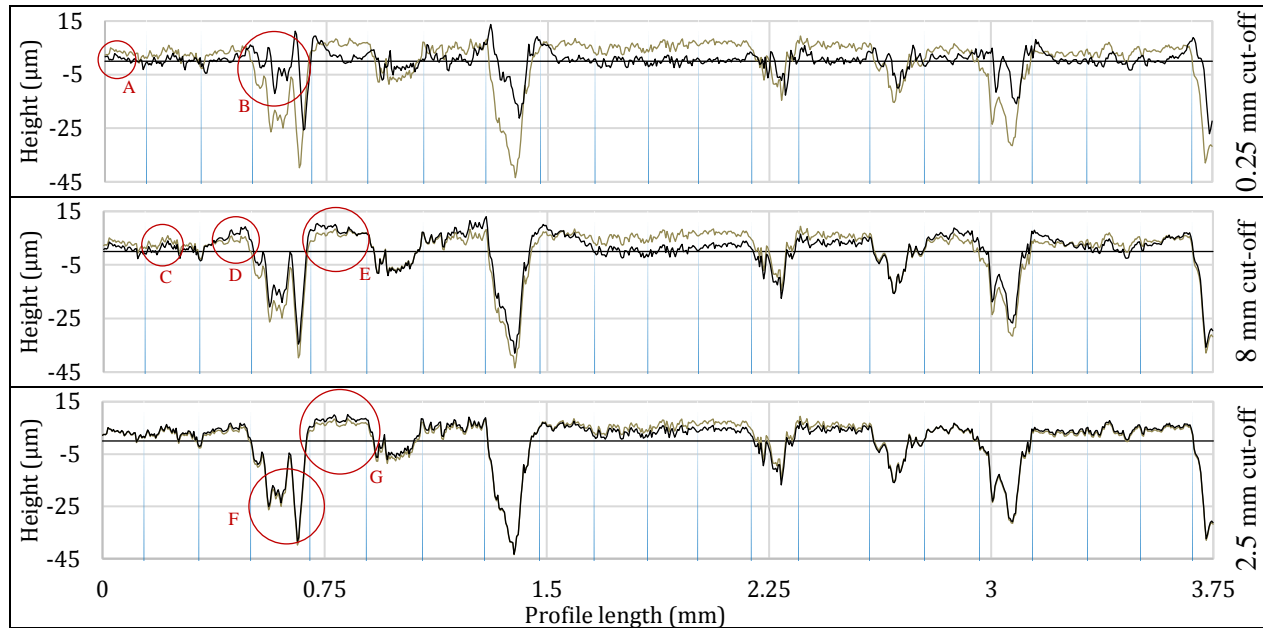


Figure 6-4: Roughness profile examples using the Gaussian probability density function filter and different cut-off lengths (roughness profiles are in black based on the primary profile in grey)

Different filtering techniques and a new filtering method are compared herein. Then, based on the profile roughness, various roughness parameters are calculated to determine the efficiency of the filtering techniques and to classify the reliability of characterizing parameters.

## 6.3 Methodology

### 6.3.1 Primary profiles filtering

The filter characteristics, presented in Table 6.1, are slightly different to the ISO standard recommendations which suggest a 2.5 mm cut-off length instead. This cut-off length is chosen depending on requirements or previously computed roughness parameters. However, based on preliminary filtering, profiles were not adequately filtered. Thus, the calculated roughness parameters are biased and so is the cut-off selection thereafter.

Secondly, setting such a cut-off length requires enough surface in the direction to perform the measurement (which is typically five cut-off lengths according to ISO standards [6, 9]). The

thickness of a laminate composite is usually no more than few millimetres. Thirdly, selecting this relatively short cut-off allows to obtain three typical and uncrossed sampling lengths per measurement.

As previously said, the linear Gaussian based filter can generate artefacts (Figure 6-4). Other filters (in linear, robust and morphologic families) were used in a preliminary study to remove the waviness from primary profiles such as spline based filter and robust Gaussian based filter. However, only low variations were noticed, and the impact on the parameters seemed insignificant. So the linear Gaussian based filter is only used in this study, due to its faster computation towards the other filters tested.

Besides the filtration limits of the linear Gaussian phase correct function filter, the filtering techniques using linear, robust or morphologic filter have pros and cons but they are not the main cause concerning issues of the composite surface texturing. The main problem would come from particular ply orientations such  $-45^\circ$  ply orientation. This ply orientation admits relatively high topographic variations and can be identified as large deep valleys (Figure 6-3).

A filtering technique of this profile type with different stratified surface properties is presented in the ISO 13565-1 standard [10]. This filtering method is particularly efficient for honing surfaces, which profiles contains a higher number of deep valleys. Even if those deep valleys are random, they are numerous and narrower. Roughness parameters generated from such profiles are less impacted by the measurement position. Thus, this ISO 13565-1 filtering technique is adapted to transverse profile composite surface texturing but it can still be improved. The amelioration proposed corresponds to the use of two different cut-offs during this filtering process instead of two identical ones (either 2.5 or 0.8 mm). Figure 6-5 displays this modified filtering technique.

From the preliminary analysis, the use of identical cut-offs has issues: mis-filtered profile parts for 2.5 mm cut-off lengths and artefacts close to the valleys for the 0.8 mm ones. The use of different cut-offs allows to reduce those problems. Firstly, the 2.5 mm cut-off length is selected to generate the first mean line (left in Figure 6-5). Secondly, the 0.25 mm cut-off length is used to generate the waviness of the profile (centre in Figure 6-5). Based on preliminary filtering, the second cut-off should be as close as possible to the ply thickness (0.185 mm in this study), and the first cut-off should be ten times greater than the second one.

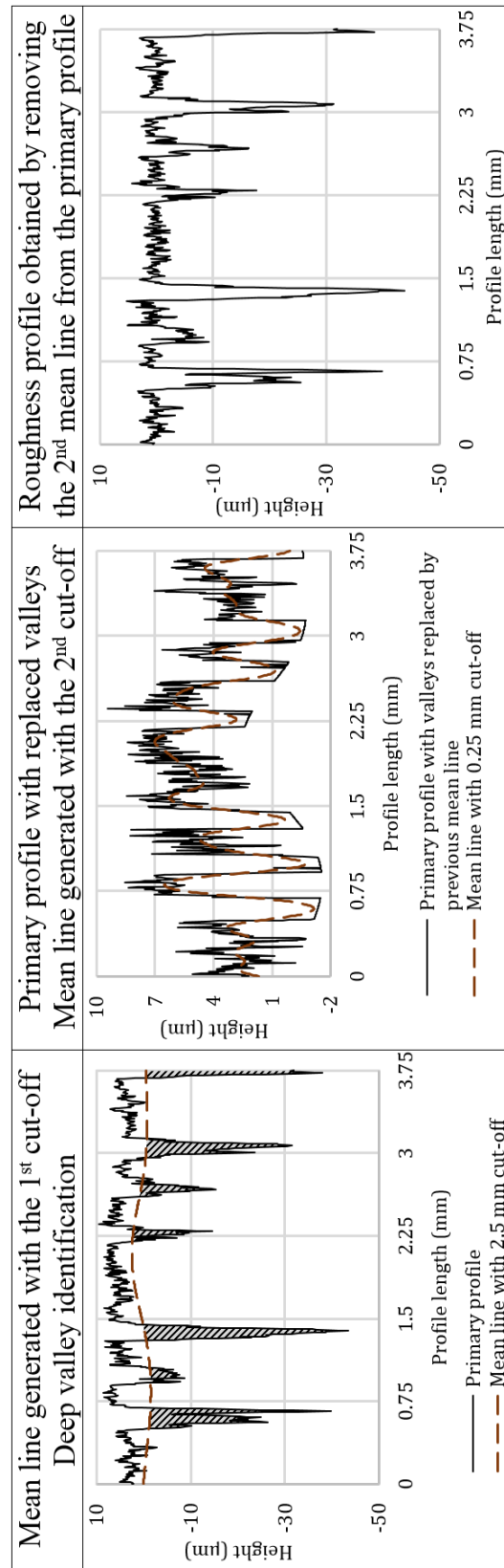


Figure 6-5: Filtering technique using the modified ISO 13565-1 method

In addition to the improvements added to the 13565-1 ISO filtering technique, a method is proposed for characterizing laminate composites in the transverse direction. This method consists in differentiating, and analysing separately, the large deep valleys and the plateaus. The so-called plateaus correspond to the upper surface of the profile. This approach is motivated by the current issue of very poor reproducibility rates of roughness parameters and by the inconsistency of the valley heights and widths.

The characterization of the valleys could be performed after the roughness profile obtained with the modified ISO 13565-1 filtering technique using global shape parameters such as the total profile height or the valley depth.

The plateaus would be obtained after removing the deep valleys from the profile as presented on the chart in Figure 6-6 and on the graph Figure 6-7. After this removal, the profile is filtered using the linear Gaussian function, giving the plateau roughness profile. From this profile, plateau roughness parameters are calculated accordingly. By removing the deep valleys, the evaluation length is reduced. To prevent comparing plateau roughness parameters from different profile lengths, the profile treated should be longer than the sampling length. Then, the plateau roughness profile is reduced to the previously selected evaluation length.

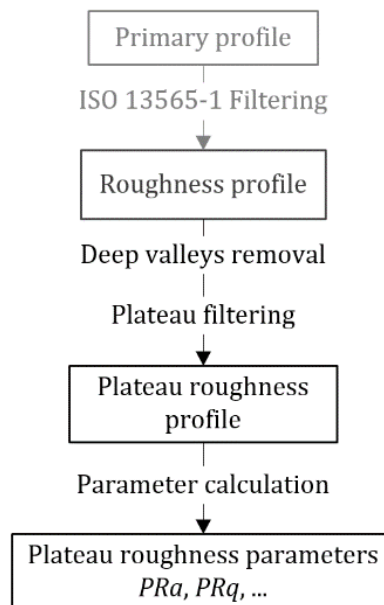


Figure 6-6: Simplified chart of the plateau roughness characterization

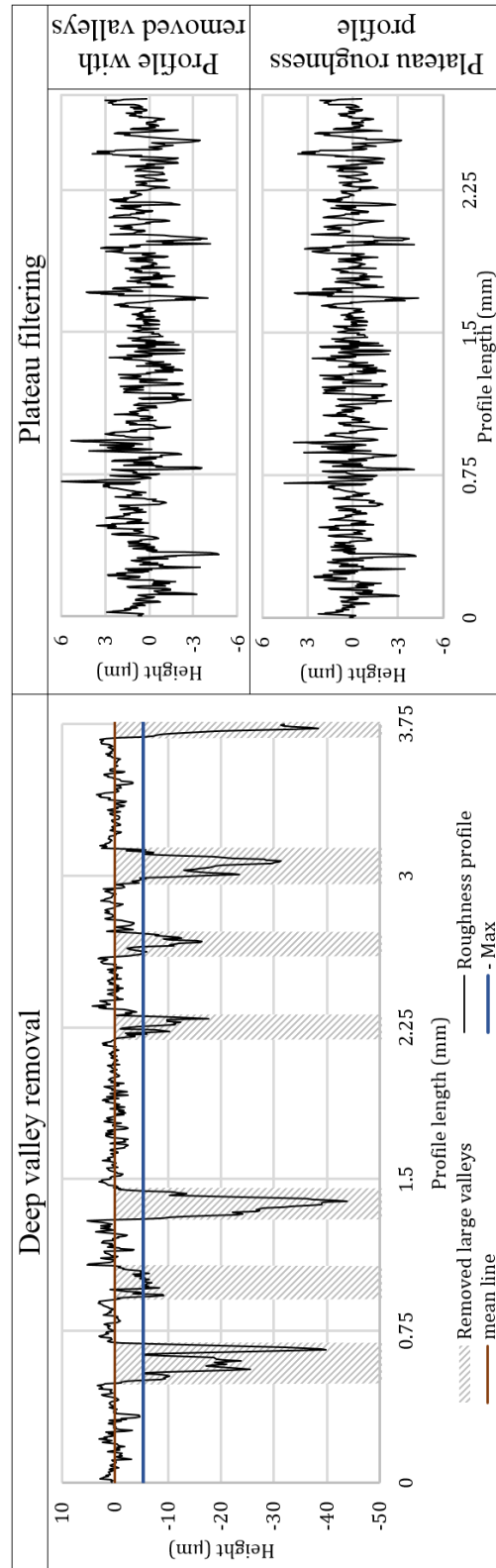


Figure 6-7: Plateau roughness profile example: removal of the profile deep valleys (left), primary and roughness plateau profiles (right)

### 6.3.2 Machining experiments

Machining tests were performed by the trimming of carbon fibre reinforced polymer (CFRP), to highlight the new characterization proposed herein. The cutting parameters, (2794 mm/min feed with a cutting speed of 300 m/min) were selected according to the best operational cutting conditions for similar tool and material from the literature [11].

A Walter Tools® end mill router with six straight flutes was selected to conduct the tests. This tool has a 3/8" diameter, a 10° relief and helix angle and a 8° rake angle as geometrical properties and a diamond chemical vapour deposition coated carbide as material properties. The tool was used with the same cutting conditions until the tool life criterion was reached. The limit was determined as the maximum average wear  $VB$  of 0.3 mm, as described in ISO 8688-2:1989 standard [12].

The machining experiments were performed with the 3-axis Huron® K2X10 computerised numerical control (CNC), geared with a dust extraction device for health and safety purposes. The setup mounted on the CNC machine allows machining short and long cuts: the long cut setup was used to generate tool wear only, the short cut setup was to utilize to machine coupons in order to inspect them fully. Short and long cuts were used alternatively until the tool life criterion was reached [13].

The laminated composite was a quasi-isotropic CFRP composite, prepared using pre-impregnated plies and autoclave-cured leading to a 64 % fibre volume fraction composite part (Figure 6-8).

The cutting tool was observed with the Keyence® VHC-600+500F optical microscope allowing to give an estimation of the tool wear  $VB_{max}$ . The tool wear  $VB$  was then calculated as the average of the tool wear  $VB_{max}$  estimated for each of the six faces of the tool.

### 6.3.3 Profile measurements

The surface texture of each coupon was examined using the Mitutoyo® SV-CS3200 profilometer. All the measurements shared common sampling length, as shown in Table 6.1. The measurements were performed for both up- and down-milling coupon faces, in the ply sequence direction. Figure 6-8 depicts the measurement area where the measurements were conducted. Five measurements of 3.75 mm in length were performed within the 50 mm central area of each face. The stylus used was the 12AAC731 standard stylus with a 2 µm tip radius and a 60° tip angle.



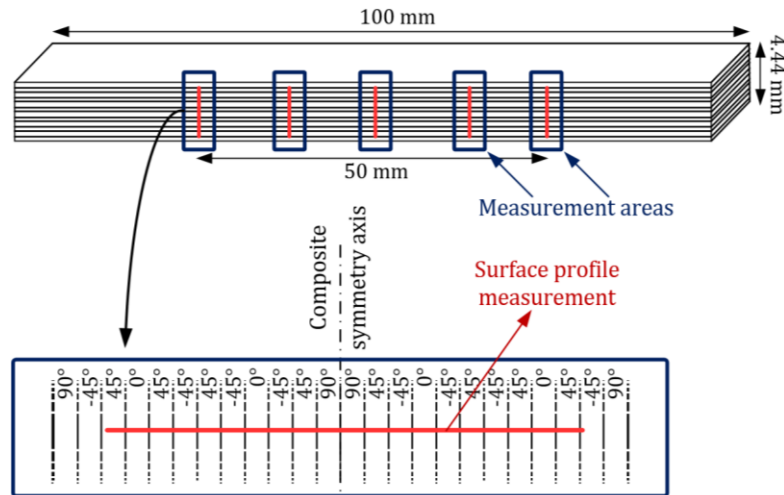


Figure 6-8: Surface profile measurement area on the coupon

### 6.3.4 Parametrization and filtering method assessment

Based on ISO standards, fifteen different parameters were calculated, from the primary profiles, the roughness profiles and the plateau roughness profiles. The fifteen parameters used are shown in Table 6.2.

To evaluate the filtering techniques and parameters reliability, those parameters were calculated with the same evaluation length of 1.25 mm taken from the 3.75 mm measurement range. To simulate the measurement position variations on the parameters, 25 profiles of 1.25 mm in length were taken along each 3.75 mm long measurement. This gives 125 profiles by face coupon and so 125 parameter calculations.

The average, median, amplitude and standard deviation were computed from the values distribution of each face. To facilitate the technique comparison, the relative standard deviation is used, which is given by calculating the standard deviation over the average of the values.

The comparative study was divided into two parts, for up- and down-milling faces. Then, for each up- and down-milling type, the maximum and average values of the relative standard deviation of parameters are presented for each method.

This approach allows to investigate the impact of the profile position within the laminate surface onto the parameters. So, this allows to assess the robustness of the filtering techniques.

Table 6.2: Chosen profile parameters

<b>Z Parameter</b>	<b>Definition</b>
$Za$	Profile average deviation
$Zq$	Profile average square deviation
$Zp$	Average of the highest peak within each cut-off length
$Zv$	Average of the deepest valley within each cut-off length
$Zz$	Sum of $Zp$ and $Zv$
$Zt$	Profile maximum amplitude
$Zsk$	Profile skewness (asymmetry)
$Zku$	Profile kurtosis (flatness)
$Zk$	Clipped profile depth
$Zkp$	Removed peak height
$Zkv$	Removed valley depth
$Mr1$	Peak material ratio curve
$Mr2$	Valley material ratio curve
$A1$	Peak material density
$A2$	Valley material density

### 6.3.5 Complementary analysis

Amplitude Distribution Curves (ADC) and Bearing Area Curves (BAC) were calculated from primary profiles of up- and down-milling faces with different tool wear. The amplitude distribution curve was computed using the height of the primary profiles and fitted using a two-term Gaussian function [14]. This function is representing the profile height probability within the evaluation length.

The bearing area curve also called Abbott-Firestone curve is technically the cumulative probability amplitude density function of the profile [15]. This BAC allows to represent the profile material ratio as a level function. Both curves were calculated for primary profiles and the modified 13565-1 filtered roughness profiles.

## 6.4 Results and discussion

### 6.4.1 Primary profiles

Before proceeding to profile filtering and parametrization, primary profiles were observed and analysed towards the tool wear and milling type. Figure 6-9 displays examples of primary profiles for five different tool wear and on both up- and down-milling faces. For the 12<sup>th</sup> pass and to a higher extent for the 14<sup>th</sup> pass, the profile height is relatively low and uncut fibres can be observed. The surface is particularly damaged for a high tool wear with a dimensional defect (unstraight surface profile). The surface roughness and waviness drastically increases comparing to a lower tool wear. The primary profiles measured on both faces until the 8<sup>th</sup> pass have similar behaviour. The first uncut fibres can be seen from the 8<sup>th</sup> pass.

Besides uncut fibres and surface shape defects, few differences can be noted between up- and down-milling face profiles. Valleys appear to be less deep in down-milling. The roughness or ruggedness of the down-milling profile plateaus seems higher. The surface plateau seems more scatter in this case.

Deep valleys which result from the machining of  $-45^\circ$  orientation ply fibres have different depths and slightly different widths. Due to the composite manufacturing process, the observable thickness of laminate plies may vary. Concerning the various valley depths, this results in the machining process and can be explained by observing profiles of  $-45^\circ$  ply orientation in the longitudinal direction. In the ply plane, the  $-45^\circ$  plies are erratic and admit a relatively high amplitude comparing to other ply orientations [2]. Depending on the measurement location in the transverse direction, the valley can reach different depths. In addition to this valley variation, the number of those deep valleys within the evaluation length can change depending on the measurement position and the composite stacking sequence. Some uncut fibres can be observed on primary profiles for a tool wear  $VB$  above 0.1 mm. Uncut fibres and non-straight machined surfaces can be easily identified in primary profiles for both up- and down-milling faces for a high tool wear ( $VB = 0.27$  mm).

BACs and ADCs of primary profiles are shown in Figure 6-10 for different tool wear and both up- and down-milling. As observed on the primary profiles, the ADCs point out the increase of the profile height with high tool wear. Concerning the BACs, two highlights are noticeable. The valley,

shortening in depth, as well as the valley density decrease, can be observed with the tool wear increase.

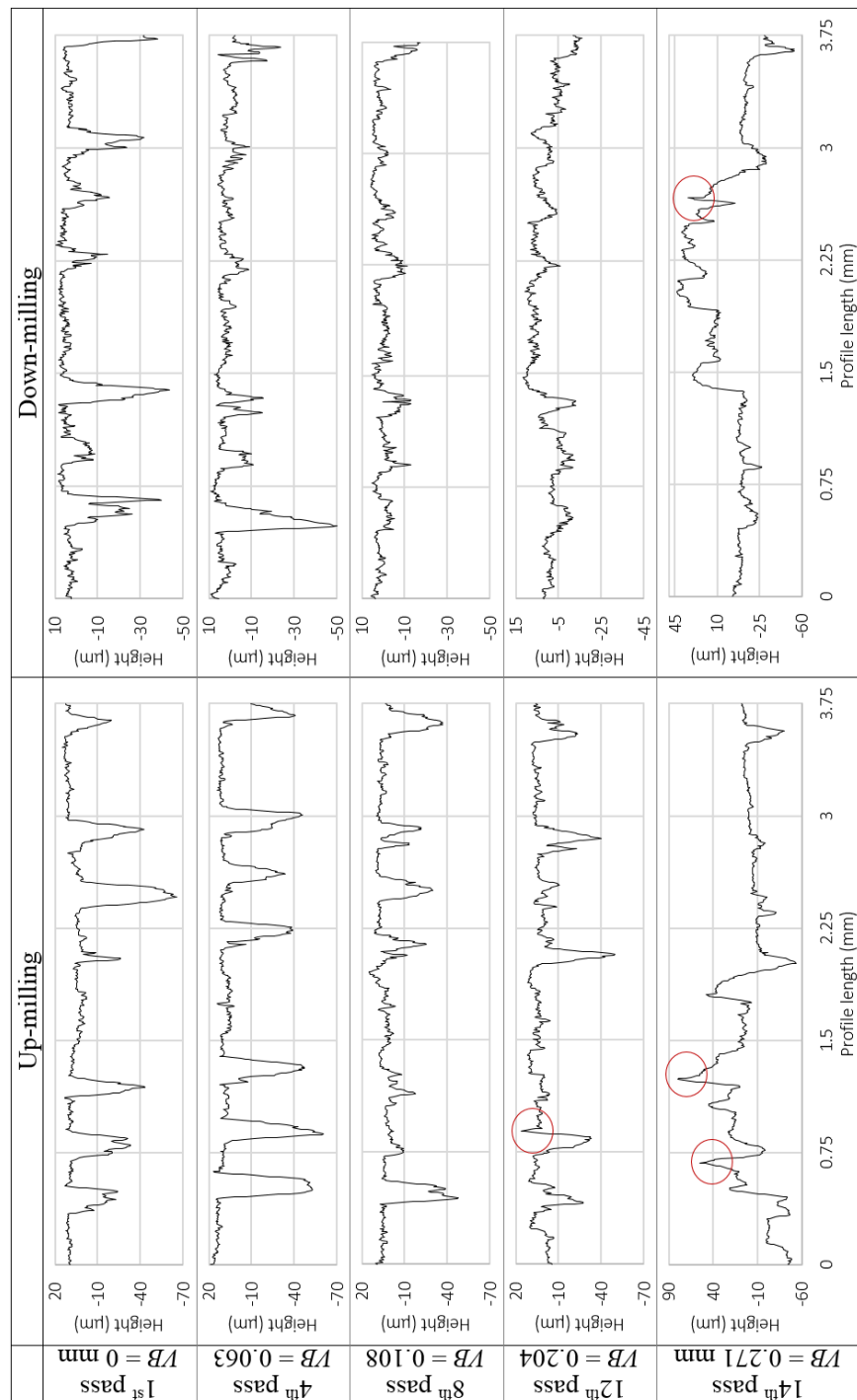


Figure 6-9: Primary profiles examples for different tool wear and both up- and down-milling with the stacking sequence from left to right for each profile:  $[0^\circ/+45^\circ/-45^\circ/+45^\circ/-45^\circ/0^\circ/-45^\circ/+45^\circ/90^\circ/90^\circ/+45^\circ/-45^\circ/0^\circ/-45^\circ/+45^\circ/-45^\circ/45^\circ/0^\circ/+45^\circ/-45^\circ]$  (uncut fibres are circled)

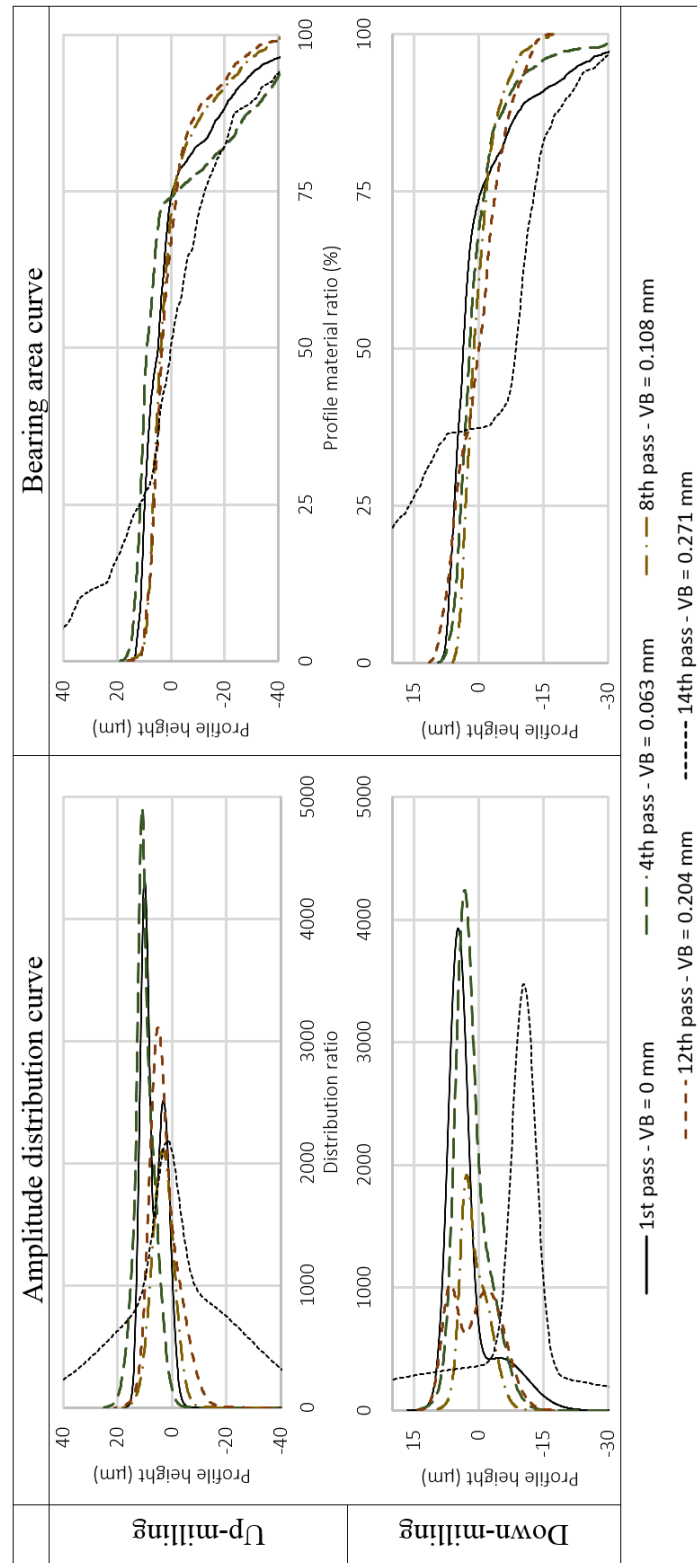


Figure 6-10: Amplitude Distribution Curves (ADC) and Bearing Area Curves (BAC) examples of primary profiles for different tool wear and both up- and down-milling

Relative standard deviations of primary parameters were calculated on each face over 125 values for each primary parameter. The averages and maximums of those relative standard deviations are presented in Table 6.3. Due to the presence of the valleys and their shape variation, primary parameters have a relatively high variability.

Because of the large distribution of the primary parameters, this characterization may not be an efficient technique for laminate composite surfaces. Only shape parameters such  $Pp$ ,  $Pv$  and  $Pt$  show tighter deviation and could be used as complementary indexes. Other parameters show similar results in terms of distribution deviation and so should be avoided as well.

#### **6.4.2 Roughness profiles obtained using linear Gaussian filter**

Most roughness parameters values indicate a lower dispersion range than for primary parameter results (Table 6.3 – b). Only the kurtosis  $Rku$  (profile flatness) shows greater value deviation for both milling types. This can be explained by artefacts introduced by the filtering process such as artificial peaks and edge distortion.

Although lower value deviations are noticed for most parameters, the standard deviation is relatively too high for the parameters to be significant enough.

As presented for primary parameters, shape roughness shape parameters such as such  $Rv$  and  $Rt$  could be used as complementary profile height indexes due to their tighter value variations.

#### **6.4.3 Roughness profiles obtained using standards filtering for different stratified properties surface**

As well as our first observations, parameters from the original technique show higher dispersion than the results obtained with the improved one. It can also be noticed that this ISO 13565-1 filtering technique, official (Table 6.3 – c) and improved (Table 6.3 – d), presents slightly higher roughness parameter deviation in comparison with the results obtained with the linear Gaussian filter. This can be explained by the presence of artefacts generated during the linear Gaussian filtering, where the filtered valleys are less deep than with the ISO 13565-1 technique.

The roughness parameters should be taken from this modified ISO 13565-1 filtering technique because of the lower deviation of the results than primary parameters and especially due to a more reliable roughness surface compared to roughness profiles obtained using the linear Gaussian filter.



Bearing Area Curves (BAC) and Amplitude Distribution Curves (ADC) of roughness profiles are shown in Figure 6-11 for different tool wear and both up- and down-milling. Several points can be noted such as the uncut fibres (seen with the peak height increase in ADC), the valley depth, width and number reduction. Those graphs also show a higher amplitude and flatter distribution of the roughness profile with the tool wear increase.

Roughness parameters, such as  $R_t$  and  $R_k$ , are considered best to describe the global shape profile and the clipped profile roughness. Results of  $R_t$  and  $R_k$  parameters using the modified 13565-1 filtering technique are depicted in Figure 6-12. The parameter dispersion is quite high but some trends can be observed with a sufficient number of measurements. The parameter  $R_t$  allows to estimate the valley height decrease with the tool wear increase. The parameter  $R_k$  can describe the quality decrease occurring at the tool life end.

#### 6.4.4 Roughness profiles with valleys removing

The averages and maximums of the relative standard deviations of roughness parameters are presented in Table 6.4 concerning plateau profile before and after filtration. Plateau roughness parameter have small variations and good reproducibility rates.

Figure 6-13 displays examples of plateau roughness profiles for five different tool wear and both up- and down-milling faces over 1.25 mm evaluation length. Few artefacts can be detected, but they remain marginal. The high plateau roughness for down milling can be observed as well as for primary profiles.

From all parameters calculated, two parameters were found particularly useful estimators of the plateau roughness texture:  $PRa$  and  $PRk$ . The variations of both those parameters vs the tool wear evolution are presented in Figure 6-14. Relatively low standard deviation can be noticed except for high tool wear. This high standard deviation could be caused by the uncut fibres increase observed in the primary profiles with the tool wear increase.

Nevertheless, the selected parameters have some limitations extracting information from the plateau profiles. A parameter able to quantify the ruggedness of the profile could be used allowing a better description of the surface quality or the tool evolution through the surface profile check.



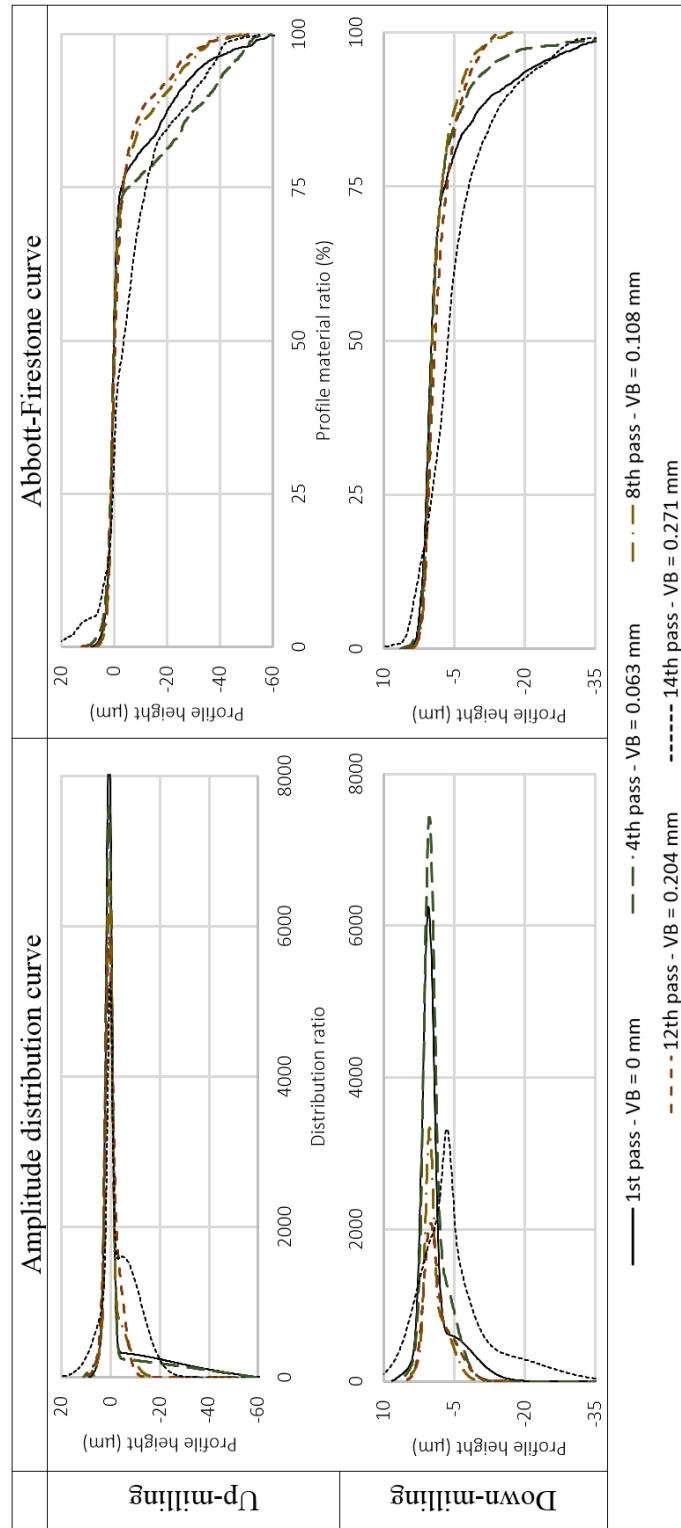


Figure 6-11: Amplitude Distribution Curves (ADC) and Bearing Area Curves (BAC) examples of roughness profiles for different tool wear obtained from filtered profiles using two different cut-off lengths during the ISO 13565-1 standard filtration

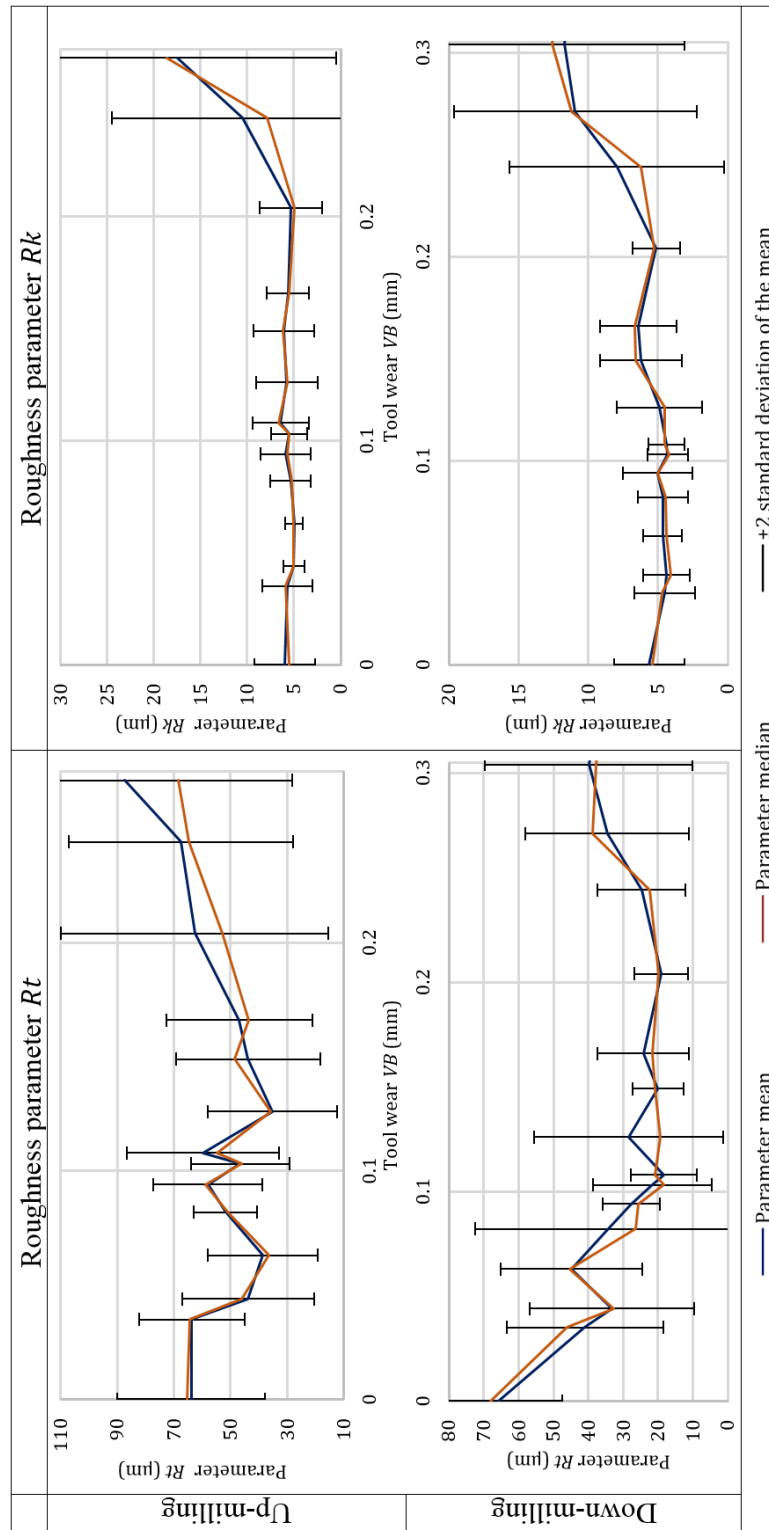


Figure 6-12: Mean and median of  $R_t$  and  $R_k$  roughness parameters for both milling type and different tool wear with the deviation of  $\pm 2$  standard deviation on the mean



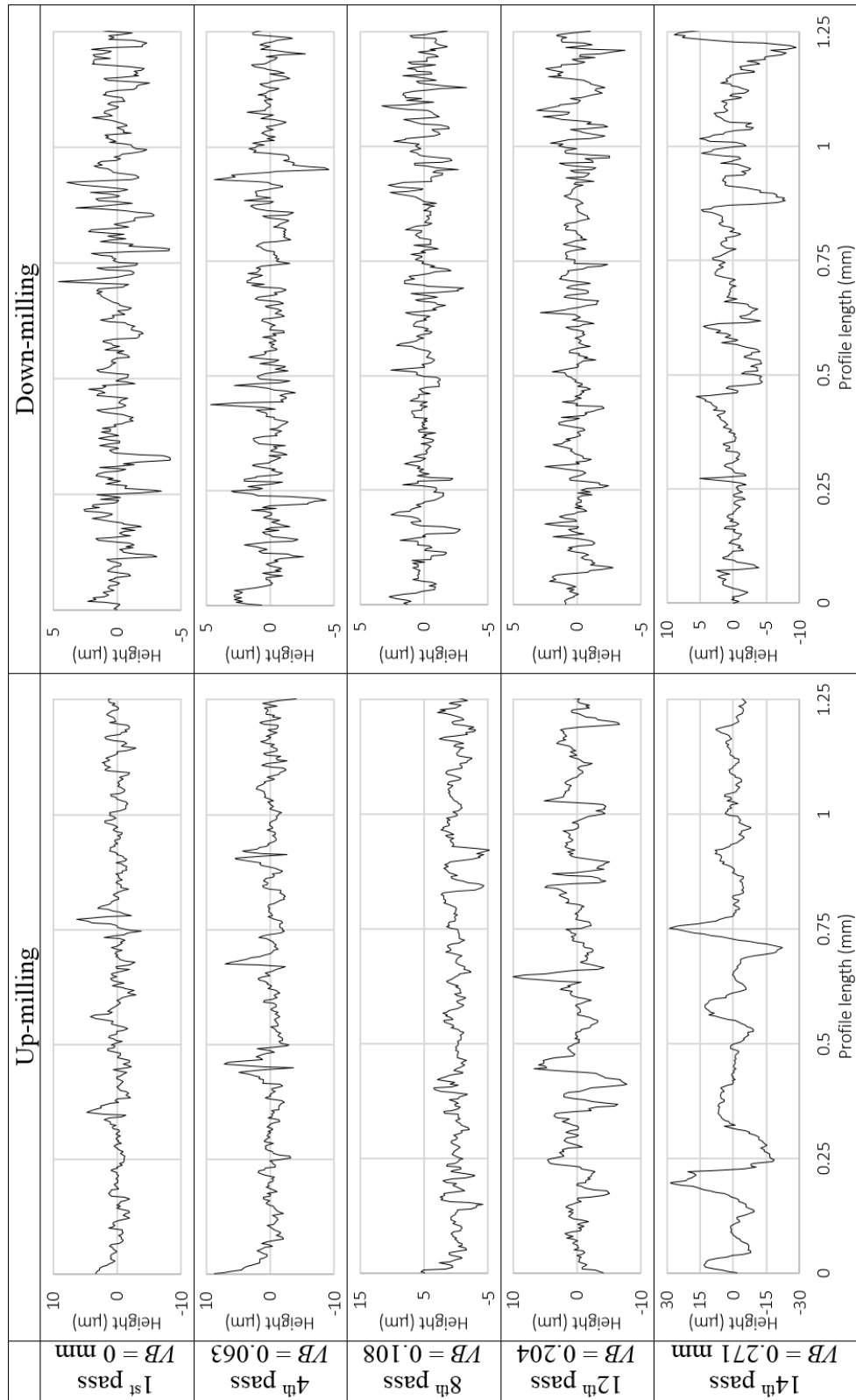


Figure 6-13: Plateau roughness profiles after removing the deep valleys and applying a second filtering

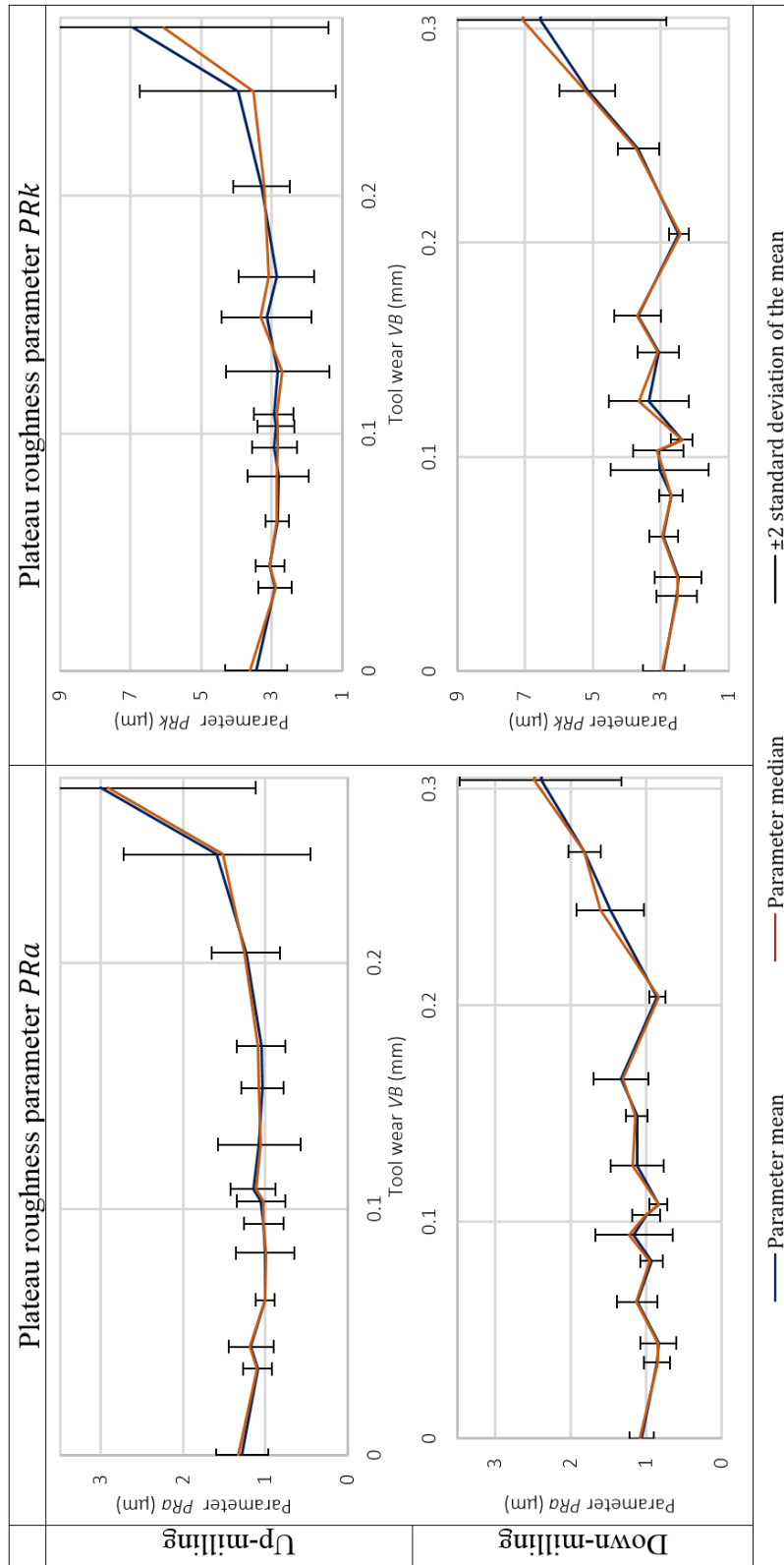


Figure 6-14: Mean and median of  $PRa$  and  $PRk$  roughness parameters for both milling type and different tool wear with the deviation of  $\pm 2$  standard deviation on the mean

## 6.5 Conclusion

A comprehensive study of the surface profile characterization of laminate composites has been conducted in the transverse direction. Different filtration techniques have been investigated, and modifications have been proposed to improve current filtering methods. Moreover, a new approach, consisting in analysing separately profile deep valleys and plateaus, is presented.

Primary and roughness profile characterizations using common parameters (such as the roughness parameters  $Ra$ ,  $Rq$ ,  $Rt$ ) are investigated through relative standard deviations of the parameters. Based on observations and current roughness parameter reproducibility issues, a novel approach is proposed consisting in characterizing separately the deep valleys (caused by the  $-45^\circ$  ply orientation machining) and the plateaus. Plateau roughness profiles are introduced and are obtained by removing the deep valleys. Plateau roughness parameters are computed from this profile, characterizing the upper composite surface texture. The developed technique allows to improve the parameter reproducibility rates (up to three times for the kurtosis results), inherent to laminate surfaces, and to perform a relatively accurate texture characterization.

Regarding this technique performance vs the milling type, this characterization technique of the down-milling CFRP surfaces shows relatively less result dispersion than of the up-milling surfaces.

This new technique is a greater help to inspect and evaluate the surface texture of a trimmed composite. This method allows a faster and simpler check than the areal surface texture or the profile surface texture analysis in the ply plane direction.

It can also be an efficient texture evaluation of drilled hole composite surfaces which are a major concern in the aerospace industry. Areal roughness inspection is usually preferred to profile roughness check because of the poor reproducibility rates of surface profile roughness parameters. However, this areal texture examination involves the hole destruction. The roughness check technique, proposed in this study, presents a reliable solution for the surface profile inspection of machined laminate composites.

## 6.6 Acknowledgements

The authors wish to thank Mr Hossein Hamedanianpour for conducting the experiments at the Centre Technologique en Aérospatial with the help of Mr Réjean Roy, and Mr David Chapelier for measuring the surface profiles.

This work was funded by the Consortium for Research and Innovation in Aerospace in Québec (CRIAQ) and its partners, the Natural Sciences and Engineering Research Council of Canada (NSERC), Bombardier Aerospace, Avior Integrated Products, Delastek and AV&R Aerospatiale.

## 6.7 References

- [1] D. Arola, M. Ramulu, and D. H. Wang, "Chip formation in orthogonal trimming of graphite/epoxy composite," *Composites Part A: Applied Science and Manufacturing*, vol. 27, pp. 121-133, // 1996.
- [2] X. Rimpault, J. F. Chatelain, J. E. Klemberg-Sapieha, and M. Balazinski, "A new approach for surface profile roughness characterization in the laminate composite ply plane," presented at the CASI Aeronautics Conference, Montreal, 2015.
- [3] J. F. Chatelain, I. Zaghbani, and J. Monier, "Effect of Ply Orientation on Roughness for the Trimming Process of CFRP Laminates," *World Academy of Science, Engineering and Technology*, vol. 68, pp. 987 - 994, 2012.
- [4] Y. Landon and M. Cherif, "Characterization of the Surface Quality of Holes Drilled in CFRP Laminates," *Advanced Materials Research*, vol. 698, pp. 107-116, 2013.
- [5] D. H. Wang, M. Ramulu, and D. Arola, "Orthogonal cutting mechanisms of graphite/epoxy composite. Part II: multi-directional laminate," *International Journal of Machine Tools and Manufacture*, vol. 35, pp. 1639-1648, 12// 1995.
- [6] I. International Standard Organization, "Geometrical Product Specifications (GPS) -- Surface texture: Profile method," in *Terms, definitions and surface texture parameters* vol. 4287:1997, ed, 1997, p. 25.
- [7] I. International Standard Organization, "Geometrical Product Specifications (GPS)," in *Filtration -- Part 1: Overview and basic* vol. 16610-1:2015, ed, 2015, p. 25.
- [8] I. International Standard Organization, "Geometrical Product Specifications (GPS) -- Surface texture: Profile method," in *Metrological characteristics of phase correct filters* vol. 11562:1996, ed, 1996, p. 7.
- [9] T. A. S. o. M. E. ASME, "Surface Texture (Surface Roughness, Waviness, and Lay)," ed. New York, NY: ASME, 2009.

- [10] I. International Standard Organization, "Geometrical Product Specifications (GPS) -- Surface texture: Profile method," in Surfaces having stratified functional properties -- Part 1: Filtering and general measurement conditions vol. 13565-1:1996, ed, 1996, p. 5.
- [11] S. Bérubé, "Évaluation de la performance d'outils de coupe dédiés au détournage de structures composites carbone/époxy," M.Sc.A., Mechanical Engineering, École de Technologie Supérieure (Université du Québec à Montréal), 2012.
- [12] I. International Standard Organization, "Tool life testing in milling," in Part 2: End milling vol. 8688-2:1989, ed, 1989, p. 26.
- [13] M. Slamani, J.-F. Chatelain, and H. Hamedanianpour, "Comparison of two models for predicting tool wear and cutting force components during high speed trimming of CFRP," International Journal of Material Forming, vol. 8, pp. 305-316, 2014.
- [14] I. International Standard Organization, "Geometrical Product Specifications (GPS) -- Surface texture: Profile method," in Surfaces having stratified functional properties -- Part 3: Height characterization using the material probability curve vol. 13565-3:1998, ed, 1996, p. 20.
- [15] I. International Standard Organization, "Geometrical Product Specifications (GPS) -- Surface texture: Profile method," in Surfaces having stratified functional properties -- Part 2: Height characterization using the linear material ratio curve vol. 13565-2:1996, ed, 1996, p. 6.



## **CHAPTER 7      GENERAL DISCUSSION**

FRP composites have been increasingly used in the industry but research and development on their manufacturing processes still need to be carried out. On a production line, the machining quality of a process needs to be evaluated to ensure parts to remain within required tolerances. In this thesis, the CFRP machining process was investigated through the tool wear and generated surface quality.

This chapter is divided in two due to the dual nature inherent to this thesis.

### **7.1 Fractal analysis of CFRP machining signals**

In this section, articles presented in Chapter 4 and Appendix A and Appendix B are discussed.

The research work led to an early development of a process monitoring technique based on fractal analysis. This innovative method is still an exploratory research but preliminary results are very promising. This technique takes ground on the noise generated during the cutting of fibres. The model evaluates, among others, the level of noise. It occurs that this noise index can be linked with the tool wear and, to a higher extent, with the surface quality as well. The usually afflicting characteristic of heterogeneity has been turned into our advantage. In practice, a considerable amount of information is lost averaging cutting force signals for instance.

In the first place (Appendix A), cutting force signals acquired during multimaterial drilling were scrutinized. An unusual shape (or noise, depending on the scale of observation) variation change was noticed in those signals. A fractal analysis known for its robustness (regularization analysis) was tried out onto those signals. Fractal analysis had already been considered in signal analysis during machining but the particularity of composite materials had been omitted. Those preliminary results pushed further investigations to this direction. Different fractal analyses were tested and compared to analyze cutting force signals acquired during the trimming of CFRP (Chapter 4). The technique was improved at this stage and results were interesting but the bandwidth limitation during the acquisition was an issue. That is why another experiment was conducted using both, the dynamometer table and acoustic sensors for the orbital drilling of CFRP/Titanium (Appendix B). Results were very promising and further steps have been made to implement this technique in the industry.

## 7.2 Topography analysis of laminated composite

In this section, papers shown in Chapter 5, Chapter 6 and Appendix C are discussed.

In the literature, there is a lack of concern regarding characterization issues of machined composite surfaces. Although few researchers criticized current roughness parameters, most of scientific researchers and engineers have kept using them. However, the surface needs to be properly parametrized or characterized to assess the machining quality.

Thanks to their physical characteristics, machined composite surfaces highly differ from e.g. metallic ones. Researchers have already investigated various problems in current characterization methods. A part of this study has been to heavily collect and observe different profiles (Appendix C). Two main profile directions have been identified to assess the surface profile characterization: longitudinal (ply plane orientation) and transversal (stacking sequence direction). Each one has specificities and different solutions to be addressed.

From the profile observation,  $-45^\circ$  fibre orientation plies admit the highest surface texture range. Surface disparities between plies with different fibre orientation leads to surface condition characterization problems. As previously mentioned, current surface profile characterization was built for homogeneous material purposes. In the transversal direction (Chapter 3), the filtration technique is the main issue problem and in the longitudinal one (Chapter 2), the parametrization is the critical point. For each, easily applicable solutions have been proposed. Those characterization techniques were developed in the line with current characterization found in the standards, including specificities caused by the type of material.

## **CHAPTER 8      GENERAL CONCLUSION AND RECOMMENDATIONS**

Machining heterogeneous materials such as CFRP is a challenging process and should be monitored closely. The surface quality is one of the most significant evaluating elements. In this thesis, surface texture characterization issues have been raised and explained. Current surface profile characterization is found inadequate to evaluate the machined laminate composites. New filtering technique and new roughness parameters have been proposed in this thesis. The filtering technique requires removing deep cavities cause by  $-45^\circ$  orientation plies in order to increase consistency and reliability in the transversal direction. In this transversal direction, current roughness parameters were found adequate to assess the surface condition if used after this new filtering technique.

In the longitudinal direction, the impact of filtering techniques on results were found insignificant. However, the new roughness parameters based on fractal analysis and autocorrelation of profiles allow to more efficiently describe the surface condition whatever the fibre orientation.

Those solutions can be applied for characterization of both trimmed and drilled surface.

In addition to characterization concerns, a process monitoring model has been developed. This model is based on the fractal analysis of machining signals such as cutting forces and acoustic emissions. Trials of this technique were performed using experiments results of trimming, axial and orbital drilling of CFRP. The monitoring techniques outcomes are promising to evaluate the tool wear while machining allowing machinist to proceed to tool replacement before a part gets scrapped. This technique could also be useful to assess the machining quality and, so on, the surface condition.

### **8.1 Original contributions**

During my doctoral studies, nine communications have been disclosed in conferences and I heavily contributed to eight journal articles which five of them are already published, one is in press and two are currently in peer revision process. The publication list is synthetized in both Table 8.1 and Table 8.2 respectively for the journal and conference papers.

Table 8.1: Journal publication list (ranked by chronological order using the submission date)

<b>Journal papers</b>	
<b>Reference</b>	<b>Status</b>
1- Aramesh, M., Rimpault, X., Klim, Z., Balazinski, M., “Wear Dependent Tool Reliability Analysis during Cutting Titanium Metal Matrix Composites (Ti-MMCs)”, SAE Int. J. Aerosp. 6(2): 2013 doi: 10.4271/2013-01-2198	Published
2- Rimpault, X., Chatelain, J.-F., Klemberg-Sapieha, J.E., Balazinski, M., “Burr height monitoring while drilling CFRP/Titanium/Aluminium stacks”, Journal Mechanics and Industry, accepted in September 2013	In press
3- Rimpault, X., Chatelain, J.-F., Klemberg-Sapieha, J.E., Balazinski, M., “Tool wear and surface quality assessment of CFRP trimming using fractal analyses of the cutting force signals”, CIRP Journal of Manufacturing Science and Technology, vol. 16, pp. 72-80, 2017, <a href="http://dx.doi.org/10.1016/j.cirpj.2016.06.003">http://dx.doi.org/10.1016/j.cirpj.2016.06.003</a>	In press
4- Rimpault, X., Chatelain, J.-F., Klemberg-Sapieha, J.E., Balazinski, M., “A new approach for the surface roughness profile characterization of laminated composites in the ply plane direction”, Canadian Aeronautics and Space Journal	Submitted in July 2015
5- Rimpault, X., Chatelain, J.-F., Klemberg-Sapieha, J. E., Balazinski, M., “Surface profile texture characterization of trimmed laminated composite in the stacking sequence direction”, Measurement, vol. 91, pp. 84-92, 2016, doi: 10.1016/j.measurement.2016.05.039	Published
6- Rimpault, X., Chatelain, J.-F., Klemberg-Sapieha, J.E., Balazinski, M., “Fractal analysis of cutting force and acoustic emission signals during CFRP machining”, Procedia CIRP, vol. 46, pp. 143-146, 2016, doi: 10.1016/j.procir.2016.03.171	Published
7- Rimpault, X., Chatelain, J.-F., Klemberg-Sapieha, J.E., Balazinski, M., “Surface profile topography of trimmed and drilled carbon/epoxy composite”, Procedia CIRP, vol. 45, pp. 27-30, 2016, doi: 10.1016/j.procir.2016.02.160	Published
8- Rimpault, X., Bitar-Nehme, E., Balazinski, M., Mayer, J. R. R., “Online monitoring and failure detection of capacitive displacement sensor using fractal analysis”, Measurement	Submitted in May 2016

During the Joint Conference on Mechanical, Design Engineering & Advanced Manufacturing, at Toulouse (France) in 2014, the presented paper was rewarded with the Best Paper Award.

A significant contribution has been produced regarding the surface condition of laminated composites and signal analysis during the machining of heterogeneous materials such as CFRPs. The work performed in the signal analysis using fractal analysis is very innovative in CFRP machining. The research has led to the early development of an online monitoring during FRP machining. This innovative monitoring method is currently under investigation for application in the industry.

The surface condition work has brought solutions easily applicable in the industry as well. Those solutions are in respect with current standards' characterization guidelines. Improving the surface profile characterization method is particularly interesting in hole surface inspection. Ensuring a proper characterization could help machinists check holes without destroying them to observe the surface perpendicularly.

Table 8.2: Communication list in conferences (ranked by chronological order using the conference/symposium date as reference)

<b>Conference papers – Reference</b>
1- Aramesh, M., Rimpault, X., Klim, Z., Balazinski, M., “Wear Dependent Tool Reliability Analysis during Cutting Titanium Metal Matrix Composites (Ti-MMCs)”, SAE 2013 AeroTech Congress & Exhibition, Montreal, September 24-26, 2013
2- Rimpault, X., Chatelain, J.-F., Klemberg-Sapieha, J.E., Balazinski, M., “Cutting parameter impact on forces and on hole diameter while drilling CFRP/titanium/aluminium stacks”, VMPT 2014, University of Calgary, May 20-23, (Submission #56)
3- Rimpault, X., Chatelain, J.-F., Klemberg-Sapieha, J.E., Balazinski, M., “Burr Height Study for Drilling Carbon Epoxy Composite/Titanium/Aluminium Stacks”, JCM 2014, Joint Conference on Mechanical, Design Engineering & Advanced Manufacturing, Toulouse France, June 18-20, 2014. Best Paper Award
4- Rimpault, X., Chatelain, J.-F., Klemberg-Sapieha J.E., Balazinski, M., “Surface condition of high speed trimming of CFRP”, COMAT 2015, 6th International Conference on Science and Technology of Composite Materials, Argentina, May 7-8, 2015
5- Rimpault, X., Chatelain, J.-F., Klemberg-Sapieha J.E., Balazinski, M., “A new approach for the surface roughness profile characterization of laminated composites in the ply plane direction”, 62nd CASI Aeronautics Conference and AGM 3rd GARDN Conference 2015, Montreal, May 19-21, p.71
6- Rimpault, X., Chatelain, J.-F., Klemberg-Sapieha, J.E., Balazinski, M., “Surface quality assessment of CFRP high speed trimming using fractal analyses of the cutting force signals”, VMPT 2015, University of British Columbia, June 2-5, (Submission #61)
7- Rimpault, X., Chatelain, J.-F., Klemberg-Sapieha, J.E., Balazinski, M., “Tool wear impact on surface roughness condition of CFRP high speed trimming”, VMPT 2015, University of British Columbia, June 2-5, (Submission #62)
8- Rimpault, X., Chatelain, J.-F., Klemberg-Sapieha, J.E., Balazinski, M., “Fractal analysis of cutting force and acoustic emission signals during CFRP machining”, HPC 2016, Chemnitz, Germany, May 31-June 2, 2016
9- Rimpault, X., Chatelain, J.-F., Klemberg-Sapieha, J.E., Balazinski, M., “Surface profile topography of trimmed and drilled carbon/epoxy composite”, 3rd conference on surface integrity, Charlotte, North Carolina, June 8-10, 2016

## 8.2 Future works

In this research, the fractal analyses were monofractal (only one fractal dimension was identified). Multifractal analysis could be overviewed allowing to identify main fractal dimensions structuring the observed signal. In addition, chaos theory tools such as Lyapunov analysis might be of interest.

As a general comment, cutting process monitoring could be heavily improved on novel materials in particular by taking into consideration the singular characteristics of those materials. For instance, the ‘noise’ in the vibration signals while machining CFRPs was left aside although this feature carries relevant information that was uncovered therein.

The proposed technique could be further evaluated, for example, concerning its reproducibility and performance. Sensor types and placement, signal acquisition characteristics could be investigated to enhance the technique potential.

Regarding the surface condition, a high number of measurement (around 12 000, including preliminary measurements) were conducted during this research. Roughness parameters and filtering methods have been introduced. However, those measurements concentrate a huge amount of information which still needs to be extracted. Machine learning and data mining could be applied on those data. For instance, correlation between roughness parameters could be identified and the proper selection of roughness parameter(s) could be performed to evaluate a FRP surface condition and machining quality.

## BIBLIOGRAPHY

- Altintas, Y. (2012). *Manufacturing automation : metal cutting mechanics, machine tool vibrations, and CNC design*. Cambridge; New York: Cambridge University Press.
- Andrus, D. C. (2005). Britain fractal coastline combined. *Dimension fractale*.
- Arola, D., Ramulu, M., & Wang, D. H. (1996). Chip formation in orthogonal trimming of graphite/epoxy composite. *Composites Part A: Applied Science and Manufacturing*, 27(2), 121-133. doi: [http://dx.doi.org/10.1016/1359-835X\(95\)00013-R](http://dx.doi.org/10.1016/1359-835X(95)00013-R)
- Arul, S., Vijayaraghavan, L., & Malhotra, S. K. (2007). Online monitoring of acoustic emission for quality control in drilling of polymeric composites. *Journal of Materials Processing Technology*, 185(1-3), 184-190. doi: 10.1016/j.jmatprotec.2006.03.114
- ASME, T. A. S. o. M. E. (2009). *Surface Texture (Surface Roughness, Waviness, and Lay)*. B46.1. New York, NY: ASME.
- Berthelot, J. M. (2012). *Matériaux composites : Comportement mécanique et analyse des structures* (5e edition ed.). Paris, France: Lavoisier.
- Bérubé, S. (2012). Évaluation de la performance d'outils de coupe dédiés au détournage de structures composites carbone/époxy. (École de Technologie Supérieure (Université du Québec à Montréal)).
- Bonnet, C. (2010). Compréhension des mécanismes de coupe lors du perçage à sec de l'empilage Ti6Al4V/Composite fibre de carbone.
- Brinksmeier, E., & Janssen, R. (2002). Drilling of Multi-Layer Composite Materials consisting of Carbon Fiber Reinforced Plastics (CFRP), Titanium and Aluminum Alloys. *CIRP Annals - Manufacturing Technology*, 51(1), 87-90. doi: [http://dx.doi.org/10.1016/S0007-8506\(07\)61472-3](http://dx.doi.org/10.1016/S0007-8506(07)61472-3)
- Bukkapatnam, S. T. S., Kumara, S. R. T., & Lakhtakia, A. (1999). Fractal Estimation of Flank Wear in Turning. *Journal of Dynamic Systems, Measurement, and Control*, 122(1), 89-94. doi: 10.1115/1.482446

- Bukkapatnam, S. T. S., Lakhtakia, A., & Kumara, S. R. T. (1995). Analysis of sensor signals shows turning on a lathe exhibits low-dimensional chaos. *Physical Review E*, 52(3), 2375-2387. doi: 10.1103/PhysRevE.52.2375
- Campbell, F. C. (2010). *Structural composite materials*. Ohio: ASM International.
- Cantero, J. L., Tardio, M. M., Canteli, J. A., Marcos, M., & Miguelez, M. H. (2005). Dry drilling of alloy Ti-6Al-4V. *International Journal of Machine Tools & Manufacture*, 45(11), 1246-1255. doi: 10.1016/j.ijmachtools.2005.01.010
- Chatelain, J. F., Zagbani, I., & Monier, J. (2012). Effect of Ply Orientation on Roughness for the Trimming Process of CFRP Laminates. *World Academy of Science, Engineering and Technology*, 68 987 - 994. Retrieved from <http://waset.org/publications/1115>
- Colligan, K. R., M. (1991). Effect of Edge Trimming on surface plies. Paper presented (Vol. 5, pp. 274-283).
- Comittee, A. I. H. (1992a). Machining. In A. International (Ed.) *ASM Handbook* (Vol. 16, pp. 929): ASM International.
- Comittee, A. I. H. (1992b). Properties and Selection : Nonferrous Alloys and Special-Purpose Materials. In A. International (Ed.) *ASM Handbook* (Vol. 2, pp. 3470): ASM International.
- Davim, J., Barman, T., & Sahoo, P. (2011). *Fractal Analysis in Machining*: Springer Berlin Heidelberg.
- Davim, J. P., & Reis, P. (2005). Damage and dimensional precision on milling carbon fiber-reinforced plastics using design experiments. *Journal of Materials Processing Technology*, 160(2), 160-167.
- Dornfeld, D. A., Kim, J. S., Dechow, H., Hewson, J., & Chen, L. J. (1999). Drilling Burr Formation in Titanium Alloy, Ti-6Al-4V. *CIRP Annals - Manufacturing Technology*, 48(1), 73-76. doi: [http://dx.doi.org/10.1016/S0007-8506\(07\)63134-5](http://dx.doi.org/10.1016/S0007-8506(07)63134-5)
- ECSS, E. C. f. S. S.-. (2011). *Space Engineering*. Noordwijk, The Netherlands: ECSS Secretariat - ESA-ESTEC - Requirements & Standards Division.



- Faraz, A., Biermann, D., & Weinert, K. (2009). Cutting edge rounding: An innovative tool wear criterion in drilling CFRP composite laminates. *International Journal of Machine Tools and Manufacture*, 49(15), 1185-1196. doi: 10.1016/j.ijmachtools.2009.08.002
- Feng, Z., Zuo, M. J., & Chu, F. (2010). Application of regularization dimension to gear damage assessment. *Mechanical Systems and Signal Processing*, 24(4), 1081-1098. doi: 10.1016/j.ymssp.2009.08.006
- Fu, P., Li, W. L., & Zhu, L. Q. (2011). Cutting Tool Wear Monitoring Based on Wavelet Denoising and Fractal Theory. *Applied Mechanics and Materials*, 48-49 349-352. doi: 10.4028/www.scientific.net/AMM.48-49.349
- Gagnepain, J. J., & Roques-Carmes, C. (1986). Fractal approach to two-dimensional and three-dimensional surface roughness. *Wear*, 109(1-4), 119-126. doi: [http://dx.doi.org/10.1016/0043-1648\(86\)90257-7](http://dx.doi.org/10.1016/0043-1648(86)90257-7)
- Ghidossi, P., Mansori, M., & Pierron, F. (2006). Influence of specimen preparation by machining on the failure of polymer matrix off-axis tensile coupons. *Composites Science and Technology*, 66(11-12), 1857-1872. doi: 10.1016/j.compscitech.2005.10.009
- Gouleau, S., Garnier, S., & Furet, B. (2007). *Perçage d'empilages multi-matériaux*. Les Ulis, FRANCE: EDP Sciences.
- Guegan, P., Lemaitre, F., & Hamann, J. (1992). Contribution a l'usinage des matériaux composites.
- Hamedanianpour, H., & Chatelain, J. F. (2013). Effect of Tool Wear on Quality of Carbon Fiber Reinforced Polymer Laminate during Edge Trimming. *Applied Mechanics and Materials*, 325-326 34-39. doi: 10.4028/www.scientific.net/AMM.325-326.34
- Hintze, W., Hartmann, D., & Schütte, C. (2011). Occurrence and propagation of delamination during the machining of carbon fibre reinforced plastics (CFRPs) – An experimental study. *Composites Science and Technology*, 71(15), 1719-1726.
- Hudson, J. A., & Harrison, J. P. (1997). *Engineering Rock Mechanics: an Introduction to the Principles*. Oxford, UK: Pergamon.
- International Standard Organization, I. (1989). *Tool life testing in milling*.

- International Standard Organization, I. (1996a). Geometrical Product Specifications (GPS) -- Surface texture: Profile method.
- International Standard Organization, I. (1996b). Geometrical Product Specifications (GPS) -- Surface texture: Profile method.
- International Standard Organization, I. (1996c). Geometrical Product Specifications (GPS) -- Surface texture: Profile method.
- International Standard Organization, I. (1996d). Geometrical Product Specifications (GPS) -- Surface texture: Profile method.
- International Standard Organization, I. (1996e). Geometrical Product Specifications (GPS) -- Surface texture: Profile method.
- International Standard Organization, I. (1997a). Geometrical Product Specifications (GPS) -- Surface texture: Profile method.
- International Standard Organization, I. (1997b). Geometrical Product Specifications (GPS) -- Surface texture: Profile method.
- International Standard Organization, I. (2015). Geometrical Product Specifications (GPS).
- Jahanmir, S., Ramulu, M., & Koshy, P. (1999). Machining of ceramics and composites. New York: Marcel Dekker.
- Jawahir, I. S., Brinksmeier, E., M'Saoubi, R., Aspinwall, D. K., Outeiro, J. C., Meyer, D., . . . Jayal, A. D. (2011). Surface integrity in material removal processes: Recent advances. *CIRP Annals - Manufacturing Technology*, 60(2), 603-626. doi: 10.1016/j.cirp.2011.05.002
- Kabaldin, Y. G., Seryi, S. V., Prosolovich, A. V., & Burdasov, E. N. (2010). Improving the stability of cutting on the basis of fractal, dimensional, and wavelet analysis. *Russian Engineering Research*, 30(6), 587-595. doi: 10.3103/s1068798x10060122
- Kalla, D., Sheikh-Ahmad, J., & Twomey, J. (2010). Prediction of cutting forces in helical end milling fiber reinforced polymers. *International Journal of Machine Tools and Manufacture*, 50(10), 882-891. doi: <http://dx.doi.org/10.1016/j.ijmachtools.2010.06.005>
- Karpat, Y., Bahtiyar, O., & Değer, B. (2012a). Mechanistic force modeling for milling of unidirectional carbon fiber reinforced polymer laminates. *International Journal of Machine*

Tools and Manufacture, 56(0), 79-93. doi:  
<http://dx.doi.org/10.1016/j.ijmachtools.2012.01.001>

Karpat, Y., Bahtiyar, O., & Değer, B. (2012b). Milling Force Modelling of Multidirectional Carbon Fiber Reinforced Polymer Laminates. *Procedia CIRP*, 1 460-465. doi:  
<http://dx.doi.org/10.1016/j.procir.2012.04.082>

Kivimaa, E. (1950). Cutting force in woodworking. Helsinki.

König, W., Wulf, C., Graß, P., & Willerscheid, H. (1985). Machining of Fibre Reinforced Plastics. *CIRP Annals - Manufacturing Technology*, 34(2), 537-548. doi:  
[http://dx.doi.org/10.1016/S0007-8506\(07\)60186-3](http://dx.doi.org/10.1016/S0007-8506(07)60186-3)

Koplev, A., Lystrup, A., & Vorm, T. (1983). The cutting process, chips, and cutting forces in machining CFRP. *Composites*, 14(4), 371-376. doi: [http://dx.doi.org/10.1016/0010-4361\(83\)90157-X](http://dx.doi.org/10.1016/0010-4361(83)90157-X)

Landon, Y., & Cherif, M. (2013). Characterization of the surface quality of holes drilled in CFRP laminates. *Diffusion and Defect Data Pt.B: Solid State Phenomena - Advanced Materials Research*, 201 - 698 107-116.

Landon, Y., & Cherif, M. (2013). Characterization of the Surface Quality of Holes Drilled in CFRP Laminates. *Advanced Materials Research*, 698 107-116. doi:  
[10.4028/www.scientific.net/AMR.698.107](http://dx.doi.org/10.4028/www.scientific.net/AMR.698.107)

Lasri, L. (2009). Modélisation macromécanique et micromécanique de l'usinage des composites à matrice polymère et fibres longues. (PhD thesis, ENSAM, Chalons en Champagne). (2009 ENAM 0031)

Lévy Véhel, J., & Legrand, P. (2004). Signal and image processing with Fraclab. Paper presented at Eighth International Multidisciplinary Conference, Vancouver, Canada.

List, G., Nouari, M., Géhin, D., Gomez, S., Manaud, J. P., Le Petitcorps, Y., & Girot, F. (2005). Wear behaviour of cemented carbide tools in dry machining of aluminium alloy. *Wear*, 259(7–12), 1177-1189. doi: [10.1016/j.wear.2005.02.056](http://dx.doi.org/10.1016/j.wear.2005.02.056)

- Logan, D., & Mathew, J. (1996). Using the correlation dimension for vibration fault diagnosis of rolling element bearings—I. Basic concepts. *Mechanical Systems and Signal Processing*, 10(3), 241-250. doi: <http://dx.doi.org/10.1006/mssp.1996.0018>
- Majumdar, A., & Tien, C. L. (1990). Fractal characterization and simulation of rough surfaces. *Wear*, 136(2), 313-327. doi: [http://dx.doi.org/10.1016/0043-1648\(90\)90154-3](http://dx.doi.org/10.1016/0043-1648(90)90154-3)
- Mandelbrot, B. (1975). *Les objets fractals : Forme, hasard et dimension*. France: Flammarion.
- Mandelbrot, B. B. (1982). *The fractal geometry of nature*. San Francisco: W.H. Freeman.
- Mathew, J., Ramakrishnan, N., & Naik, N. K. (1999). Investigations into the effect of geometry of a trepanning tool on thrust and torque during drilling of GFRP composites. *Journal of Materials Processing Technology*, 91(1-3), 1-11. doi: [http://dx.doi.org/10.1016/S0924-0136\(98\)00416-6](http://dx.doi.org/10.1016/S0924-0136(98)00416-6)
- McKenzie, W. (1960). Fundamental aspects of wood cutting process. *Forest Products Journal*, 10 447-456.
- Molinari, A., Musquar, C., & Sutter, G. (2002). Adiabatic shear banding in high speed machining of Ti-6Al-4V: experiments and modeling. *International Journal of Plasticity*, 18(4), 443-459. doi: [http://dx.doi.org/10.1016/S0749-6419\(01\)00003-1](http://dx.doi.org/10.1016/S0749-6419(01)00003-1)
- Nouari, M., List, G., Girot, F., & Géhin, D. (2005). Effect of machining parameters and coating on wear mechanisms in dry drilling of aluminium alloys. *International Journal of Machine Tools and Manufacture*, 45(12-13), 1436-1442. doi: 10.1016/j.ijmachtools.2005.01.026
- Palanikumar, K., Karunamoorthy, L., & Karthikeyan, R. (2006). Assessment of factors influencing surface roughness on the machining of glass fiber-reinforced polymer composites. *Materials & Design*, 27(10), 862-871. doi: 10.1016/j.matdes.2005.03.011
- Persson, E., Eriksson, I., & Zackrisson, L. (1997). Effects of hole machining defects on strength and fatigue life of composite laminates. *Composites Part A: Applied Science and Manufacturing*, 28(2), 141-151. doi: 10.1016/s1359-835x(96)00106-6
- Piquet, R., Ferret, B., Lachaud, F., & Swider, P. (2000). Experimental analysis of drilling damage in thin carbon/epoxy plate using special drills. *Composites Part A: Applied Science and Manufacturing*, 31(10), 1107-1115. doi: [http://dx.doi.org/10.1016/S1359-835X\(00\)00069-5](http://dx.doi.org/10.1016/S1359-835X(00)00069-5)

- Polmear, I. J. (1996). *Light Alloys - Metallurgy of the Light Metals*: Halsted Press.
- Rimpault, X., Chatelain, J. F., Klemberg-Sapieha, J. E., & Balazinski, M. (2015). A new approach for surface profile roughness characterization in the laminate composite ply plane. Paper presented at CASI Aeronautics Conference, Montreal.
- Robert, B. (2001). *Les fractales en Physique*. Techniques de l'ingénieur Mécanique physique, base documentaire : TIB110DUO(ref. article : af4500). Retrieved from <http://www.techniques-ingenieur.fr/base-documentaire/sciences-fondamentales-th8/mecanique-physique-42110210/les-fractales-en-physique-af4500/>
- Roudgé, M. (2011). *Modélisation expérimentale par les réseaux de neurones du perçage multi-matériaux*. (Université Bordeaux 1, Bordeaux).
- Roueff, F., & Lévy Véhel, J. (1998, 1998-10). A Regularization Approach to Fractional Dimension Estimation. Paper presented at Fractals 98. Retrieved from <http://hal.inria.fr/inria-00593254>
- Russ, J. (1994). *Fractal Surfaces*: Springer US.
- Sapoval, B. (1997). *Universalités et fractales* (Science ed.). France: Flammarion.
- Sheikh-Ahmad, J., Urban, N., & Cheraghi, H. (2012). Machining Damage in Edge Trimming of CFRP. *Materials and Manufacturing Processes*, 27(7), 802-808. doi: 10.1080/10426914.2011.648253
- Sheikh-Ahmad, J. Y. (2009). *Machining of Polymer Composites*.
- Shyha, I. S., Soo, S. L., Aspinwall, D. K., Bradley, S., Perry, R., Harden, P., & Dawson, S. (2011). Hole quality assessment following drilling of metallic-composite stacks. *International Journal of Machine Tools and Manufacture*, 51(7-8), 569-578. doi: <http://dx.doi.org/10.1016/j.ijmachtools.2011.04.007>
- Slamani, M., Chatelain, J.-F., & Hamedanianpour, H. (2014). Comparison of two models for predicting tool wear and cutting force components during high speed trimming of CFRP. *International Journal of Material Forming*, 8(2), 305-316. doi: 10.1007/s12289-014-1170-2
- Stephenson, D. A., & Agapiou, J. S. (2005). *Metal cutting theory and practice* (Vol. 68): CRC press.

- Tönsheff, H. K., Friemuth, T., & Groppe, M. (2001, June 27-28). A solution for an economical machining of bore holes in composite materials (CFK, aluminum). Paper presented at Proceedings of 3rd International Conference on Metal Cutting and High Speed Machining, Metz (France).
- Tsao, C. C., & Hocheng, H. (2007). Effect of tool wear on delamination in drilling composite materials. *International Journal of Mechanical Sciences*, 49(8), 983-988. doi: <http://dx.doi.org/10.1016/j.ijmecsci.2007.01.001>
- Wang, D. H. (1993). Machining characteristics of graphite/epoxy composite. (University of Washington).
- Wang, D. H., Ramulu, M., & Arola, D. (1995a). Orthogonal cutting mechanisms of graphite/epoxy composite. Part I: unidirectional laminate. *International Journal of Machine Tools and Manufacture*, 35(12), 1623-1638. doi: 10.1016/0890-6955(95)00014-o
- Wang, D. H., Ramulu, M., & Arola, D. (1995b). Orthogonal cutting mechanisms of graphite/epoxy composite. Part II: multi-directional laminate. *International Journal of Machine Tools and Manufacture*, 35(12), 1639-1648. doi: [http://dx.doi.org/10.1016/0890-6955\(95\)00015-P](http://dx.doi.org/10.1016/0890-6955(95)00015-P)
- Wang, X. M., & Zhang, L. C. (2003). An experimental investigation into the orthogonal cutting of unidirectional fibre reinforced plastics. *International Journal of Machine Tools and Manufacture*, 43(10), 1015-1022. doi: 10.1016/S0890-6955(03)00090-7
- Wern, C. W., Ramulu, M., & Colligan, K. (1993). A study of the surface texture of composite drilled holes. *Journal of Materials Processing Technology*, 37(1-4), 373-389. doi: [http://dx.doi.org/10.1016/0924-0136\(93\)90103-D](http://dx.doi.org/10.1016/0924-0136(93)90103-D)

## **APPENDIX A – ARTICLE 4: BURR HEIGHT MONITORING WHILE DRILLING CFRP/TITANIUM/ALUMINIUM STACKS**

Xavier Rimpault<sup>a</sup>, Jean-François Chatelain<sup>b</sup>, Jolanta E. Klemberg-Sapieha<sup>c</sup>, Marek Balazinski<sup>a</sup>

<sup>a</sup>Department of Mechanical Engineering, Polytechnique Montréal, Canada

<sup>b</sup>Department of Mechanical Engineering, École de Technologie Supérieure, Canada

<sup>c</sup>Department of Engineering Physics, Polytechnique Montréal, Canada

\* Accepted in *Mechanics and Industry* in September 2015.

### **A.1 Abstract**

In the aerospace industry, deburring operations are often difficult to achieve and can be very costly. Hence, burrs generated during the machining should be studied. In this research, the drilling operations were performed and analysed for a stack composed of carbon fibre reinforced polymer (CFRP), titanium and aluminium alloys, using three cutting feeds and three cutting speeds for each material.

A monitoring method is presented to predict the burr heights in the titanium and aluminium layers. The cutting force signals obtained during the drilling of the CFRP layer were analysed using the regularization fractal analysis, resulting in an estimation of the fractal dimension. This fractal analysis was optimized in order to monitor the clearance tool wear and the burr heights. The burr heights, measured at the outlet of the titanium and aluminium alloys, were observed in terms of the thrust force, the torque, the hole diameter and circularity, and the clearance tool wear. This fractal analysis technique can be implemented for an on-line control to predict the generated burr heights in the metallic layers while drilling the previous CFRP layer.

*Keywords:* Stack drilling, burr height, fractal analysis.

### **A.2 Introduction**

The use of carbon fibre reinforced polymer (CFRP) has been increasing over the past decades in the aircraft structures, notably due to its high strength/weight ratio. During airplane assembly, CFRP panels are used alongside with metallic parts, e.g. made of aluminium or titanium alloys. In the aerospace industry, to assemble and fasten those parts together, traditional drilling and

mechanical bolting operations are usually conducted. The drilling process can be operated on different types of stacks, such as: CFRP/titanium, CFRP/aluminium, aluminium/CFRP/titanium, etc. Bolting is used in order to assemble the parts and also to easily dismantle them for maintenance and repair purposes. Nevertheless, to increase the hole precision, all layers of the stack should be machined at once. Therefore, one-shot drilling is preferred [1].

On the other hand, the one-shot drilling process yields additional problems. Tönsheff *et al.* [2] found that when drilling of sandwiched materials, various problems may occur, such as dissimilar diameter, intense tool wear, heat damage, intra- and inter-laminate delamination, erosion, etc.

Moreover, the hole quality, such as the hole surface roughness and the hole straightness to the generating line, greatly impacts the efficiency of the bolting joints. It is therefore desirable to machine holes with tight hole straightness tolerances. However, drilling operation is more challenging to control, particularly due to the different machining characteristics of the layers within the stack [3]. In this study, the diameter of the hole is measured at different heights along the hole depth.

Burr formation is a critical factor occurring during the drilling of metallic parts. After machining operations, parts are deburred which cost can account for up to 30% of the total cost of the components [4]. However, in the aerospace industry, before stacking and drilling of the parts together, a shim resin is usually applied between each layer. That complicates the observation of one part only and the measurement of its burr heights [5].

In this paper, two main aspects were studied. The first one is the burr heights measured at the outlet of the metallic layers. The second one is the monitoring and diagnosis of the burr heights and the tool wear thanks to the fractal analysis of the cutting force signals from the CFRP machining. The generated burrs remain a challenge in the industry and needs to be evaluated through the scope of various elements such as the tool wear, the cutting parameters and the cutting forces. The fractal analysis of the cutting force signals allows monitoring the burr height generated and so keeping required inside burr height tolerance.

### **A.3 Fractal analysis**

The term “fractal” was first introduced by Mandelbrot [6] to describe the “roughness” or singularities or length of the coastline of Britain. Depending on the scale of the observation of a



coastline, the length may vary. The traditional geometrical approach is ineffective to provide an accurate measurement of the coastline length. A fractal is an object or a set which owns a self-affine or self-similar pattern or singularity [7]. Fractals can be defined by their fractal dimension. This parameter may be estimated through few fractal analyses. One of the simplest and probably the most commonly used is the capacity fractal analysis, also called the box counting fractal analysis. This technique is illustrated in Figure A-1. The object is observed through a mesh with a box size of  $\varepsilon$ . For each mesh size, boxes that contain a part of the object are numbered giving the minimal number of boxes number  $N_\varepsilon$  required to cover the object.

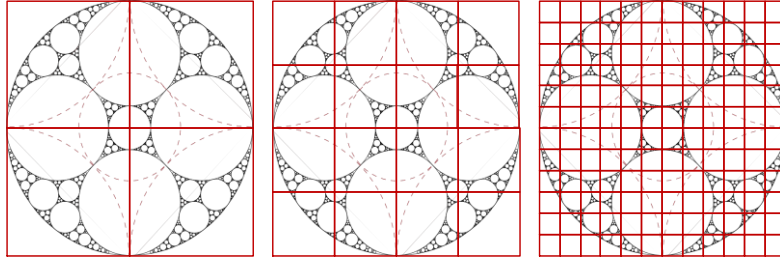


Figure A-1: Box counting example for a five circle inversion fractal

Then, the capacity dimension can be expressed as follows:

$$D_C = -\lim_{\varepsilon \rightarrow 0} \frac{\ln(N_\varepsilon)}{\ln \varepsilon} \quad (\text{A.1})$$

For the example from Figure A-1, the calculated capacity dimension  $D_C$  is close to 1.328, the fractal dimension of this object.

Fractal analysis is used to provide a measure of the irregularity or “roughness” of a signal from a dynamic system. The health information of a machine or its subset parts can be extracted from the fractal analysis of their vibration signals [8, 9].

Few fractal analysis methods can be found in the literature. One of them, the regularization analysis, was used for signals analysis in order to describe the irregularities in non-linear dynamical systems [8]. This method is used in this study to show its possibilities to analyse the cutting force signals. One of the main reasons of choosing this method is its robustness [10]. Feng *et al.* [8] used it for processing the accelerometer signal to assess the gear damage.

Besides, contrary to isotropic and homogenous materials such as metal alloys, CFRP is made of two different components – carbon fibres which are very hard to machine and epoxy resin which

has a high machinability index. During the machining of CFRP, the carbon fibres are fractured due to the mechanical load of the tool applied on the fibre.

The fracture of the carbon fibres causes an additional noise on the cutting forces signals comparing to the signals obtained during the machining of the homogenous metallic materials. This noise may depend on the wear state of the tool, the nose radius, the cutting parameters, etc.

Usually, this noise is not taken into account in the analysis of the cutting forces. However, it may give additional information relative to the machining such as the tool condition, the quality of the surface generated and the hole surface condition. With the increase of the tool wear or the change of the cutting parameters, the noise – or “roughness” – on the signal might change. Indeed, to fracture the fibres with a worn tool, the mechanical load applied may need to be higher. In this case, the use of fractal analysis could give a possibility of monitoring the tool condition by analysing the noise from the cutting force signals.

## **A.4 Workpiece materials**

### **A.4.1 CFRP**

Besides problems occurring due to the stacking of different materials, various issues may appear from the drilling process: fibre-resin delamination which could appear at the inlet or outlet of the hole, burnt composite, pulled and uncut fibres, etc. [11-13].

Due to the high sensibility of the epoxy resin to the heat, the temperature generated during the drilling can locally burn the resin. Due to the low conductivity of the epoxy resin, the temperature is difficult to ease. Thus, during dry drilling, the machining generates higher temperatures than with coolant use.

Due to the abrasiveness and hardness of the carbon fibres, abrasion is the main wear mechanism affecting the tool [14]. Tsao *et al.* [15] shown that the tool condition has an impact on the tool wear: an increased tool wear leads to more delamination. They found that delamination can also be influenced by the feed rate and the drill diameter.

### **A.4.2 Titanium alloy**

Titanium alloys are widely used in the aerospace industry thanks to their superior properties e.g. a high strength/weight ratio, a low density, a high fatigue and a high corrosion resistance. But, titanium alloys are also known to be difficult-to-machine materials [16].

Their low thermal conductivity causes high temperatures generated in the primary cutting zone during machining That results in an intense and rapid tool wear [17, 18].

In addition to the severe tool wear, the surface integrity and the quality of the holes drilled are influenced mostly by the high temperature in the cutting zone. This impact may be observed through the surface roughness parameters, the burr height, the hole diameter, as well as the changes in the microstructure near the surface of the walls of the holes [19].

Because of the generated heat caused by the drilling of the titanium layer, the experiments were conducted using peck drilling to, consequently, reduce this heat [4, 20, 21].

### **A.4.3 Aluminium alloy**

Contrary to titanium alloys, aluminium alloys have excellent machinability properties. Although the aluminium machinability index is relatively high, problems occur when drilling such alloys. One of the main problems is the adhesion of cut material on the tool cutting edges. This causes a tool wear increase and consequently to a low surface quality. On one hand, increasing the cutting speed can reduce this adhesion effect. But, on the other hand, the cutting speed increase raises as well the temperature in the cutting zone [22, 23].

Commonly used in the aerospace industry, the aluminium grade selected is one of the 7000 aluminium series. This grade was chosen for its good characteristics, such as high machinability index, high strength and heat treatment capacity. The drawback of this grade is its low resistance to corrosion [24, 25].

## **A.5 Experimental set-up**

The upper layer of the composite/metal stack tested was a CFRP laminate manufactured with an autoclave-cured 24-ply CFRP laminate using the pre-impregnated ply technology. This CFRP was prepared with lay-up continuous unidirectional fibre layers with  $0^\circ$ ,  $90^\circ$  and  $\pm 45^\circ$  orientations, with

a total thickness of 3.3 mm and a volume fibre fraction of 64%. The titanium layer was a Ti-6Al-4V, with a thickness of 2.0 mm. The aluminium layer was comprised of one 3.5 mm thick 7000 series aluminium grade.

The machining experiments were carried out using the high speed machining centre Huron<sup>®</sup> K2X10. This 3-axis computerised numerical control (CNC) machine allows a maximum spindle speed of 28 000 RPM at 40 kW. For health and safety purposes, a dust extraction system was mounted onto the machine.

Figure A-2 depicts the components of the workpiece used for the experiments. In industrial application, shim resin is applied between each layer of the stack. However, to allow the measurement and the analysis of the burr heights, shim was not applied and a thermoreactive paper Thermex<sup>®</sup> was placed instead. Due to the high heat generated during the machining of the titanium layer, the thermoreactive paper side was placed towards the titanium layer. This 0.05 mm thick paper allows a temperature range detection at the interface of two materials to see if the temperature generated at the interfaces was not too high to affect the materials of the stack. The reactive range of this colour-reacted paper detects temperatures between 90 °C and 150 °C. Above the upper limit, the paper becomes darker and darker until it combusts.



Figure A-2: Stack material specifications

The experimental set-up is shown in Figure A-3. A sponge filled with coolant was placed close to the working area allowing to slightly lubricate the tool tip during the drilling of the metallic layers.

Figure A-4 shows the mounting that allows the drilling of 120 holes, with a maximum diameter of 6 mm in an 80 mm x 300 mm workpiece.

The torque and thrust force were measured for each drilling using a 9255B Kistler<sup>®</sup> piezoelectric dynamometer table. The signals obtained were transmitted through an amplifier. Then, the signals were digitalised using an A/D converter with a 24 KHz frequency rate and recorded with a data acquisition set.

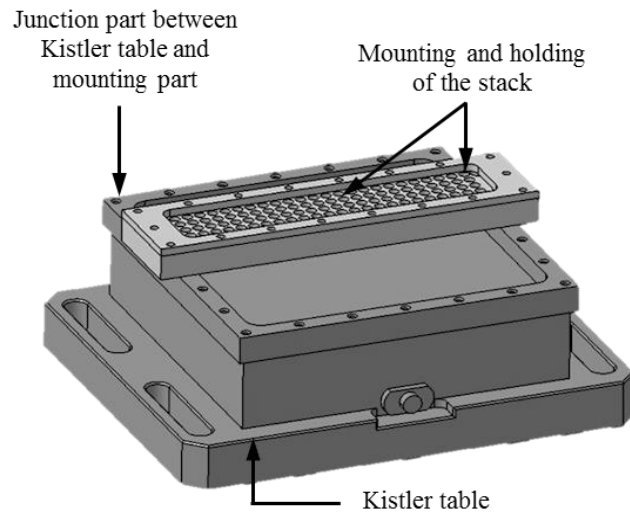


Figure A-3: Experimental set-up of the fixture of the workpiece, mounted over the Kistler force measurement table and a junction part

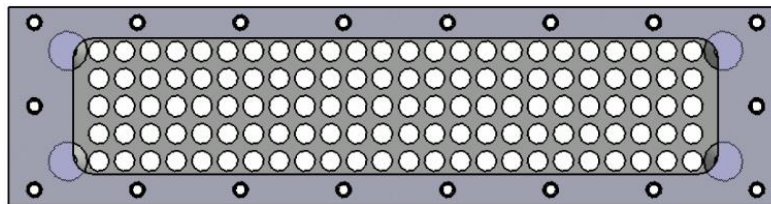


Figure A-4: Top view of the holding table and frame of the stack

## A.6 Methodology

### A.6.1 Design of experiments

The aim of the conducted experiments was to improve the stability of the process, as well as the hole quality during the drilling of the multimaterial stack composed of CFRP, titanium and aluminium alloys. Therefore, burr heights were inspected in the outlets of the metallic layers. Different cutting parameters, as well as different drilling strategies, were applied during those experiments. The heights of pecks during peck drilling, the feed variations while cutting, and the heights of cutting parameter changes (from one material cutting parameters to another) were the chosen parameters for the drilling strategy. Nevertheless, due to a minor impact of the selected drilling strategies, only the cutting parameters variations versus the burr heights were presented. Three cutting feed and three cutting speed levels were selected for each type of material within the

stack. The design of experiments, which was divided into two parts, included a  $L_{27}(3^6)$  Taguchi plan of experiment and a full plan of the couple feed-speed for each of the three materials.

Only the cutting parameters were selected as experiment variables for these two plans of experiments. Each design of experiments was performed three times and the order of the drillings was randomized for each repetition.

Three twist drills, with a common geometry and coating, were used to perform two series of 120 holes. During the experiments, the drills were put in contact with a sponge filled with coolant before each change of cutting parameters. The use of these diamond-coated tools is listed in Table A.1.

The levels of the cutting parameters are presented as normalised values using the central selected point as the cutting parameter reference.

Table A.1: Conducted plans of experiments for the twist drills

Tool #	Number of holes drilled	Experiments
1	118	2 Taguchi + 1 Full
2	64	1 Taguchi + 1 Strategy
3	56	1 Full + 1 Strategy

### A.6.2 Analyses performed

Analyses of variance (ANOVA) were performed for the thrust force, the torque burr height, the hole diameter and the circularity, allowing an identification of their impact and the quantification of the different cutting parameters.

The fractal dimensions of the CFRP cutting force signals were calculated using the regularization fractal analysis to evaluate the complexity of the signal. The regularization fractal analysis was chosen for its relative robustness [8, 10].

Regularization dimension is obtained after convolutions of the signal  $s$  with different Gaussian kernel  $g_a$  with a width of  $a$ . Then, the convolution product  $s_a$  can be expressed:

$$s_a = s * g_a \quad (\text{A.2})$$

The Gaussian kernel  $g_a$  used in our calculation was the first derivative of the 1-D Gaussian function with a width of  $a$ .

The hypothesis is that  $s_a$  has a finite length called  $l_a$ , for the size of  $a$  [10, 26]. The regularization dimension  $D_R$  is then obtained with:

$$D_R = 1 - \lim_{a \rightarrow 0} \frac{\ln l_a}{\ln a} \quad (\text{A.3})$$

The limit, in the equation 3, is usually estimated as the slope value when  $a$  values are close to 0 and when the coefficient of determination  $R$ -squared of the linear regression of a part of the curve is close to 1.

The thrust force signals obtained during the machining of the CFRP layer were analysed with this regularization technique giving the fractal dimensions. The relation between the computed fractal dimensions and the number of holes previously drilled was observed, as well the relations between the calculated fractal dimensions and the tool wear  $VB_{Bmax}$  and between the calculated fractal dimensions and the burr height ratio in the titanium and in the aluminium outlets.

Although the fractal dimension was computed on the torque and the thrust force signals acquired during the machining of the CFRP, titanium and aluminium, only the results of the thrust force fractal dimension during the CFRP machining are presented in this article.

### A.6.3 Measurements

The on-line measurements of cutting forces – thrust force and torque – were performed. The average values, calculated from the cutting force signals, were compared to the burr height ratio. As well as for the cutting parameter values, the results of the burr heights are presented as normalized, in percentage. The burr height ratio corresponds to the measured burr height over the maximum burr height obtained for the layer.

A digital probe indicator was used to measure the hole burr heights at the outlet of the titanium and aluminium layers. For each hole, the burr height value was assessed as an average of three measurements.

Both clearance faces of the twist drills were inspected every five drillings using the digital optical microscope VHX-600+500F Keyence. The tool wear  $VB_{Bmax}$  was estimated using the digital images captured with the microscope. The tool wear  $VB_{Bmax}$  presented in this article is expressed as the average of the tool wear estimated on both drill faces.

The hole dimensions were measured using the Mitutoyo Bright Strato coordinate measuring machine (CMM) in order to check the hole straightness to the generating line. The diameter and circularity were measured for each hole, and at the same depths from their references A, B and C, for CFRP, titanium and aluminium, respectively, as depicted in Figure A-5.

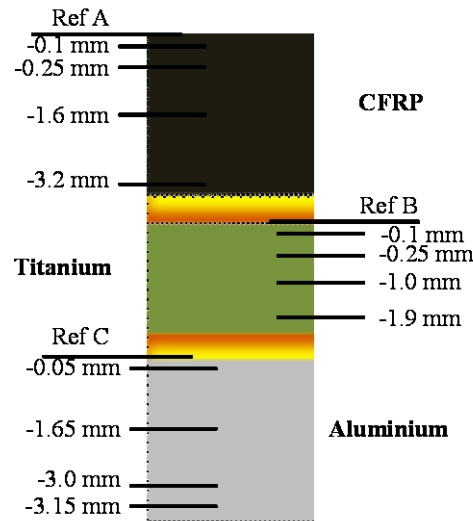


Figure A-5: Depths for the measurements of hole diameter and circularity (the references are at the top of each layer in the stack)

The presented thrust force and torque values are the averages of the signal obtained during one peck when the drill cutting edges are fully engaged in a same material. The final thrust force and torque values are estimated by the average of all the pecks.

## A.7 Results and discussion

### A.7.1 Burr height analysis

#### A.7.1.1 Titanium burr height analysis

The tool wear of identical tools can differ from the same cutting conditions after a certain number of drilled holes. This is why the burr height versus the tool wear was preferred to the burr height versus the number of drilled holes. The evolution of the measured titanium burr heights versus the measured clearance tool wear  $VB_{Bmax}$  is shown in Figure A-6. A regression was calculated using a third-order polynomial function showing the dependency between the burr height ratio and the tool wear.



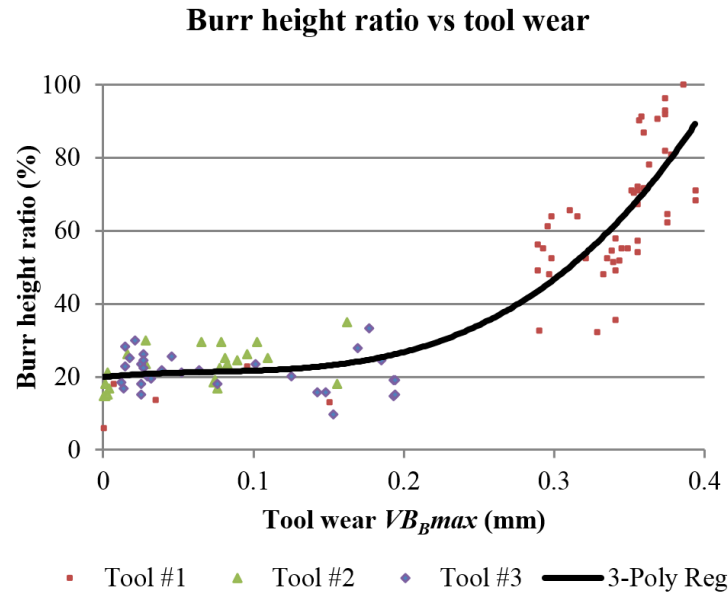


Figure A-6: Titanium burr height ratio versus the tool wear  $VB_{Bmax}$

Moreover, although the experiments were conducted on the stack of materials where there was no clearance at the titanium layer outlet, no limit seems to be reached by the burr heights. Nonetheless, the burr heights measured should instinctively tend to a maximum value for a high tool wear, due to the presence of the aluminium layer at the outlet side of the titanium layer. Two possible reasons can be taken into consideration. Firstly, the limit of the tool wear may not have been reached in our tests. In this case, further experiments might show a maximum or at least a reduction in the burr height increase versus the tool wear. The second reason may be that the mechanical characteristic differs for the titanium and aluminium alloys. Under the pressure applied from the tool during machining, the titanium burr is pushed onto the aluminium layer. Due to the lower hardness of the aluminium comparatively to the titanium, the aluminium part is locally deformed by the titanium burr.

The results of the titanium burr heights versus the thrust force and the torque are presented in Figure A-7 and in Figure A-8, respectively. The presented results were obtained from the titanium machining with the same cutting conditions in the titanium layer, which cutting parameters were selected at the central point of the titanium cutting speed and feed levels. The  $R$ -squared coefficient, calculated from the linear regression, is lower for the torque due to a higher dispersion, which equals 0.77 for Figure A-7 and 0.5 for Figure A-8.

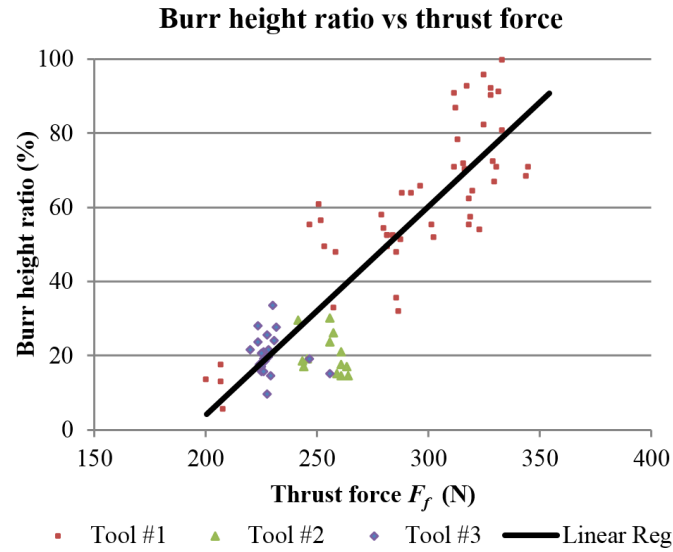


Figure A-7: Titanium burr height ratio versus the thrust force under same cutting parameters corresponding to the central point of the variation parameters for titanium

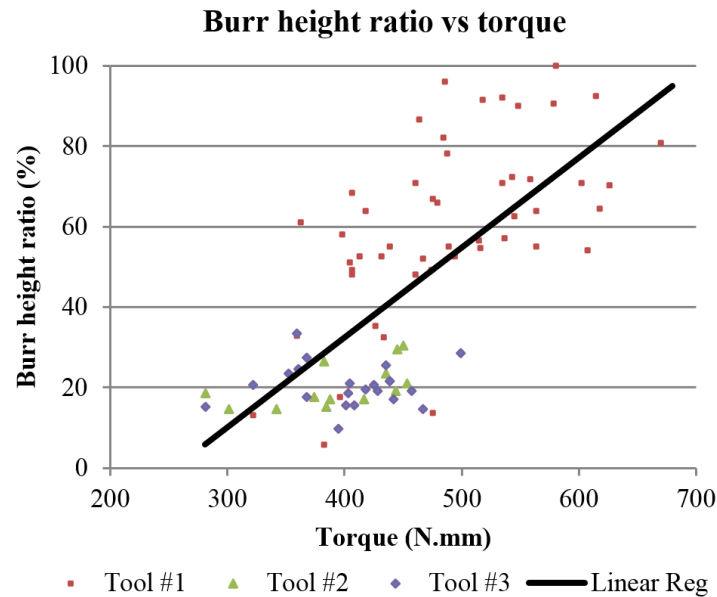


Figure A-8: Titanium burr height ratio versus the torque under same cutting parameters corresponding to the central point of the variation parameters for titanium

The means of the burr height ratio measured for each set of cutting parameters are shown in Table A.2. According to the results, the cutting speed in the titanium layer does not affect significantly the burr height as opposed to the cutting feed. The higher the feed is, the lower the burr heights are.

The relative standard deviation of the burr height was calculated using the measurement results of the holes drilled with the same cutting conditions with a tool wear lower than 0.20 mm, giving the result of 5.5 %.

Table A.2: Means of the titanium burr height ratios for each couple of feed and speed corresponding to the titanium layer

<b>Feed/Speed Levels</b>	<b>Titanium Speed 70%</b>	<b>Titanium Speed 100%</b>	<b>Titanium Speed 130%</b>
<b>Titanium Feed 60%</b>	51.3	48.5	50.6
<b>Titanium Feed 100%</b>	42.9	43.9	42.2
<b>Titanium Feed 140%</b>	36.6	40.4	26.8

On the thermoreactive paper, a dark halo around the hole was observed for each hole. The radial value of the halo was measured on the thermoreactive paper placed between the titanium and aluminium layers where the titanium burrs are investigated. The measured radial values of the halo were within the range between 0.02 mm and 0.05 mm. No other colour could be identified around this halo. Thus, the temperature gradient at the outer limits of the halo was high.

#### **A.7.1.2 Aluminium burr height analysis**

Firstly, the observations at the outlet of the holes on the aluminium layer presented no attachment onto the exit surface such as ring or drill cap. This statement was valid for all the cutting feed or speed levels and for all the cutting strategy selected.

The evolution of the measured aluminium burr height versus the tool wear  $VB_{Bmax}$  is depicted in Figure A-9. A regression was calculated using a third-order polynomial function showing the dependency between the burr height ratio and the tool wear.

Figure A-10 shows the measured aluminium burr height versus the thrust force. The dependency between the burr height and the thrust force is illustrated by the calculated exponential regression function drawn in Figure A-10. The  $R$ -squared coefficient calculated from the exponential regression equals 0.54. Although a correlation can be observed between the burr height and thrust force, no significant correlation can be detected between the torque and the aluminium burr heights. Dispersion of the results is relatively high and the correlation coefficient calculated was close to zero.

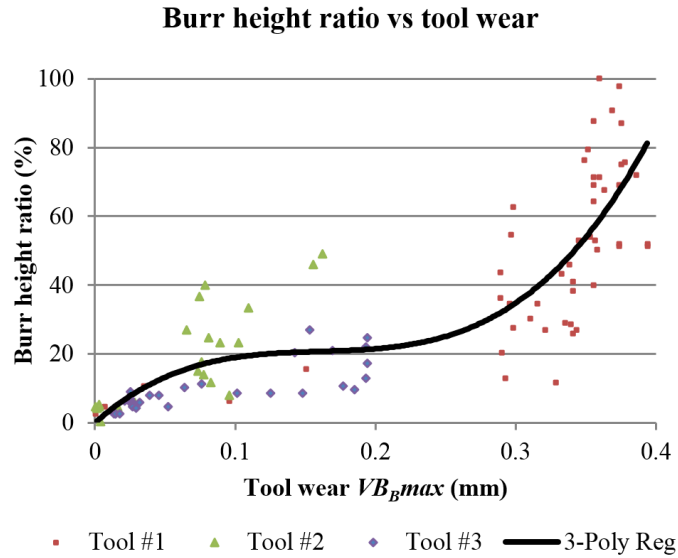


Figure A-9: Aluminium burr height ratio versus the tool wear  $VB_{Bmax}$

Table A.3 shows the means of the burr height ratios measured for each set of aluminium cutting parameters. According to these results, for high cutting speed, the aluminium burr heights remains steady whatever the feed is. However, for low and central cutting speed levels, higher burr heights are generated for higher cutting feed levels.

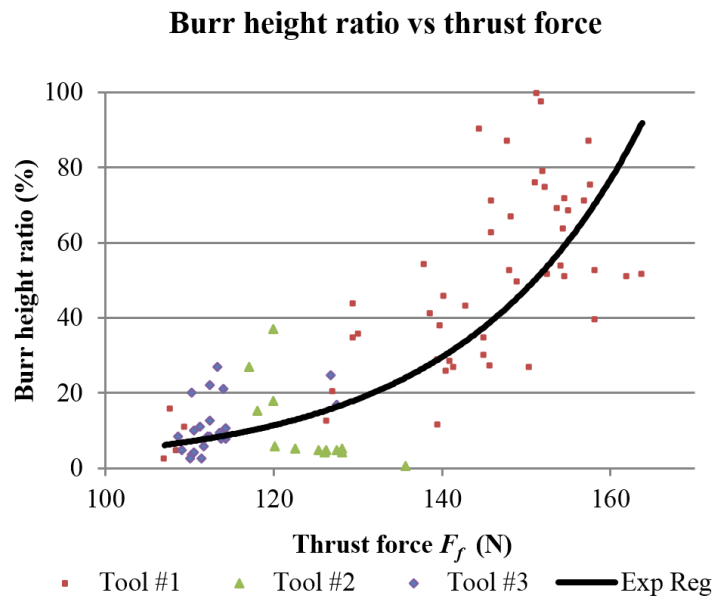


Figure A-10: Aluminium burr height ratio versus the thrust force under same cutting parameters corresponding to the central point of the variation parameters for titanium

The relative standard deviation calculated for the aluminium burr height was computed using the measurement results of the holes drilled with the same cutting conditions with a tool wear inferior to 0.20 mm, giving the result of approximately 10%.

Table A.3: Means of the aluminium burr height ratios for each couple of feed and speed corresponding to the aluminium layer

Feed/Speed Levels	Al Speed 60%	Al Speed 100%	Al Speed 140%
Al Feed 75%	29.2	31.0	33.7
Al Feed 100%	34.6	35.7	32.2
Al Feed 125%	40.5	42.0	32.9

### A.7.2 Fractal analysis of cutting forces

The observation of the cutting force signals during drilling the CFRP, titanium and aluminium suggested performing fractal analysis on those signals. Figure A-11 and Figure A-12 show an example of the measured thrust force signals during the machining of CFRP, obtained with a sharp tool and a worn tool.

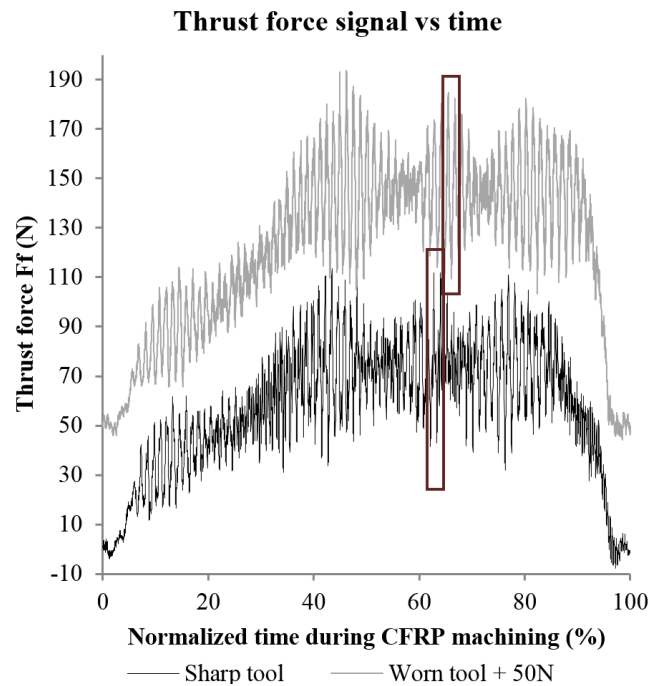


Figure A-11: Measured thrust force signals for sharp and worn tools during CFRP machining

The signal acquired during the whole CFRP machining, shown in Figure A-11, highlights the more erratic character of the sharp tool comparing to the worn one. This observation is confirmed with

the graph presented in Figure A-12 which is a magnification of the frames from Figure A-11. The worn tool signal over a period seems to be close to a periodical function whereas the signal is more irregular.

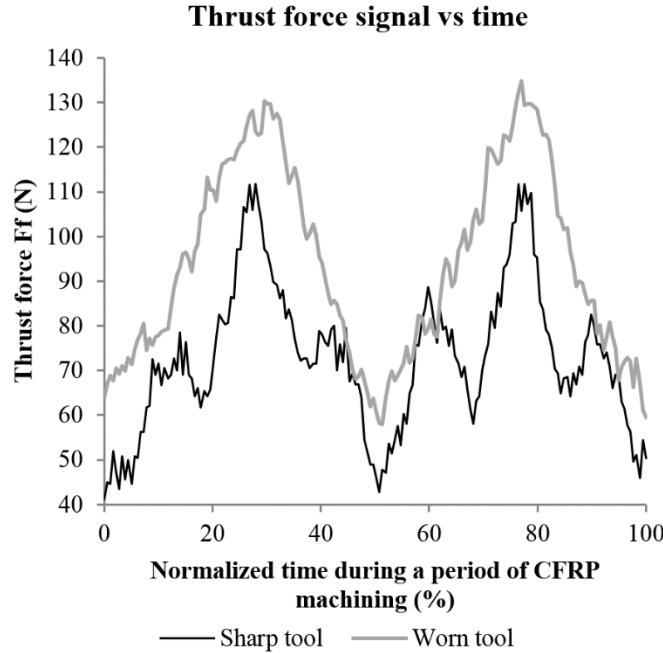


Figure A-12: Measured thrust force signals for sharp and worn tools over a period during CFRP drilling (magnification of the frames from Figure A-11)

As mentioned above, the regularization fractal analysis was processed on the signals of the cutting force. In the preliminary study, it was performed for the thrust force signals obtained with one tool at different tool wear levels under the same cutting conditions. Figure A-13 shows the graph  $\ln l_a$  (length of the convolution product estimated for the size  $a$ ) versus  $\ln a$ , for one tool while drilling the hole numbers 1, 17, 34, 55, 82 and 115. In order to estimate the slope value and so, the fractal dimension, the least square (LS) method was used. However, it is crucial to determine the range where the slope value is calculated. According to the fractal dimension definition, this range is selected where the slope derivative remains stable and for the lowest values of  $a$ . Nevertheless, we found that the obtained results from such a range show very low impact towards the number of holes drilled or the tool wear. Depending on the scale of observation, the noise from the dynamometer or the CNC machine prevails on the signal of the cutting forces. This is why the range determination needs to be re-established.

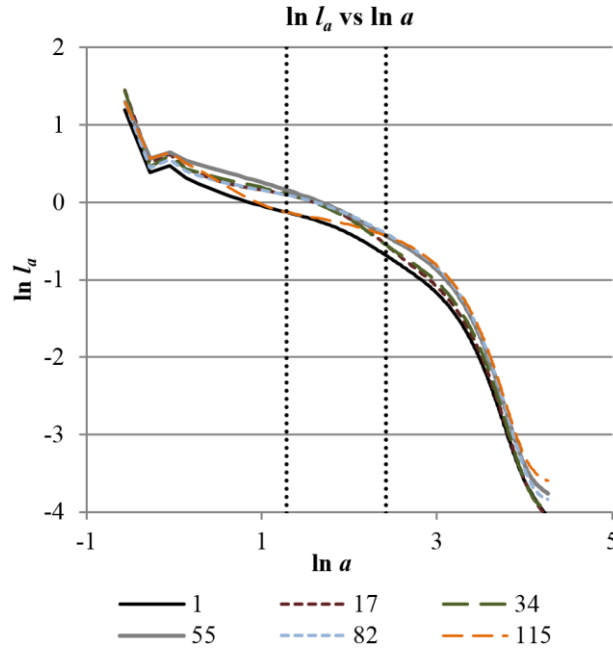


Figure A-13: Graphs  $\ln l_a$  (length of the convolution product estimated for the size  $a$ ) versus  $\ln a$  computed from the thrust force signals obtained during the CFRP machining using one tool after drilling the holes 1, 17, 34, 55, 82 and 115

From preliminary analyses, the best fit for the upper limit of this range was found for the sampling points acquired during one third of the tool rotation period. The lower limit was selected for a fixed sampling length, which does not depend on the cutting speed. No relevant feed rate impact was found over those two limits. This range selection was used for the following fractal dimension estimations. The selected range between those upper and lower limits is represented by dot lines in Figure A-13. The graph presented in Figure A-14 corresponds to the magnification of the graph area within the selected range in Figure A-13.

For each hole, the regularization fractal analysis was performed on the thrust force and on the torque signals from the CFRP machining. Though, only the results computed from the thrust force show less dispersion and are presented.

This analysis was similarly realized on the torque and on the thrust force signals obtained during the titanium and aluminium machining. From this investigation, the computed fractal dimensions show an even higher dispersion. However, the use of the fractal analysis on the cutting force signals in these homogeneous materials, such as employed aluminium and titanium alloys, may not be relevant. Even if the shape of the cutting force signals is more jagged with a worn tool, the

difference is not as visible as for the signals from the CFRP machining. Figure A-15 depicts the thrust force signals for a sharp tool and a worn tool over one tool rotation period. Admittedly, the amplitudes of both periodical curves are different, but they share, relatively, similar curvature and similar noise.

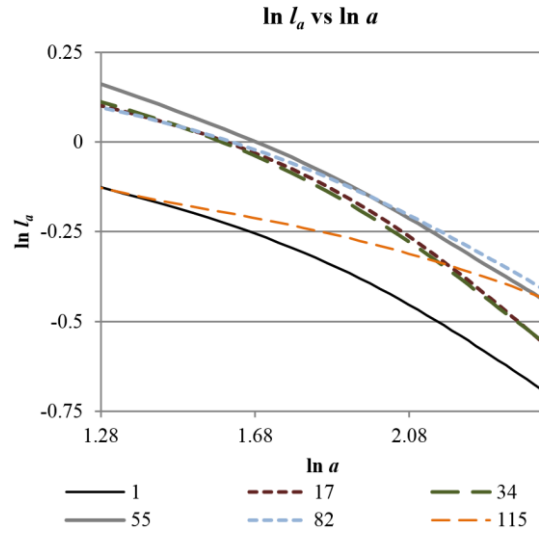


Figure A-14: Graphs  $\ln l_a$  (length of the convolution product estimated for the size  $\mathbf{a}$ ) versus  $\ln a$  from the thrust force signals obtained from the CFRP machining using one tool after drilling the holes 1, 17, 34, 55, 82 and 115 (magnification of the area between the vertical lines from Figure A-13)

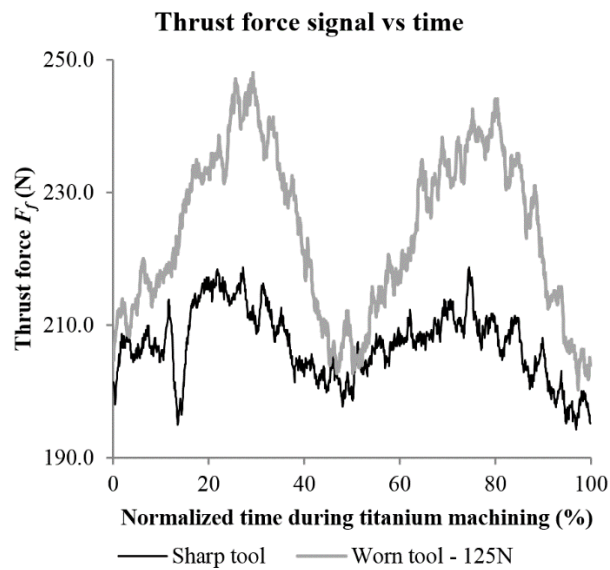


Figure A-15: Measured thrust force signals for sharp and worn tools over a period during titanium machining



After adapting the regularization fractal analysis to our case, the repeatability of this analysis needs to be checked to evaluate the results. Fractal dimension was calculated for different sampling lengths of a single thrust force signal. Each relative standard deviation was computed from one hundred fractal dimensions  $D_R$  calculated from signal sections. The relative standard deviations were calculated using different sampling lengths, which is presented in Figure A-16.

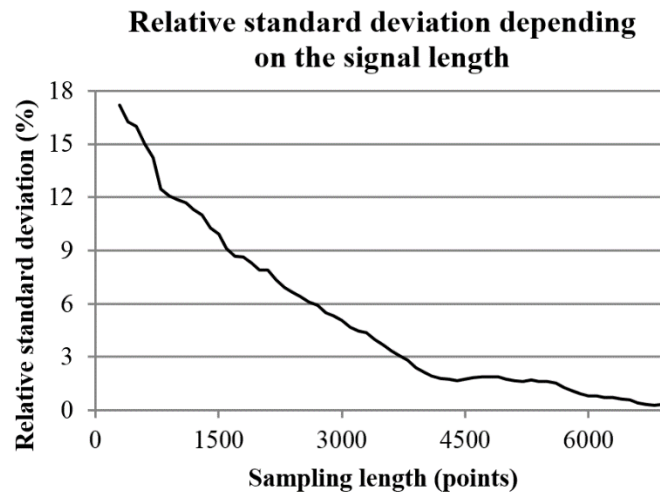


Figure A-16: Relative standard deviations of fractal dimensions  $D_R$ , calculated for different sampling lengths

The relative standard deviation is around 17% for short signal lengths (around 300 points). For a treated signal of 4000 points and more, the relative standard deviation drops under 2%. All the signals analysed from the CFRP machining had a wider length than 4000 points.

Table A.4: Means of the calculated force signal fractal dimensions  $D_R$  for each couple of feed and speed levels corresponding to the CFRP layer

Feed/Speed Levels	CFRP Speed 60%	CFRP Speed 100%	CFRP Speed 140%
<b>CFRP Feed 70%</b>	1.66	1.59	1.50
<b>CFRP Feed 100%</b>	1.65	1.53	1.46
<b>CFRP Feed 130%</b>	1.57	1.56	1.45

Table A.4 shows the means of the fractal dimensions  $D_R$ , computed on the thrust force signals during the CFRP drilling for each hole. The means were calculated for each level of the CFRP cutting parameters (feed and speed). Those mean values point a maximum of 15% variation and need to be taken into account for further considerations. Figure A-17 depicts the calculated dimensions for cutting speed and feed at 100%. For each signal, three slope values were estimated

using the LS method and the minimum (Min) and maximum (Max) limits by consecutives eliminations.

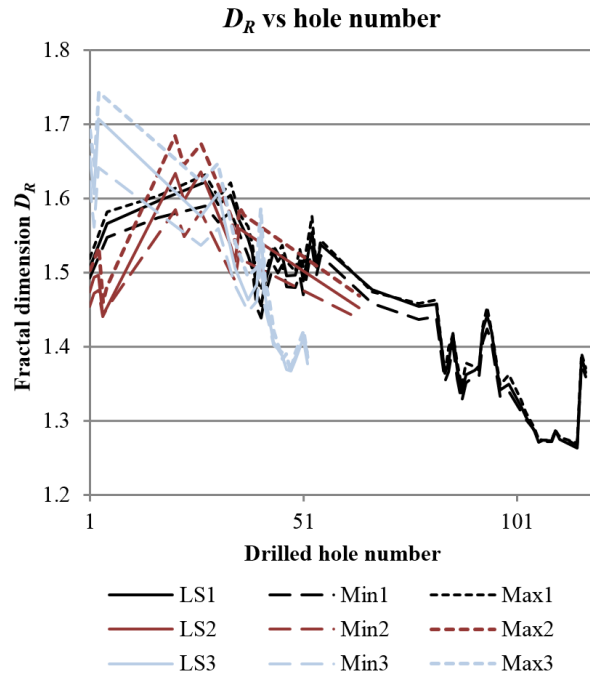


Figure A-17: Fractal dimension  $D_R$  versus the number of hole drilled for 100% CFRP cutting speed and feed levels (LS 1-3: Fractal dimension  $D_R$  estimated with least square method for tools 1-3, Min: minimum limit of Fractal dimension  $D_R$ , Max: maximum limit of Fractal dimension  $D_R$ )

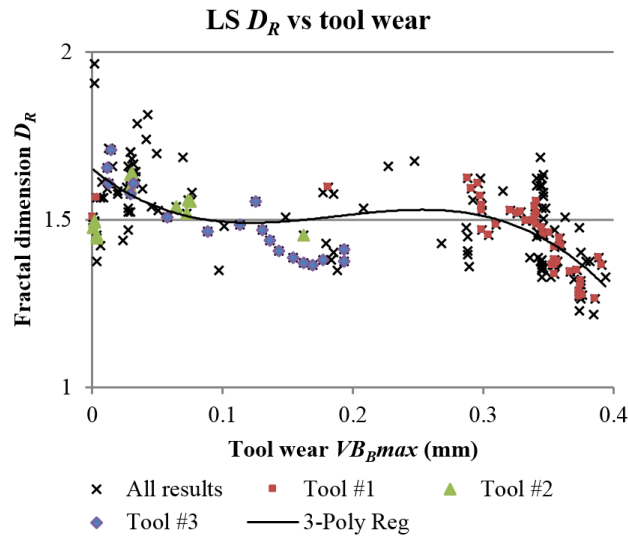


Figure A-18: Fractal dimensions  $D_R$  using least square (LS) method versus the tool wear  $VB_{Bmax}$

All the results of the calculated fractal dimension versus the tool wear  $VB_{Bmax}$  are presented in Figure A-18. A third degree polynomial regression was drawn with a 0.52  $R$ -squared value. The fractal dimension remains relatively constant until it drastically drops for a higher tool wear.

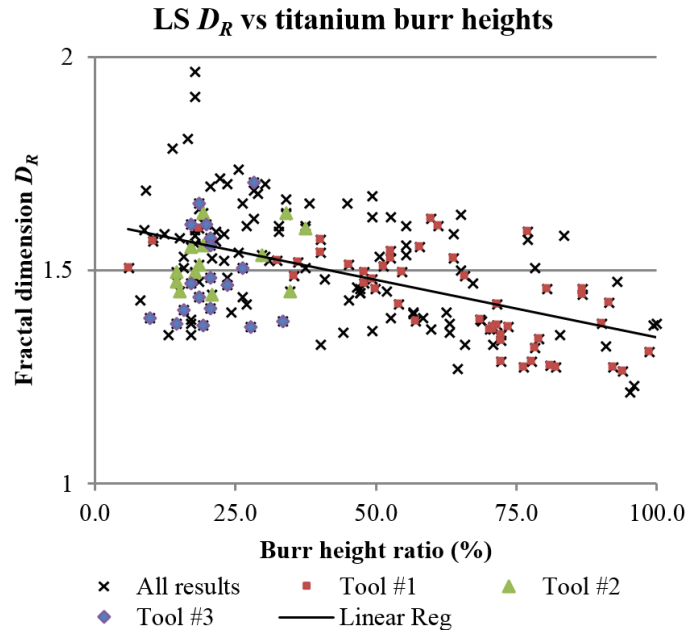


Figure A-19: Fractal dimensions  $D_R$  using least square (LS) method versus titanium burr height ratio

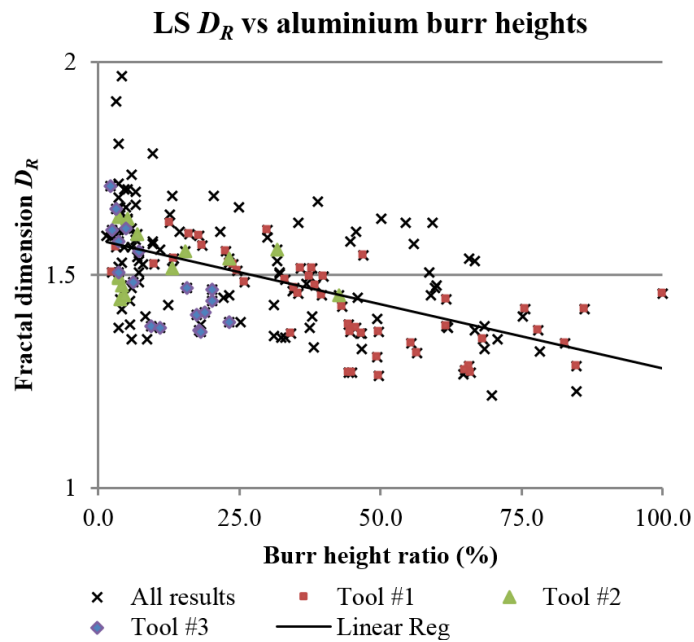


Figure A-20: Fractal dimensions  $D_R$  using least square (LS) method versus aluminium burr height ratio

Figure A-19 and Figure A-20 depict the fractal dimensions versus the titanium burr height ratio and the aluminium burr height ratio, respectively. For all the results, regardless the cutting parameters of any layer, a linear regression was drawn as an approximation of the results with a  $R$ -squared value of 0.45 for both, titanium and aluminium, burr heights. Regarding the results of the aluminium burrs for one tool used with same cutting parameters selected, the  $R$ -squared score jumps to 0.65 and 0.84 with a two and three degree polynomial regression, respectively.

In addition to the tool wear or cutting forces in titanium and aluminium layers, fractal dimension  $D_R$  calculated from the thrust force signals during the CFRP machining can be another feature to monitor the burr generation. It may also be possible to evaluate the tool wear. The advantage of this method results in the prediction of the burr heights in the titanium and aluminium outlets before the tool drills these layers. This allows preventing off-tolerance burr heights without altering the production time.

## A.8 Conclusion

A method to monitor the burr heights in a multimaterial stack was developed based on the regularization fractal analysis. Because, in the industry, a deburring process may not be performed following the drilling of a multimaterial stack, the burr heights need to be monitored. The thrust force signals acquired during the drilling of the CFRP layer were analysed using an adaptation of the regularization analysis, giving the fractal dimension. This fractal dimension allows to monitor and to estimate the burr heights in the metallic layers of the stack composed of CFRP, titanium and aluminium. Using the cutting forces obtained from a dynamometer table, the burr heights can be estimated when the tool is drilling the CFRP layer and before it reaches the titanium and aluminium layers. Hence, this technique allows preventing to generate hole burr heights outside tolerance requirements and improving production efficiency. Even if the use of a dynamometer table remains complicated to integrate in some industry processes, this analysis and monitoring technique may be implemented e.g. for signals from AE sensors placed onto the CNC machine relatively close to the spindle.

To feature this monitoring technique, multimaterial stack drilling experiments were conducted using diamond-coated twist drills. The burr heights versus factors such as speed and feed levels, tool wear, thrust force, torque, diameter and circularity were studied. The results show that the

titanium burr heights can be reduced using a higher feed. For titanium burrs, the process can be observed thanks to the torque average while drilling the titanium layer and, for more accuracy, with the thrust force average. The tool wear is also an effective way to check the burr height. The aluminium burrs can be reduced by increasing the cutting speed or by decreasing the feed. The aluminium burrs can be monitored as well with the thrust force average while drilling the aluminium layer, and also with the tool wear.

## A.9 Acknowledgements

The authors wish to thank the Consortium for Research and Innovation in Aerospace in Québec (CRIAQ) and its partners, the Natural Sciences and Engineering Research Council of Canada (NSERC), Mitacs, Bombardier Aerospace, Avior Integrated Products, Delastek and AVR&R Aerospatiale, for their financial support. The regularization fractal dimensions were computed based on the program code of the FracLab software developed by INRIA France.

## A.10 References

- [1] I.S. Shyha, S.L. Soo, D.K. Aspinwall, S. Bradley, R. Perry, P. Harden, S. Dawson. Hole quality assessment following drilling of metallic-composite stacks, *International Journal of Machine Tools and Manufacture*, 51 (2011) 569-578.
- [2] H.K. Tönsheff, T. Friemuth, M. Groppe. A solution for an economical machining of bore holes in composite materials (CFK, aluminum), in: *Proceedings of 3rd International Conference on Metal Cutting and High Speed Machining*, Metz (France), 2001.
- [3] J. Mathew, N. Ramakrishnan, N.K. Naik. Investigations into the effect of geometry of a trepanning tool on thrust and torque during drilling of GFRP composites, *Journal of Materials Processing Technology*, 91 (1999) 1-11.
- [4] D.A. Dornfeld, J.S. Kim, H. Dechow, J. Hewson, L.J. Chen. Drilling Burr Formation in Titanium Alloy, Ti-6Al-4V, *CIRP Annals - Manufacturing Technology*, 48 (1999) 73-76.
- [5] E. Brinksmeier, R. Janssen. Drilling of Multi-Layer Composite Materials consisting of Carbon Fiber Reinforced Plastics (CFRP), Titanium and Aluminum Alloys, *CIRP Annals - Manufacturing Technology*, 51 (2002) 87-90.
- [6] B. Mandelbrot. *Les objets fractals : Forme, hasard et dimension*, France: Flammarion, 1975.
- [7] B. Sapoval. *Universalités et fractales*, Science ed., France: Flammarion, 1997.
- [8] Z. Feng, M.J. Zuo, F. Chu. Application of regularization dimension to gear damage assessment, *Mechanical Systems and Signal Processing*, 24 (2010) 1081-1098.

- [9] J. Yang, Y. Zhang, Y. Zhu. Intelligent fault diagnosis of rolling element bearing based on SVMs and fractal dimension, *Mechanical Systems and Signal Processing*, 21 (2007) 2012-2024.
- [10] F. Roueff, J. Lévy Véhel. A Regularization Approach to Fractional Dimension Estimation, in: M.M. Novak (Ed.) *Fractals 98: World Scientific*, 1998.
- [11] E. Persson, I. Eriksson, L. Zackrisson. Effects of hole machining defects on strength and fatigue life of composite laminates, *Composites Part A: Applied Science and Manufacturing*, 28 (1997) 141-151.
- [12] W. König, C. Wulf, P. Graß, H. Willerscheid. Machining of Fibre Reinforced Plastics, *CIRP Annals - Manufacturing Technology*, 34 (1985) 537-548.
- [13] P. Guegan, F. Lemaitre, J. Hamann. Contribution à l'usinage des matériaux composites, in: I. Brest (Ed.) *La Construction Navale en Composites*, Paris (France), 1992, pp. 11.
- [14] D.A. Stephenson, J.S. Agapiou. *Metal cutting theory and practice: CRC press*, 2005.
- [15] C.C. Tsao, H. Hocheng. Effect of tool wear on delamination in drilling composite materials, *International Journal of Mechanical Sciences*, 49 (2007) 983-988.
- [16] X. Yang, C. Richard Liu. Machining titanium and its alloys, *Machining Science and Technology*, 3 (1999) 107-139.
- [17] A. Molinari, C. Musquar, G. Sutter. Adiabatic shear banding in high speed machining of Ti-6Al-4V: experiments and modeling, *International Journal of Plasticity*, 18 (2002) 443-459.
- [18] I.J. Polmear. *Light Alloys - Metallurgy of the Light Metals: Halsted Press*, 1996.
- [19] J.L. Cantero, M.M. Tardio, J.A. Canteli, M. Marcos, M.H. Miguelez. Dry drilling of alloy Ti-6Al-4V, *International Journal of Machine Tools & Manufacture*, 45 (2005) 1246-1255.
- [20] M. Ramulu, T. Branson, D. Kim. A study on the drilling of composite and titanium stacks, *Composite Structures*, 54 (2001) 67-77.
- [21] P.F. Zhang, N.J. Churi, Z.J. Pei, C. Treadwell. Mechanical drilling processes for titanium alloys: a literature review, *Machining Science and Technology*, 12 (2008) 417-444.
- [22] G. List, M. Nouari, D. Géhin, S. Gomez, J.P. Manaud, Y. Le Petitcorps, F. Girot. Wear behaviour of cemented carbide tools in dry machining of aluminium alloy, *Wear*, 259 (2005) 1177-1189.
- [23] M. Nouari, G. List, F. Girot, D. Géhin. Effect of machining parameters and coating on wear mechanisms in dry drilling of aluminium alloys, *International Journal of Machine Tools and Manufacture*, 45 (2005) 1436-1442.
- [24] A.I.H. Committee. Properties and Selection : Nonferrous Alloys and Special-Purpose Materials, in: A. International (Ed.) *ASM Handbook: ASM International*, 1992, pp. 3470.
- [25] A.I.H. Committee. Machining, in: A. International (Ed.) *ASM Handbook: ASM International*, 1992, pp. 929.
- [26] J. Lévy Véhel, P. Legrand. Signal and image processing with Fraclab, in: C.a.F.i.N. *Proceedings of Fractal04 (Ed.) Eighth International Multidisciplinary Conference*, Vancouver, Canada, 2004.

## **APPENDIX B – ARTICLE 5: FRACTAL ANALYSIS OF CUTTING FORCE AND ACOUSTIC EMISSION SIGNALS DURING CFRP MACHINING**

Xavier Rimpault<sup>a</sup>, Jean-François Chatelain<sup>b</sup>, Jolanta E. Klemberg-Sapieha<sup>c</sup>, Marek Balazinski<sup>a</sup>

<sup>a</sup>Department of Mechanical Engineering, Polytechnique Montréal, Canada

<sup>b</sup>Department of Mechanical Engineering, École de Technologie Supérieure, Canada

<sup>c</sup>Department of Engineering Physics, Polytechnique Montréal, Canada

\* Published in *Procedia CIRP*, vol.46, pp.143-146, 2016.

### **B.1 Abstract**

Cutting forces and acoustic emissions signals while machining Fiber Reinforced Plastics (FRP) depends strongly on the tool wear. Fractal analysis can be adapted to those signals to characterize their variations. This tool wear monitoring technique is presented herein for the carbon FRP (CFRP) orbital drilling. Fractal parameters, characterizing the signal complexity and ruggedness, are very efficient for machining quality estimation and to follow the tool wear evolution.

*Keywords:* Fiber reinforced plastic, orbital drilling, fractal analysis, cutting force, acoustic emission, tool wear.

### **B.2 Introduction**

Carbon fiber reinforced plastics (CFRPs) have been increasingly used in the aerospace industry over the past decades due to its lightweight vs mechanical properties. CFRP is constituted of two very different materials (carbon fiber and epoxy resin). The CFRP machining usually involves only finishing operations, thanks to its manufacturing, allowing CFRP components to be produced close to their final shape. To evaluate the machining quality, surface integrity is examined. Several problems may occur during fibre reinforced plastic (FRP) machining, e.g. uncut fibres, pulled fibres, delamination and burnt resin [1-4]. Due to the abrasiveness and hardness of the carbon fibres, abrasion is considered as the main tool wear mechanism [5, 6]. With the tool wear increase, keeping sufficient machining quality is challenging, and the surface quality should be examined through the tool life. Hamedanianpour et al. found that, even if the tool wear is still considered as

functional, the resin may be burnt during the CFRP machining leading to a lower surface quality [7].

New techniques of tool wear monitoring can emerge due to the FRP heterogeneity. With the tool wear increase, the cutting tool edge radius increases resulting in lower surface quality and the signals' change of cutting forces and acoustic emissions (AEs). In addition to statistical parameters to extract quantitative data from such signals, fractal analysis was used to estimate the complexity of the signal [8, 9]. Therein, cutting force and vibratory signals were analyzed during homogeneous materials machining. However, the changes of the signal complexity through the tool life seem to be relatively low during the machining of homogeneous materials. Nevertheless, the cutting force and AE signals observed while machining CFRP show relatively high signal complexity variations for different tool wear. Thus, performing the fractal analysis of such signals would be relevant. In this study, the orbital drilling of composite/metal stack is investigated. The drilling of such stack is a major concern in the aerospace industry, which is part of the last assembly process of current airplanes' structural parts. In addition to issues specific to each material of the stack, machining stacks constituted of very different characteristics materials leads to further problems. So, process monitoring is crucial to maintain sufficient machining quality.

## **B.3 Materials and methodology**

### **B.3.1 Machining setup**

The machined part was a stack composed of a quasi-isotropic CFRP, prepared using 24 pre-impregnated plies, with a 3.3 mm thickness, and Ti-6Al-4V titanium alloy, with a 3.0 mm thickness. The K2X10 Huron® high-speed machining center was used to conduct the machining tests. A dust extraction system was mounted onto the machine for health and safety purposes. The stack was machined by orbital drilling with different cutting parameters for each material of the stack. The cutting parameters, used to drill the 5.85 mm diameter holes, are presented in Table B.1. The tool was a four flutes uncoated carbide shoulder mill with a 4 mm diameter, 30° helix angle and 11 mm maximum depth of cut. The composite/metal stack was drilled using the same setup until the complete tool failure. A total of 44 holes was achieved even though the tool had already reached the end of its tool life.



Table B.1: Cutting parameters

Material	Helix step (mm)	Feed (mm/min)	Speed (RPM)
CFRP	0.7	800	11 000
Titanium	0.35	300	3 200

### B.3.2 Measurements

The cutting force and AE signals were acquired during the tests using a dynamometer table and an AE sensor. The experimental setup is presented in Figure B-1. The input signal from both systems were acquired using the same amplifier and DAQ system at the 48 kHz frequency rate. The cutting force and AE signals from the CFRP machining were analyzed. The machining of titanium allowed generating a faster tool wear.

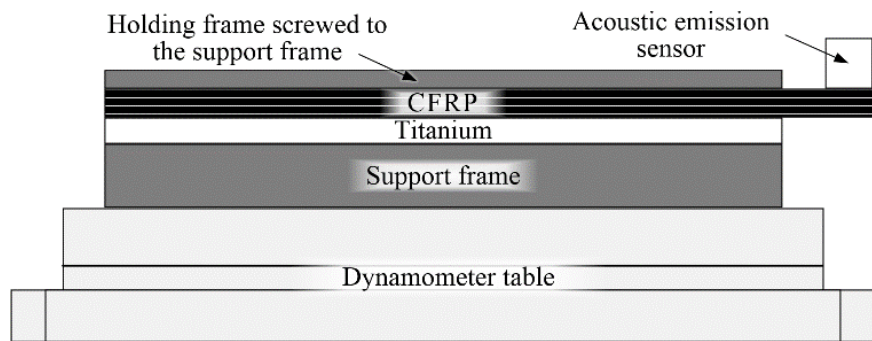


Figure B-1: Experimental setup representation

The tool wear was estimated between each drilling in order to evaluate the fractal parameters along the tool life. The tool wear was estimated using VHC 600+500F Keyence<sup>®</sup> optical microscope pictures which were taken on the clearance face of the tool tip edges. The maximum tool wear  $VB_{max}$  was estimated according to ISO standard recommendations [10]. The tool wear  $VB$  is introduced as the  $VB_{max}$  average of the four tool cutting edges.

Figure B-2 depicts the acquired signals (the cutting forces signals, the total cutting force signal and the AE signal) during the first drilling. The signal section analyzed corresponds to the area between the dash lines (Figure B-2), which is the relatively stable part of the CFRP machining using CFRP cutting parameters.

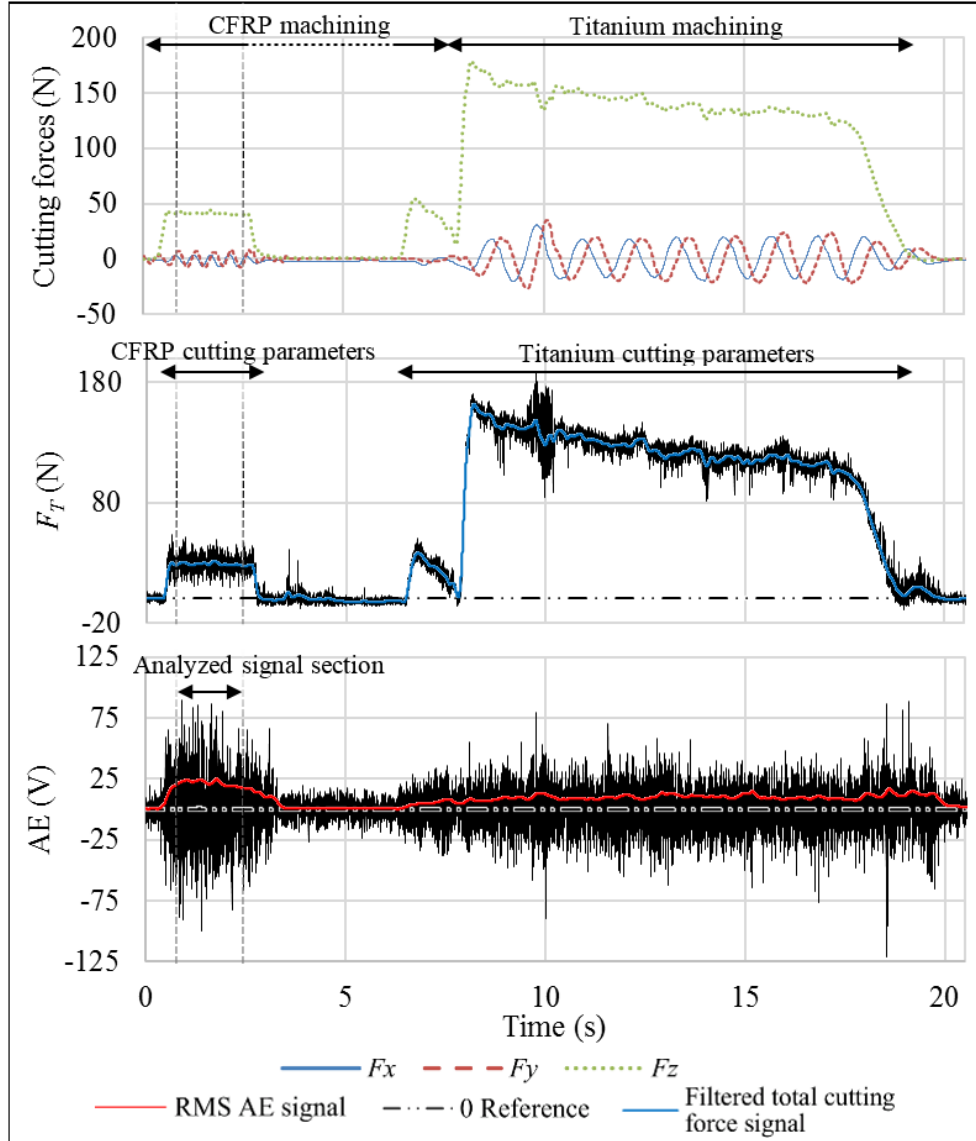


Figure B-2: Filtered cutting forces (top), total cutting force (center) and filtered and root mean square (RMS) acoustic emission (AE – bottom) signals

To highlight the changes of the signals' shape through the tool life, Figure B-3 show magnified signal samples from the analyzed section for different tool wear. In Figure B-3, the signal sample of the total cutting force  $F_T$  is relatively steady for a new tool. Then, the passes due to the cutting edges, can be identified on the cutting force signal with higher tool wear.

The signal samples from the AE sensor acquisition for different tool wear show similar trends (Figure B-3), in comparison with the cutting force signal samples. However, the periodic oscillation in those samples is more distinct with the tool wear increase.

From the signals observation of the AE and the cutting force, two outlines can be identified. At high frequency (so at low scale) the signal seems affected with noise for the first holes and becomes sharper with the tool wear increase. At a higher scale (around the tool rotation frequency), both signal types turns from a steady signal for the first holes, to increasingly clearer periodic oscillations for higher tool wear. The period corresponds to the tool rotation time per tooth.

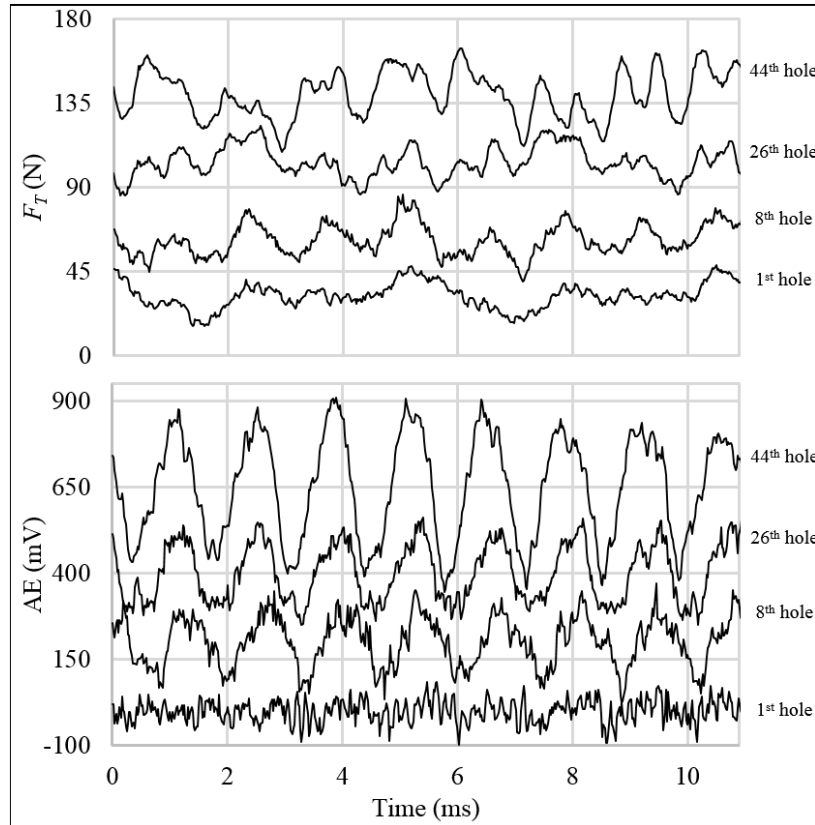


Figure B-3: Zoom samples, from the analyzed section presented in Fig. 2, of the total cutting force ( $F_T$ ) signals – up – and of the acoustic emission (AE) signals – down – over two tool rotation periods for different holes

### B.3.3 Fractal analysis

Fractal analysis allows quantifying the signal complexity by a single value, the fractal dimension. Adapted to the cutting force and AE signal, several signal features changes (e.g. complexity, shape) can be tracked along the tool life.

Various fractal analysis emerged such as box-counting but have some constraints e.g. relatively low robustness. The regularization fractal analysis, selected herein, was used to assess gear damage

using accelerometer signals [11] and showed relatively good repeatability rates. This regularization dimension is estimated from the convolutions of the signal ‘ $s$ ’ with different kernels  $g_a$  with a width of ‘ $a$ ’ [12, 13]. Each convolution product  $s_a$  is written:

$$s_a = s * g_a \quad (\text{B.1})$$

The kernels  $g_a$  are based on a rectangle kernel which is an affine function. Then, the hypothesis that  $s_a$  has a finite length called  $l_a$ , for the size of ‘ $a$ ’, is set. The regularization dimension  $D_R$  is calculated using:

$$D_R = 1 - \lim_{a \rightarrow 0} \frac{\log l_a}{\log a} \quad (\text{B.2})$$

The limit, in the equation B.2, is usually estimated as the slope estimation, where the ‘ $a$ ’ values are the smallest and the coefficient of determination,  $R^2$ , of the linear regression of a part of the curve ( $\log l_a$  vs  $\log a$ ) is close to 1. From preliminary analyses, the range of the slope determination was selected for the low scale (from 2 kHz to 6 kHz so between eight and 23 sampling points). In the case where the cutting parameters would change, the range determination could be selected accordingly, and adapted depending on the cutting speed.

Samples of curves ( $\log l_a$  vs  $\log a$ ) determining the fractal dimension and fractal parameters are shown in Figure B-4. For both, cutting forces and AEs, the tool wear influence is easily identified from the fractal dimension determination curve characteristics. The curve is relatively straight for the first holes. With higher tool wear, the curves becomes bumpy with higher and more distinct arches. Those periodic arches illustrate the tool tooth rotations observable in the AE and cutting force signals (Figure B-3).

## B.4 Results and discussion

The fractal analysis results are shown in Figure B-5. The fractal dimension  $D$ , the topothesy  $G$  and the  $R^2$  calculated for each drilling from the total cutting force and AE signals are presented hereafter. The fractal dimension  $D$  (slope value in the selected range) is a factor characterizing the signal complexity, the topothesy  $G$  (slope offset) quantifies the signal ruggedness and the  $R^2$  (slope coefficient of determination) stands for the auto-scale regularity of the signal. Results from the AE signals analysis reflect the tool wear evolution more efficiently than for the cutting force signals.

A fractal index  $I_F$  is introduced in order to propose an efficient machining quality factor improving the monitoring process:

$$I_F = \frac{D \cdot G}{R^2} \quad (\text{B.2})$$

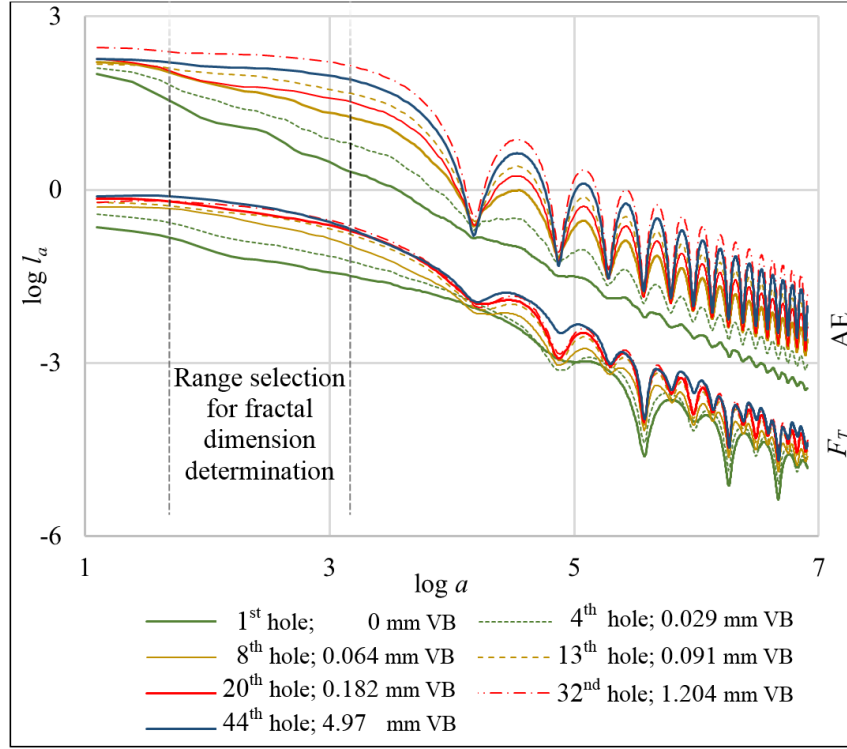


Figure B-4: Graph of curve samples for the fractal dimension determination using the rectangular kernel of total cutting force and acoustic emission signals

Figure B-6 depicts this index, and the tool wear, vs the holes drilled, including the three wear stages. Due to the complexity of the tool wear evaluation for such a tool, the stages are fairly an indication of their positions. The primary stage (**I**) is found to end around the third hole and the steady state stage (**II**) to end around the 20<sup>th</sup> hole with the beginning of the rapid wear stage (**III**). All parameters and so the fractal index vs the holes drilled show humps, during the initial wear stage (A in Figure B-6) and at the beginning of the third stage (B in Figure B-6), characterized by a rapid tool wear increase. Both humps in the fractal index (A and B in Figure B-6) are linked to the changes of the tool wear derivate. This  $I_F$  index humps point out high curve variations of the tool wear.

In Figure B-6, the fractal index of AE signals analysis also presents a continuous decrease during the second stage which could be linked to the machining quality decreasing along the tool wear evolution. This stage **II** is crucial due to the critical point presence of machining quality turnaround within this second stage. This abrupt change of surface quality occurs around the 15<sup>th</sup> hole. So, by setting up an  $I_F$  index threshold at 0.5, low machining quality could be avoided.

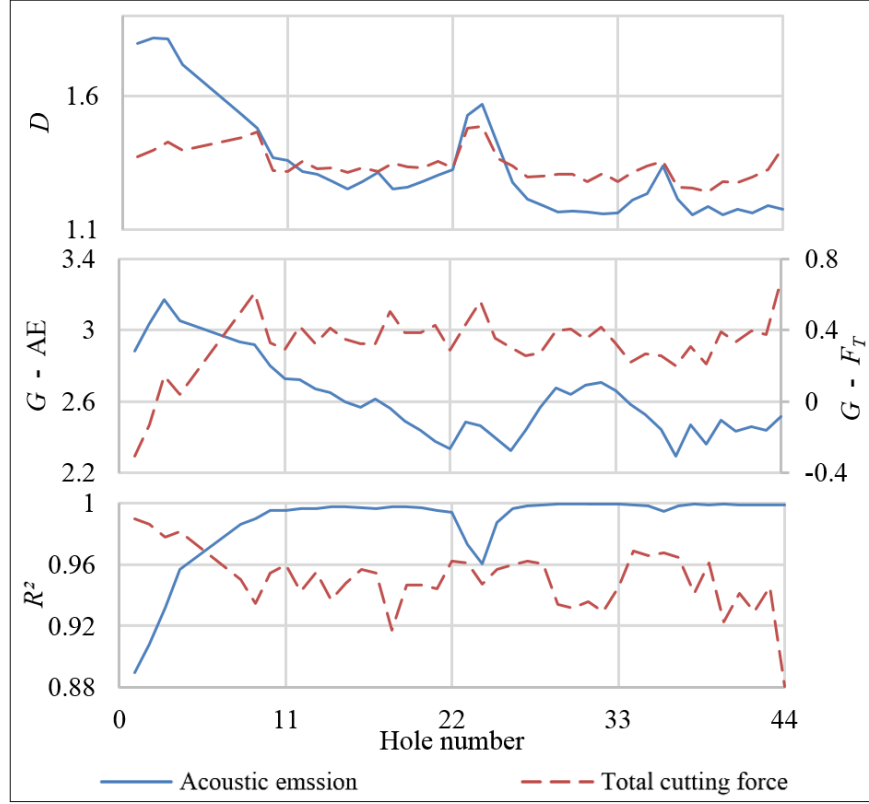


Figure B-5: Results of the fractal dimension  $D$ , the topothesy  $G$  and the  $R^2$  from the analysis of  $F_T$  and AE signals vs the number of holes drilled

## B.5 Conclusion

A promising online monitoring method of tool wear while machining composite is presented in this study based on fractal analysis of cutting force and AE signals. The fractal parameters and index are found efficient to assess the tool wear during CFRP machining. The fractal analysis used herein admits for only inputs the range of the observation scale for the fractal dimension determination. Adapting this monitoring technique is easy to setup contrary to e.g. statistical parameters which require rather long preliminary machining tests.

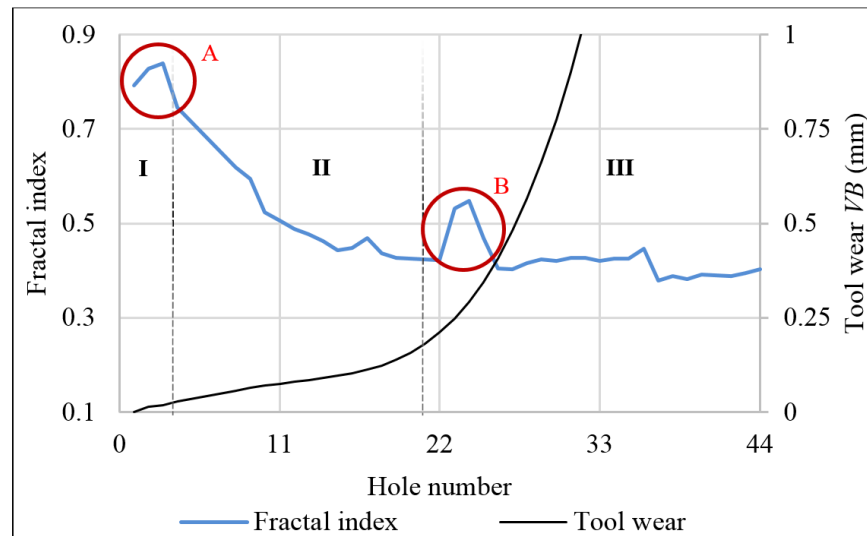


Figure B-6: Fractal index,  $I_F$ , results and the tool wear in function of the number of holes drilled

Fractal parameters (fractal dimension  $D$ , topothesy  $G$  and  $R^2$ ) obtained from AE signal analysis are efficient to describe the tool wear evolution and, to a further extent, the machining quality. In order to improve this technique further, the fractal index  $I_F$  can be calculated based on parameters such as fractal dimension and topothesy. In this study, this index is confirmed to be an excellent factor to evaluate the tool wear while drilling CFRP. Further experiments could be performed to investigate the robustness of this method e.g. with the online change of the cutting parameters.

## B.6 Acknowledgements

This work was funded by the Consortium for Research and Innovation in Aerospace in Québec and its partners, the Natural Sciences and Engineering Research Council of Canada, Bombardier Aerospace, Avior Integrated Products, Delastek and AV&R Aerospatiale. The authors wish to thank Mr Éric Marcoux for his help in conducting the experiments. The regularization analysis was performed using a program part from the Matlab® Toolbox FracLab engineered by INRIA in France.

## B.6 References

- [1] E. Persson, I. Eriksson, and L. Zackrisson, "Effects of hole machining defects on strength and fatigue life of composite laminates," *Composites Part A: Applied Science and Manufacturing*, vol. 28, pp. 141-151, 1997.

- [2] W. König, C. Wulf, P. Graß, and H. Willerscheid, "Machining of Fibre Reinforced Plastics," *CIRP Annals - Manufacturing Technology*, vol. 34, pp. 537-548, // 1985.
- [3] P. Guegan, F. Lemaitre, and J. Hamann, "Contribution a l'usinage des materiaux composites," ed, 1992.
- [4] S. Jahanmir, M. Ramulu, and P. Koshy, *Machining of ceramics and composites*. New York: Marcel Dekker, 1999.
- [5] D. A. Stephenson and J. S. Agapiou, *Metal cutting theory and practice* vol. 68: CRC press, 2005.
- [6] C. C. Tsao and H. Hocheng, "Effect of tool wear on delamination in drilling composite materials," *International Journal of Mechanical Sciences*, vol. 49, pp. 983-988, 8// 2007.
- [7] H. Hamedanianpour and J. F. Chatelain, "Effect of Tool Wear on Quality of Carbon Fiber Reinforced Polymer Laminate during Edge Trimming," *Applied Mechanics and Materials*, vol. 325-326, pp. 34-39, 2013.
- [8] Y. G. Kabaldin, S. V. Seryi, A. V. Prosolovich, and E. N. Burdasov, "Improving the stability of cutting on the basis of fractal, dimensional, and wavelet analysis," *Russian Engineering Research*, vol. 30, pp. 587-595, 2010.
- [9] P. Fu, W. L. Li, and L. Q. Zhu, "Cutting Tool Wear Monitoring Based on Wavelet Denoising and Fractal Theory," *Applied Mechanics and Materials*, vol. 48-49, pp. 349-352, 2011.
- [10] I. International Standard Organization, "Tool life testing in milling," in *Part 2: End milling* vol. 8688-2:1989, ed, 1989, p. 26.
- [11] Z. Feng, M. J. Zuo, and F. Chu, "Application of regularization dimension to gear damage assessment," *Mechanical Systems and Signal Processing*, vol. 24, pp. 1081-1098, 2010.
- [12] J. Lévy Véhel and P. Legrand, "Signal and image processing with Fraclab," in *Eighth International Multidisciplinary Conference*, Vancouver, Canada, 2004.
- [13] F. Roueff and J. Lévy Véhel, "A Regularization Approach to Fractional Dimension Estimation," in *Fractals* 98, 1998.



## **APPENDIX C – ARTICLE 6: SURFACE PROFILE TOPOGRAPHY OF TRIMMED AND DRILLED CARBON/EPOXY COMPOSITE**

Xavier Rimpault<sup>a</sup>, Jean-François Chatelain<sup>b</sup>, Jolanta E. Klemberg-Sapieha<sup>c</sup>, Marek Balazinski<sup>a</sup>

<sup>a</sup>Department of Mechanical Engineering, Polytechnique Montréal, Canada

<sup>b</sup>Department of Mechanical Engineering, École de Technologie Supérieure, Canada

<sup>c</sup>Department of Engineering Physics, Polytechnique Montréal, Canada

\* Published in *Procedia CIRP*, vol.46, pp.27-30, 2016.

### **C.1 Abstract**

The surface finish of Fiber Reinforced Plastic (FRP) laminate is challenging to characterize, due to the heterogeneous structure of the composite. Profile roughness parameters are highly impacted by the different layer properties, and their distributions are relatively spread out. In this paper, the surface topography of a 24-ply quasi-isotropic Carbon FRP (CFRP) is observed through primary profiles and the roughness parameter  $R_a$  in the transverse direction on trimmed and drilled CFRP surfaces. The surface characterization using the  $R_a$  parameter is found inadequate in providing useful information as to the machined surface quality.

*Keywords:* Fiber reinforced plastic, topography, roughness.

### **C.2 Introduction**

Due to high strength-to-weight ratios of composite materials, they have been increasingly used in the aerospace industry. Composites are produced close to their final shape, but finishing operations are still required, e.g. trimming and drilling. The composite surface topography after such machining operations needs to be investigated for assembly purpose. The laminate composite mechanisms are different depending on the tool-fiber angle due to the different fiber orientations. In consequence, the surface topography is impacted as well [1, 2]. Profile roughness parameters obtained in the ply plane direction of trimmed laminated composite surfaces are highly different depending on e.g. the fiber angle and the tool wear. It was found a radical difference of surface profile behavior of trimmed,  $0^\circ$  and  $45^\circ$  vs the  $-45^\circ$  ply orientations [3, 4]. In the transverse direction, the surface topography analysis is more complex. Due to its laminated structure, the

composite stacking sequence leads to different stratified surface properties. Each layer surface should be examined separately to perform an accurate roughness profile analysis. But such solution would be time-consuming. Due to a relatively high thickness variation of each ply, an automation procedure of the profile analysis would be extremely complicated to implement. Thus, the surface profile analysis should be carried out using traditional techniques. However, Landon et al. found a very poor reproducibility rate for the roughness parameter  $Ra$  from measurements taken at different heights and different angular positions along the hole axis [5]. This is caused by the deep valleys, generated during the machining of  $-45^\circ$  plies, in the roughness profile. Surface profile in the transverse direction should be investigated further to identify additional problems and propose a viable surface profile characterization solution. Besides, profiling contact measurement, which is preferred in hole inspection, leads to a slight surface alteration of the composite. Because of this and to reduce the characterizing time of composite surfaces in the industry, the smallest number of measurement repetitions should be reached to achieve a reliable surface characterization.

This study raises the problems of the surface profile characterization of holes in carbon fiber reinforced plastic (CFRP) material. To have a clearer understanding of the challenges involved, the profile characterization of CFRP trimmed surfaces was performed for different tool wear. For both machining processes (trimming and drilling), primary profiles as well as roughness parameters are presented and discussed to highlight the characterization difficulties.

## **C.3 Materials and methodology**

### **C.3.1 Material and machining setup**

For drilling and trimming experiments, the laminated composite was a quasi-isotropic CFRP prepared using 24 pre-impregnated plies. The K2X10 Huron<sup>®</sup> high-speed machining center was used to perform the machining tests. A dust extraction system was mounted onto the machine for health and safety purposes. A 3/8" diameter end-mill router with six flutes was selected to conduct the trimming experiments and a twist drill for the drilling tests. The tool wear was estimated using images taken with VHC 600+500F Keyence<sup>®</sup> optical microscope. The maximum tool wear was evaluated based on images taken at the tool edge clearance faces, according to ISO standards recommendations [6]. The tool wear  $VB$  corresponds herein to the average of the six maximum tool wear values estimated for each of the tool cutting edges.

### C.3.2 Measurement setup

The surface topography was extracted from profiles taken with Mitutoyo® SV-CS3200 profilometer. All measurements, on both hole and trimmed surfaces, were performed using the same cut-off lengths (0.25 mm) and the same 0.2  $\mu\text{m}$  pitch. Two different stylus configurations (standard and deep-hole) with the same tip geometry (2  $\mu\text{m}$  tip radius and 60° tip angle) were used.

According to ISO standards, the typical profile sampling length (1.25 mm herein) was selected to calculate roughness parameters, based on five cut-off lengths (0.25 mm each) [7]. Primary profiles were obtained after linear correction of the measured raw profiles [8]. The parameter  $Ra$  was calculated using the roughness profiles which were obtained after the primary profile filtering, to remove the profile waviness. This parameter  $Ra$  was selected due to its extensive use and to highlight the characterization issues.

#### C.3.2.1 Profile topography in trimming

Figure C 1 depicts the measurement location on the trimmed coupons. Five measurements of 3.75 mm were performed for each machined side. Out of each measurement, five roughness parameters  $Ra$  were calculated from profile length (1.25 mm), giving a total of 25  $Ra$  values per face. This allows to estimate the  $Ra$  parameter deviation influenced by the measurement position in the composite height thickness.

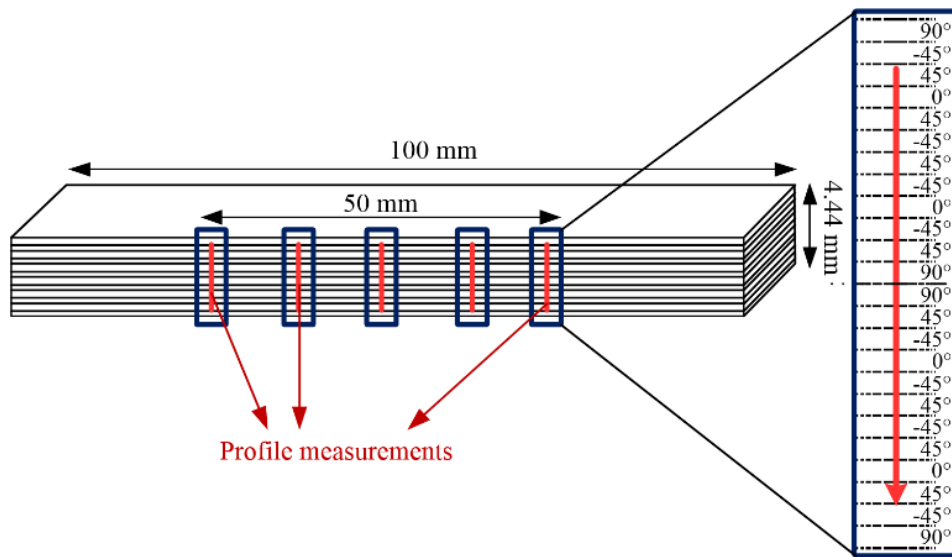


Figure C-1: Measurement positions on trimmed surfaces in the transverse direction

### C.3.2.2 Profile topography in drilling

Figure C 2 shows the location and orientation of the hole topography profile measurements. Five profiles of 2.25 mm were measured for each of the 36 angular positions along the hole generating line, so every 10° increment. Three roughness parameters  $Ra$  were calculated from each measured profile, giving, in total, fifteen roughness parameter repetitions per angular position per hole.

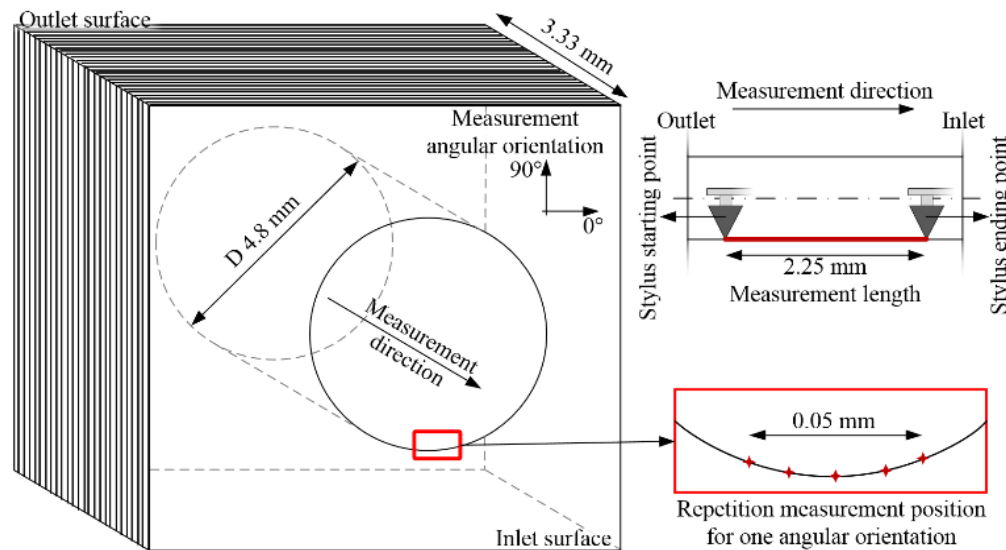


Figure C-2: Measurement positions diagram on hole surfaces

## C.4 Results and discussion

### C.4.1 Trimmed surface profiles

Samples of primary profiles for different tool wear are presented in Figure C 3. Plies with various fiber orientations can be relatively easily identified, in particular for low tool wear. In agreement with the literature, the deep cavities correspond to the -45° plies. The other ply orientations are difficult to distinguish from one to another. Up- and down-milling coupon sides also have different characteristics. Down-milling surfaces for different tool wear are similar. But down-milling surfaces are smoother at a low scale, as well as the total height of the primary profile rises, with the tool wear increase. Regarding up-milling surfaces, the -45° plies become more difficult to track with the tool wear increase. The profile roughness becomes higher with the tool wear increase.

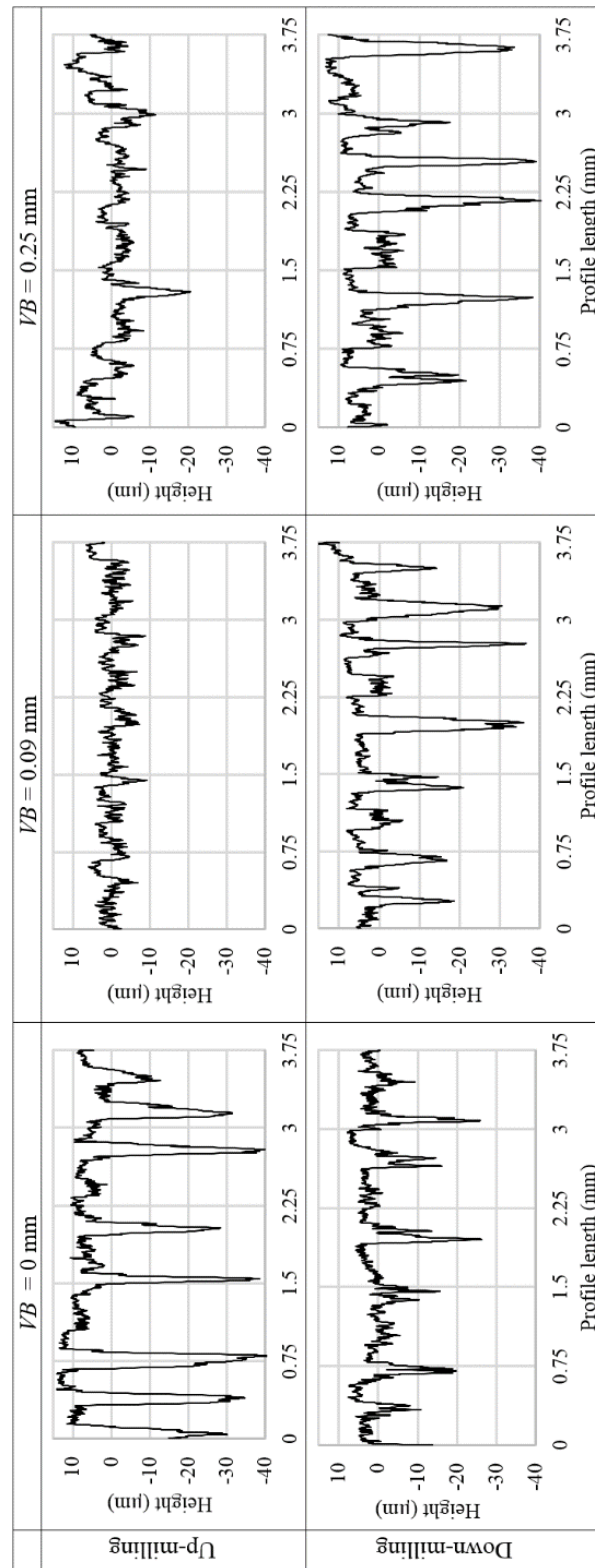


Figure C-3: Primary profiles of up- and down-milling trimmed surfaces  
for three different tool wear

Figure C 4 depicts the  $Ra$  results in up- and down-milling. Due to the different properties of the laminated composite surface, characterization parameters are strongly impacted by the measurement position. The value distribution of  $Ra$  is relatively large. The average variation of  $Ra$  remains relatively stable along the tool life for both up- and down-milling. However, based on surface analysis in the ply plane direction, such surface characterization is inadequate and misrepresentative of the composite topography [9]. Due to the  $Ra$  calculation characteristics, this parameter shrinks the surface characterization into a single number corresponding to the profile height deviation average. This cuts out any profile singularity impact on the parameter value. Though, averaging is preferred for the surface analysis of homogeneous materials allowing the reduction in the effect of outliers but should be investigated in composite surface case.

The mischaracterization can be the consequence of the composite lamination characteristics, such as the number of  $-45^\circ$  plies, their thickness and the composite stacking sequence.

In addition to the reduced information involved in the parametrization, the filtering, generating roughness profiles, can cause artifacts [5].

The profile misrepresentation of  $Ra$ , presented in Figure C 4, is instigated by the characterization process itself (filtering and parametrization). This explains why the same roughness parameter  $Ra$  value can be calculated from such different primary profile samples, shown in Figure C 3.

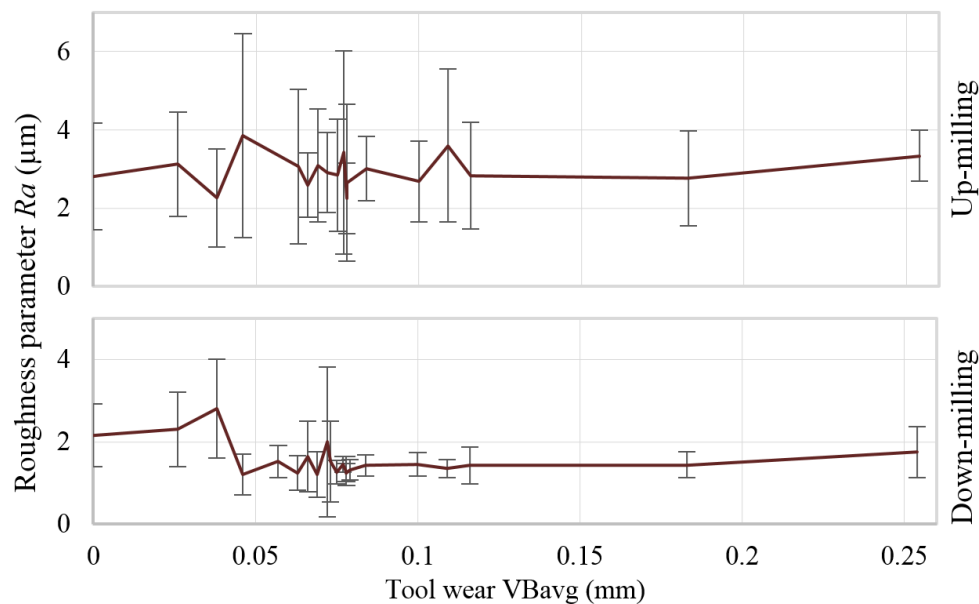


Figure C-4:  $Ra$  average results with  $\pm 2$  standard deviations obtained on up- and down-milling faces

### C.4.2 Drilled surface profiles

Figure C 5 depicts the results of the roughness parameter  $Ra$  vs the hole orientation for a new tool. Depending on the measurement position, the  $Ra$  deviation admits a relatively high difference ratio up to twelve (standard deviation values of 0.07 mm for  $20^\circ$  and 0.88 mm for  $270^\circ$  in Figure C 5).

Figure C 6 displays the averages and dispersions of the parameter  $Ra$  for medium and high tool wear. For medium tool wear (0.09 mm VB) compared to Figure C 5 results, the  $Ra$  average and deviation tends to be lower but the  $Ra$  deviation still varies widely. For high tool wear (0.25 mm VB), the deviation difference tends to be limited. But the parameter  $Ra$  increases so the roughness average is higher.

Figure C 7 shows primary profile examples measured in a hole quarter for different tool wear. The tool wear estimation varies between the drilling and trimming operations because of the tooling difference, so the tool wear comparisons are fairly limited. However, similar trends are observed in the primary profiles measured for different tool wear. With a new tool, the machined surface is relatively rough and erratic. Above a tool wear limit, the surface generated is smoother and stable due to the cutting mechanism change. When the tool wear becomes even higher, the number of topographic defect raises highly which leads to a rougher surface.

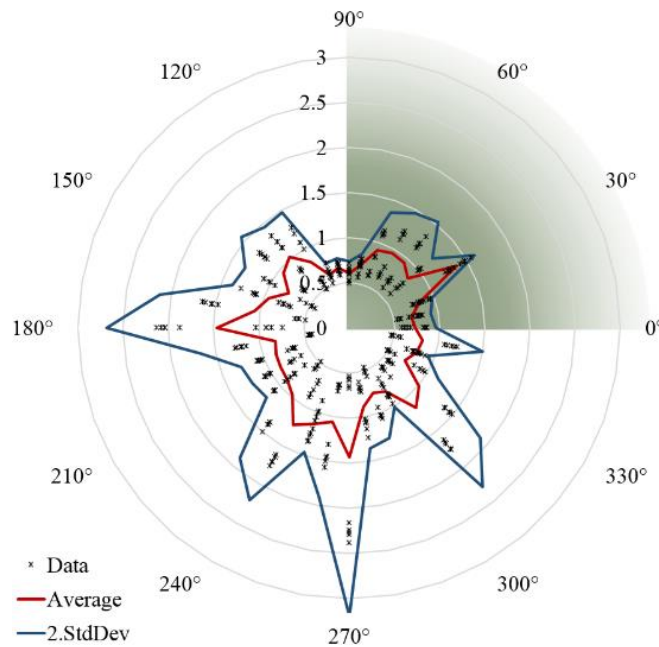


Figure C-5: Roughness parameters  $Ra$  along the hole orientation for a sharp tool

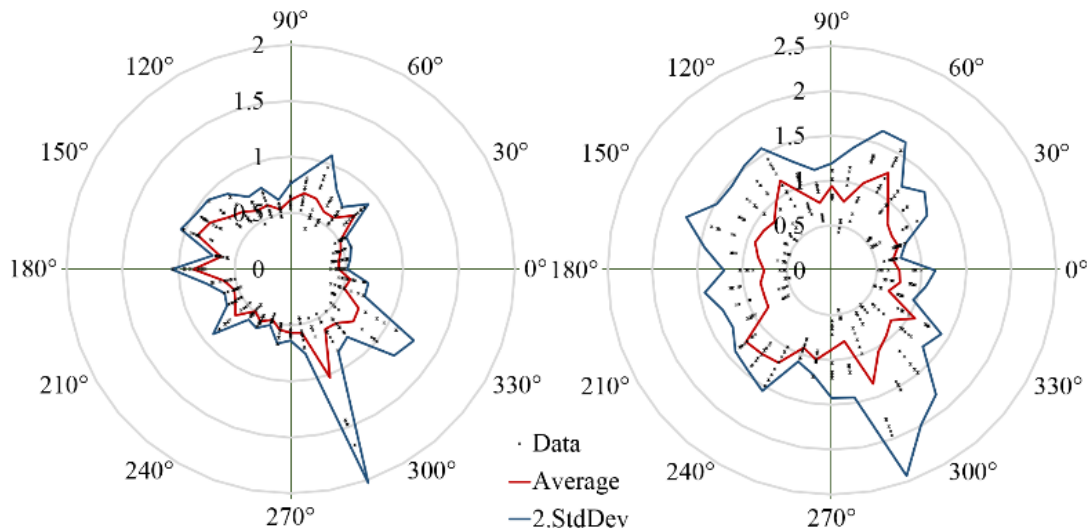


Figure C-6: Roughness parameters  $Ra$  for medium (left) and high (right) tool wear

The  $-45^\circ$  plies seem relatively easy to be spotted but, in some locations, those plies are particularly difficult to observe. Moreover, with the tool wear increase, the  $-45^\circ$  plies become highly difficult to be differentiated from the other. This issue is due to the topography of the machined  $-45^\circ$  plies. In the ply plane, those plies admit large variations. So depending on the measurement position, the  $-45^\circ$  ply can be measured at the high or at the bottom location of its surface in the transverse direction. In the case of the former location, the profile prevents exposing the  $-45^\circ$  plies. The filtering and parametrization problems, identified in the surface profile analysis in trimming, remain present for the hole surface case. In addition to those problems, the measurement position and orientation accuracy is another problem source in the hole surface analysis.

## C.5 Conclusion

In this study, the machined surface topography of CFRP drilled and trimmed surface was investigated. Trimmed and hole surfaces were measured in the transverse direction of the composite lamination. Due to the heterogeneous structure of laminated composite, the machined surface has different stratified surface topography properties. The  $-45^\circ$  ply orientation admits higher surface roughness than the other ply orientations ( $0^\circ$ ,  $45^\circ$  and  $90^\circ$ ). Based on the measurement results, the roughness parameter  $Ra$  is found inadequate to characterize such surfaces. Depending on the composite ply stacking sequence and the measurement position, the results deviation can be relatively high. The filtering and the parameterization can influence the deviation of the results. In hole surfaces, another problem may be highlighted. Set up position and



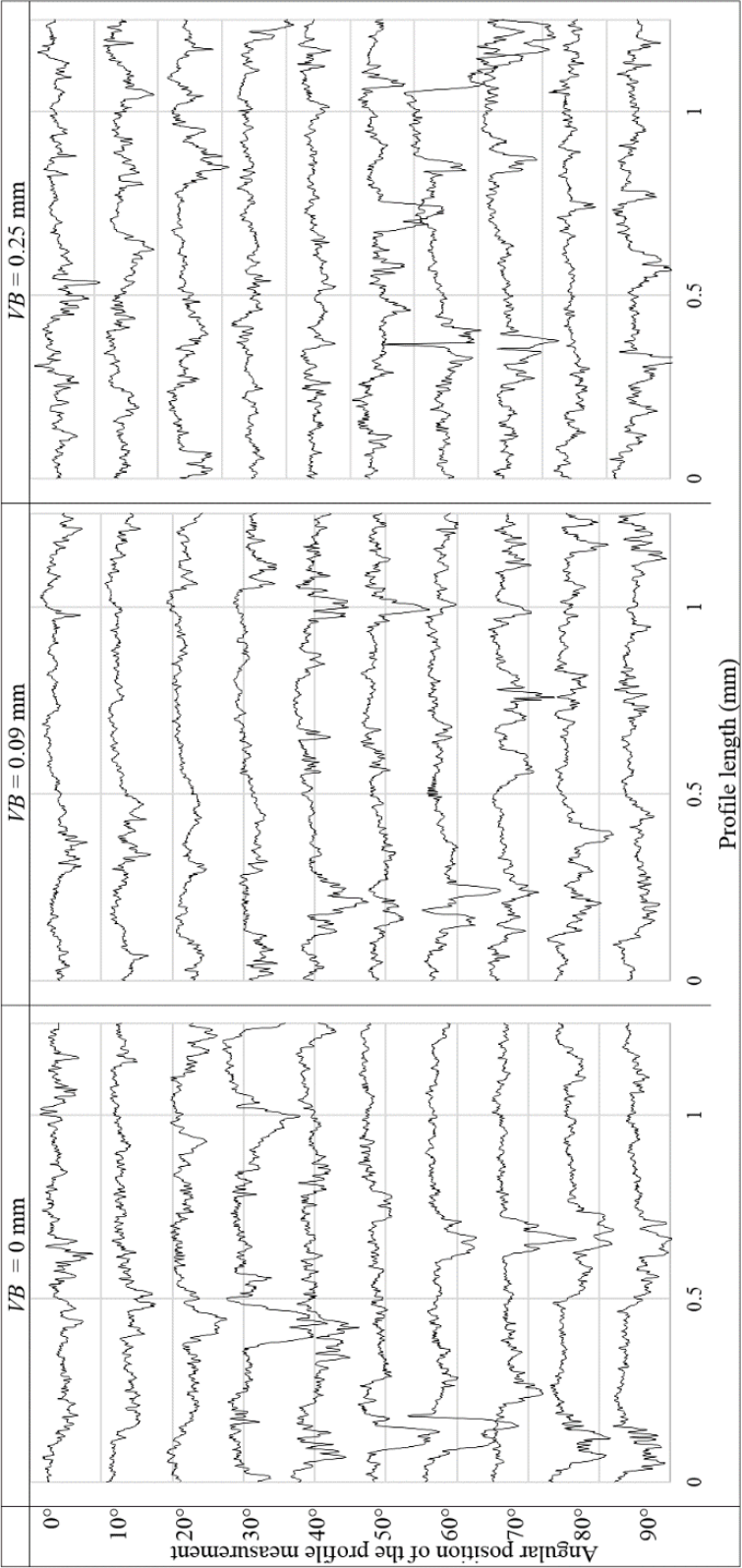


Figure C-7: Profile samples for different tool wear at several hole angular positions (colored section in Figure C 5)

orientation variations between the measurements are an additional source of the variations in the roughness parameters. Using the *Ra* parameter should be avoided for composites' surfaces and different approaches may be considered such as the introduction of new roughness parameters and alternative filtering techniques.

## C.6 Acknowledgements

This work was funded by the Consortium for Research and Innovation in Aerospace in Québec and its partners, the Natural Sciences and Engineering Research Council of Canada, Bombardier Aerospace, Avior Integrated Products, Delastek and AV&R. The authors wish to thank Mr Hossein Hamedanianpour for conducting the trimming experiments at the Centre Technologique en Aérospatial with the help of Mr Réjean Roy, and Mr David Chapelier and Mr Gang Zhao for measuring profiles of trimmed and hole surfaces.

## C.7 References

- [1] Arola D, Ramulu M, Wang DH. Chip formation in orthogonal trimming of graphite/epoxy composite. *Composites Part A: Applied Science and Manufacturing*. 1996;27:121-33.
- [2] Wang DH, Ramulu M, Arola D. Orthogonal cutting mechanisms of graphite/epoxy composite. Part II: multi-directional laminate. *International Journal of Machine Tools and Manufacture*. 1995;35:1639-48.
- [3] Rimpault X, Chatelain JF, Klemberg-Sapieha JE, Balazinski M. A new approach for surface profile roughness characterization in the laminate composite ply plane. In: Institute CAaS, editor. CASI Aeronautics Conference Montreal2015.
- [4] Chatelain JF, Zaghibani I, Monier J. Effect of Ply Orientation on Roughness for the Trimming Process of CFRP Laminates. *World Academy of Science, Engineering and Technology*. 2012;68:987 - 94.
- [5] Landon Y, Cherif M. Characterization of the Surface Quality of Holes Drilled in CFRP Laminates. *Advanced Materials Research*. 2013;698:107-16.
- [6] International Standard Organization I. Tool life testing in milling. Part 2: End milling1989. p. 26.
- [7] International Standard Organization I. Geometrical Product Specifications (GPS) -- Surface texture: Profile method. Rules and procedures for the assessment of surface texture1996. p. 8.

- [8] International Standard Organization I. Geometrical Product Specifications (GPS) -- Surface texture: Profile method. Terms, definitions and surface texture parameters 1997. p. 25.
- [9] Wern CW, Ramulu M, Colligan K. A study of the surface texture of composite drilled holes. *Journal of Materials Processing Technology*. 1993;37:373-89.